GROUND-WATER CAPTURE-ZONE DELINEATION: METHOD COMPARISON IN SYNTHETIC CASE STUDIES AND A FIELD EXAMPLE ON FORT WAINWRIGHT, ALASKA

By

Julie Anne Ahern

RECOMMENDED: _____

_____

_____

_____

Advisory Committee Chair

_____

Chair, Department of Civil and Environmental Engineering

APPROVED: _____

Dean, College of Engineering and Mines

_____

Dean of the Graduate School

_____

Date

GROUND-WATER CAPTURE-ZONE DELINEATION: METHOD COMPARISON IN SYNTHETIC CASE STUDIES AND A FIELD EXAMPLE ON FORT WAINWRIGHT, ALASKA

A

THESIS

Presented to the Faculty

of the University of Alaska Fairbanks

in Partial Fulfillment of the Requirements

for the Degree of

MASTER OF SCIENCE

By

Julie Anne Ahern, B.S.

Fairbanks, Alaska

May 2005

ABSTRACT

Ground-water capture zone delineation is an integral part of the recent Source Water Assessments performed nation-wide. Delineations are used to identify where protection from contamination is critical. The objectives of our study were to compare commonly-used methods by quantifying the differences in capture-zone areas and evaluating whether the differences increase with system complexity. We delineated capture zones of hypothetical case studies. We began with a very simple hydrogeologic system and gradually added complexity. Four methods were applied to each case: Calculated fixed-radius (CFR), two analytical solutions (WHPA and UFE-Thiem), and a numerical model (MODFLOW). Area comparisons revealed that, in comparison to the numerical model, CFR consistently overestimated, WHPA underestimated, and UFE-Thiem was variable and the most similar.

We then compared the methods in a field case on Fort Wainwright, Alaska. As our numerical method, we used a sub-regional ground-water flow model. Area comparisons were similar to case-study results. Surface-water features were the most influential complexity in the field case. We concluded that each method is only as accurate as its assumptions. Any added margin of error must be appropriate for both the aquifer complexities and required assumptions specific to a given ground-water system.

TABLE OF CONTENTS

LIST OF FIGURES

LIST OF TABLES

LIST OF APPENDICES

LIST OF OTHER MATERIALS

ABBREVIATIONS

ADEC =	Alaska Department of Environmental Conservation
asl =	above sea level
BCF =	MODFLOW's Block-Centered Flow Package
CFR =	calculated fixed radius
D =	dimensional
DRO =	diesel range organic
EPA =	Environmental Protection Agency
ET =	evapotranspiration
FWM =	Fort Wainwright monitoring well
MPATH =	MODPATH
NTL =	Northern Testing Laboratories
P =	precipitation
SDWA =	Safe Drinking Water Act
SVS =	simplified variable shapes
SWA =	Source Water Assessment
TOT =	time of travel
UAF =	University of Alaska Fairbanks
UFE =	Uniform Flow Equation
USGS =	United States Geological Survey
WHP =	Wellhead Protection
WHPA =	Wellhead Protection Area (EPA analytical model)
WS =	water supply
ZOC =	zone of contribution

NOMENCLATURE

a = anisotropy ratio

b = aquifer thickness

B_{eff} = effective aquifer thickness

C = conductance

h = hydraulic head

i = hydraulic gradient

K = hydraulic conductivity

L = length of stream reach

l = length of well-screen interval

M = thickness of streambed

n = porosity

q = specific discharge

Q = volumetric flow rate

r = radial distance from well

S = storativity

S_s = specific storage

t = time

v = average linear velocity

W = width of stream

x_{sp} = stagnation point of flow paths down-gradient of pumping well (UFE)

y_{max} = maximum width of capture zone up-gradient of pumping well (UFE)

Φ = complex velocity potential

ϕ = velocity potential

φ = stream function

UNITS

cfs = cubic feet per second

cfu = colony forming units

d = days

^{o}F = degrees Fahrenheit

fbgs = feet below ground surface

ft = feet

gpm = gallons per minute

in = inches

mi = miles

min = minutes

ml = milliliter

sq mi = square miles

yr = year

ACKNOWLEDGEMENTS

Funding for this project was provided by primarily by Alaska EPSCoR and the US Army Alaska. Additional funding sources include GW Scientific and the University of Alaska Fairbanks. I would like to thank those who worked with me on the Fort Wainwright Geohydrologic Monitoring Project, namely Matt Dusenbury and Mathias Eriksson. Bob Busey and Emily Youcha provided useful technical assistance as well.

Thanks to the USGS instructors of the 2003 MODFLOW-2000 short course, especially Arlen Harbaugh and Dave Pollock, who provided modeling insight both during and after the class. Thanks to the USGS ground-water modelers who created the Fairbanks sub-regional model: Michael Lilly, Stan Leake, Dave Claar, and Alan Nakanishi; they developed an extremely valuable tool in studying ground-water flow of the Fairbanks area. Useful information was also provided by former staff of ADEC's Drinking Water Protection Program, namely Sarah Rygh and Sue Braumiller, regarding ADEC's SWA delineation method.

My committee members, Larry Hinzman, Dave Barnes, Doug Kane, and Michael Lilly, have given me much of their time, resources, and knowledge; all are greatly appreciated. Thanks to the rest of those in the Water and Environmental Research Center, especially Greta Myerchin, Danielle Kitover, and Sarah Seelan. Lastly, the thoughtfulness and support of my family and friends have helped immensely. Special thanks to Jeff Oatley and Heather Best; their humor and wisdom will never be forgotten.

GROUND-WATER CAPTURE-ZONE DELINEATION: METHOD COMPARISON IN SYNTHETIC CASE STUDIES AND A FIELD EXAMPLE ON FORT WAINWRIGHT, ALASKA

INTRODUCTION

In recent years, ground-water protection has become a national priority. Policy-makers have shifted their approach, focusing less on remediation and more on prevention. A major step in the prevention of contaminated ground water is capture-zone delineation. A capture zone is the volume through which ground water flows to a pumping well over a given time (Hansen, 1991). Figure 1 illustrates a simple example. Delineating a well's capture zone aids in water-supply management by creating an awareness of the recharge source. This helps ensure sustainable pumping operations and outlines areas where protection from contamination is critical. Delineations are also useful for extraction wells in pump-and-treat remediation systems (Fetter, 1994).

The accuracy of the delineation often depends on the method used because the sophistication of available techniques varies widely. Since simpler methods cannot account for complexities within real systems, using them can result in either an over- or underestimation of the capture zone. An underestimation may lead to contamination or over-pumping of the source, while an overestimation may cause unnecessary monitoring and land-use restrictions.

The EPA has recommended several delineation methods for states to use in their Source Water Assessment (SWA) Programs. Because no single method is mandatory, state and local agencies have applied a variety of techniques. Their choices were based on resource and data availability, as well as the hydrogeologic setting of individual water-supply systems.

Our study compares delineation methods commonly-used by state and local agencies. The methods have varying levels of sophistication. Our objectives are to quantify the differences in the size and shape of the capture zone, and evaluate the degree of differences as hydrogeologic complexity increases. The selected methods are as follows:

1. **Calculated Fixed Radius (CFR)**. This is the simplest method. It assumes one-dimensional flow around the well screen, which creates a cylindrical capture zone.
2. **Analytical solution**: This is a solution used in the Alaska Department of Environmental Conservation (ADEC) Source Water Assessment Program (Braumiller, 2000). It is based on the superposition of radial flow on a uniform flow field. It is a unique solution that combines the Thiem and uniform flow equations. We refer to it here as the **UFE-Thiem** method.
3. **Analytical solution: WHPA** (Wellhead Protection Area). This is an EPA-derived analytical model that has been widely used by states in their Wellhead Protection and Source Water Assessment Programs. It is based on the same analytical equations as in the UFE-Thiem solution, but uses particle-tracking to delineate capture zones.
4. **Numerical model: MODFLOW and MODPATH**. MODFLOW is a ground-water flow model designed by the U.S. Geological Survey (USGS). MODPATH is a particle-tracking code associated with MODFLOW.

We test the following hypothesis:

Under the same hydrogeologic and pumping conditions, CFR, UFE-Thiem, and WHPA will delineate capture areas that significantly differ from those delineated by the numerical method. The magnitude of difference will increase with both aquifer complexity and the invalid assumptions made by each method.

To test the hypothesis, we apply the methods to four synthetic case studies. Hydrogeologic complexity increases with each case to examine the affect on the capture zones. We overlay the delineations of all methods for each case to compare their two-dimensional capture areas. Results produced by MODPATH are assumed to be the best estimation of true conditions, and so we find the differences in area between the first three methods as compared to MODPATH. We then examine whether the differences increase with site complexity. Lastly, we identify the effects of the complexities and the limits of method assumptions.

After comparing the methods in synthetic case studies, we apply them to a field case. The site is located at the primary water-supply wells on Fort Wainwright, Alaska. The first three methods use the same amount of inputs as with the synthetic cases. However, our numerical model incorporates far more detailed data than in previous cases. We use a sub-regional flow model of the Fairbanks floodplain, which was developed by the USGS. The model uses more data than in past capture-zone delineations of the Fort Wainwright water-supply wells, and it is therefore more capable of producing a higher level of accuracy.

This study comes at a critical time: most states have recently completed their SWA programs and some are now tailoring their plans to fit local conditions. Our results demonstrate the need for using a method with an appropriate level of accuracy. Furthermore, alluvial aquifers such as those in our case studies are a common water-supply source due to their high yields. Our results can therefore be applied to many regions throughout the country.

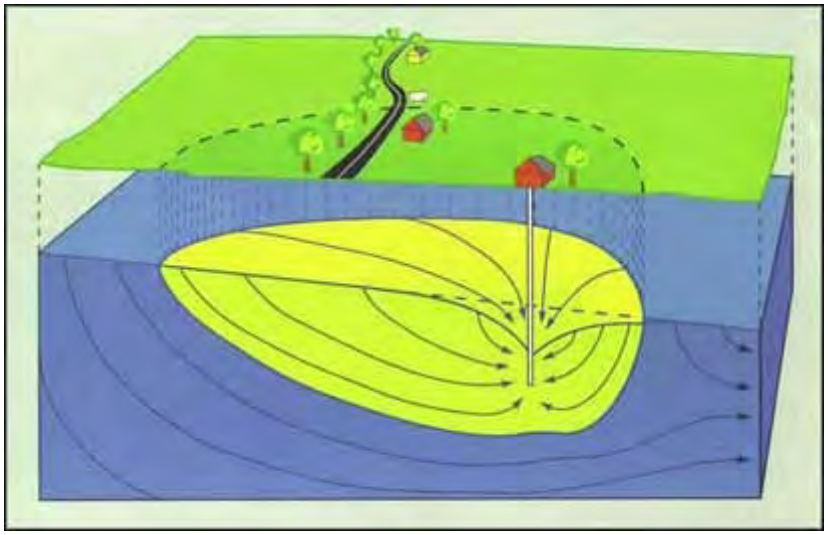

Figure 1. Example of a capture zone (US EPA, 2003)

1 CAPTURE ZONE DELINEATION BACKGROUND

1.1 LITERATURE REVIEW

1.1.1 Ground-Water Protection in the US

Before 1986, the US EPA had enacted several laws aiming in part to control potential sources of ground-water contamination. They include the 1976 Safe Drinking Water Act (SDWA), the Resource Conservation and Recovery Act (1976), and the Clean Water Act (1977), among others. These federal policies leave the responsibility of implementation with state and local governments (Gallagher, 1990). As such, the degree and type of enforcement may vary widely. A potential drawback is their focus on specific contaminants. Such an approach fails to identify the vulnerability of water-supply systems as a whole. Furthermore, contaminant-specific legislation can lead to action that is responsive in nature (i.e., efforts that are remedial rather than preventative).

A comprehensive federal ground-water protection program first appeared in the 1986 SDWA Amendments (Gallagher, 1990). Known as the Wellhead Protection (WHP) Program, it was designed to prevent contamination of ground-water supplies in conjunction with the traditional treatment approach. Rather than focus on individual contaminant sources, the WHP approach examines each well's recharge area and identifies existing and potential sources of contamination. The program was to be administered by state and local governments, and consisted of four parts:

1) delineation of Wellhead Protection Areas (WHPA),
2) inventory of potential contaminant sources within the delineated area,
3) management controls for potential contaminant sources, and
4) contingency plans for emergency situations.

A decade later, the 1996 SDWA Amendments established the Source Water Assessment (SWA) Program. This program is very similar to WHP program with two main differences: the Source Water Protection Areas (SWPA) include surface-water as well as ground-water supplies, and the program requires that states make all SWA reports accessible to the public. Currently, most states have completed their SWA reports.

As listed above, the first step of both programs involves the delineation of the public water supply's protection area. A WHPA is defined as "the surface and subsurface area surrounding a well or wellfield, supplying a public water system, through which contaminants are reasonably likely to move toward and reach such a well or wellfield." (US EPA, 1987). This area can be thought of as a two-dimensional, aerial view of the capture zone.

1.1.2 Common Methods of Capture Zone Delineation

States have used a variety of delineation methods because the EPA does not require any particular technique in either WHP or SWA programs. Instead, the EPA provided a list of six approved methods, based on current U.S. and European ground-water protection programs, from which states could choose. They are:

- arbitrary fixed radius,
- calculated fixed radius,
- analytical solutions,
- simplified variable shapes,
- hydrogeologic mapping, and
- numerical modeling.

1.1.2.1 Arbitrary Fixed Radius

The simplest type of delineation is the arbitrary fixed radius. The method consists simply of selecting a radial distance around the wellhead. The distance has no hydrogeologic basis; instead, the radius is based on the delineator's judgment of what will constitute a reasonably protective area. Existing regulatory drinking water-supply setback distances may be taken into consideration. Because no information on the ground-water system or well is taken into account, this method has a high degree of uncertainty.

1.1.2.2 Calculated Fixed Radius

Calculated fixed radius also draws a circle around the wellhead. However, the radius is not determined by the user, but rather by a one-dimensional volumetric flow equation:

$$r = \sqrt{\frac{Qt}{nl\pi}} \quad (1)$$

where r is the radius, Q is the volumetric discharge rate of the well, n is the aquifer porosity, l is the length of the well's screened interval, and t is the user-specified time of travel, or TOT. The TOT is the time period in which recharge travels from its origin to the well. Note that the travel time pertains to the advective movement of water in the saturated zone rather than unsaturated flow or contaminant transport.

The radius calculation assumes 1-D horizontal flow, homogeneity, isotropy, steady-state conditions, and negligible well interference. The resulting delineation is a cylinder around the screened interval that is large enough to yield the well discharge over the given TOT (Figure 2). The simple nature of the equation causes certain variables to exercise considerable control over the solution. For example, altering the screened interval (l) strongly impacts the radius. Figure 3 shows that a decrease in l of 40 feet more than doubles the radius. Such influence within a real aquifer system is improbable.

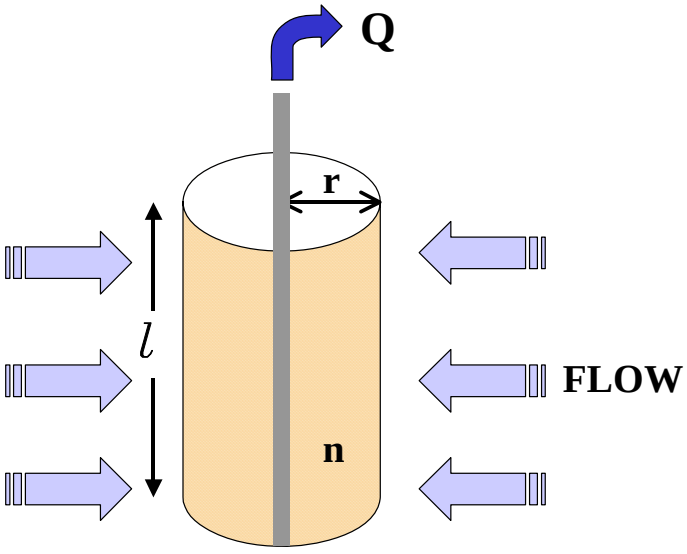

Figure2: Capture zone delineation using CFR. Modified from Muldoon and Payton (1993).

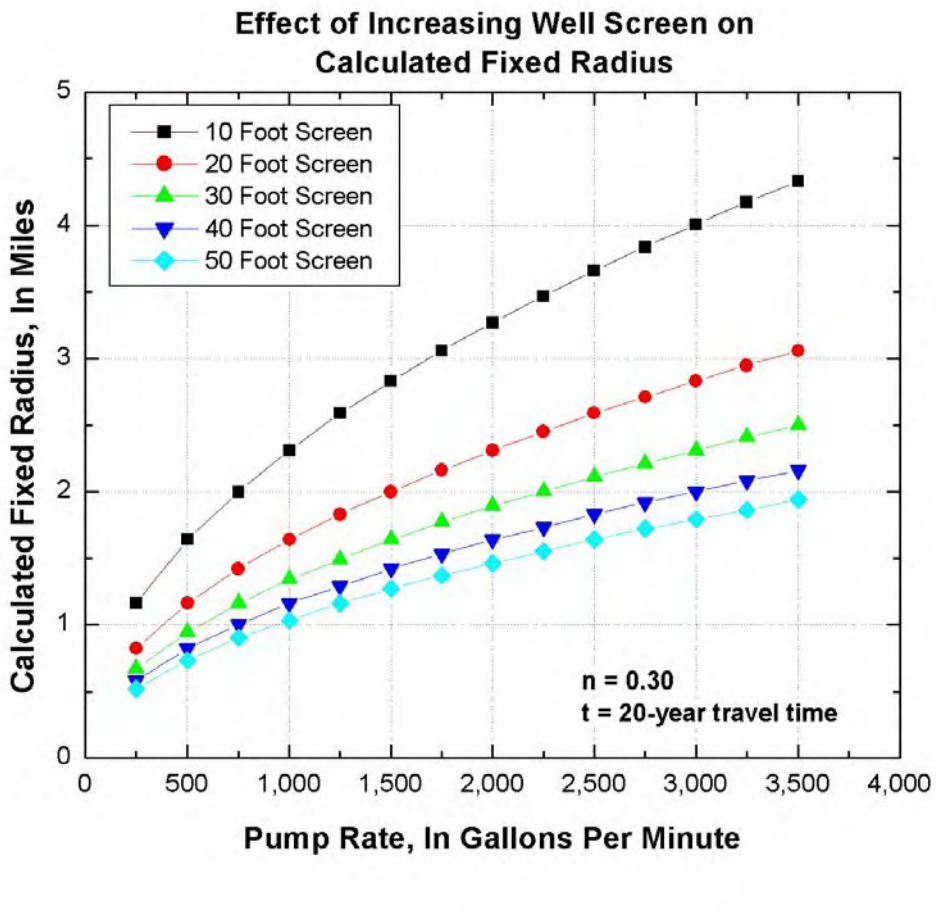

Figure 3: CFR as a function of well screen length and pumping rate.

1.1.2.3 *Analytical Solutions*

One of the major differences between analytical solutions and CFR is the addition of a second dimension. CFR assumes that flow to the well arrives equally from all directions. In contrast, an analytical solution accounts for the aquifer's regional (or natural) hydraulic gradient. Under steady-state pumping conditions, the flow is drawn primarily from the up-gradient direction. When a pumping gradient exists in addition to the natural gradient, the natural gradient will reverse a short distance down-gradient of the well (Fetter, 1994). The analytical capture zone outlines the ground-water flow divide that encompasses the well. In other words, all streamlines outside of the zone bypass the

well. In plan view, the area forms a parabolic shape rather than a circle. This section describes the methodology in further detail.

Analytical methods employ exact, closed-form solutions to the governing differential equation of an ideal flow system. In a two-dimensional x-y plane, the equation is:

$$\frac{\partial^2 \phi}{\partial x^2} + \frac{\partial^2 \phi}{\partial y^2} = 0 \tag{2}$$

ϕ is the velocity potential, defined as $\phi = Kh$, where K is hydraulic conductivity and h is hydraulic head (Javandel et al., 1984). Equation 2 is the Laplace equation, which is a continuity relationship that establishes the conservation of a fluid mass (Freeze and Cherry, 1979). It is one of the most commonly-applied equations in mathematical physics.

Bear and Jacobs (1965) were the first to derive an analytical equation describing the effects of a discharging well on uniform flow paths. They defined the boundaries of a capture zone in a confined, homogeneous and isotropic aquifer under conditions of uniform flow and a fully-penetrating pumping well. Superposition of a regional flow term and a point-sink term is used to solve for flow in a two-dimensional (x,y) plane. Javandel et al. (1984) and Javandel and Tsang (1986) further developed this method to examine the extent of subsurface contamination.

The solution is based on an analytic function known as the complex velocity potential (Φ):

$$\Phi = \phi + i\varphi \tag{3}$$

where i is $\sqrt{-1}$ and φ is the stream function. Stream functions are everywhere tangent to the specific discharge (McWhorter and Sunada, 1977). Thus, the specific discharge field is found by taking the derivative of ϕ:

$$q_x = -\frac{\partial \phi}{\partial x} = -K\frac{\partial h}{\partial x} \tag{4}$$

where K is hydraulic conductivity. This relationship is known as Darcy's Law. Since ϕ and φ are conjugate functions, φ can be determined if ϕ is known (Javandel et al., 1984):

$$\frac{\partial \phi}{\partial x} = \frac{\partial \varphi}{\partial y} \tag{5}$$

$$\frac{\partial \phi}{\partial y} = -\frac{\partial \varphi}{\partial x} \tag{6}$$

Note that the slopes of equipotentials (i.e., lines of equal velocity potential) and streamlines (i.e., lines of equal stream function) are negative reciprocals of each other. This implies that ϕ and φ are everywhere orthogonal (Gorelick et al., 1993), as Figure 4 illustrates.

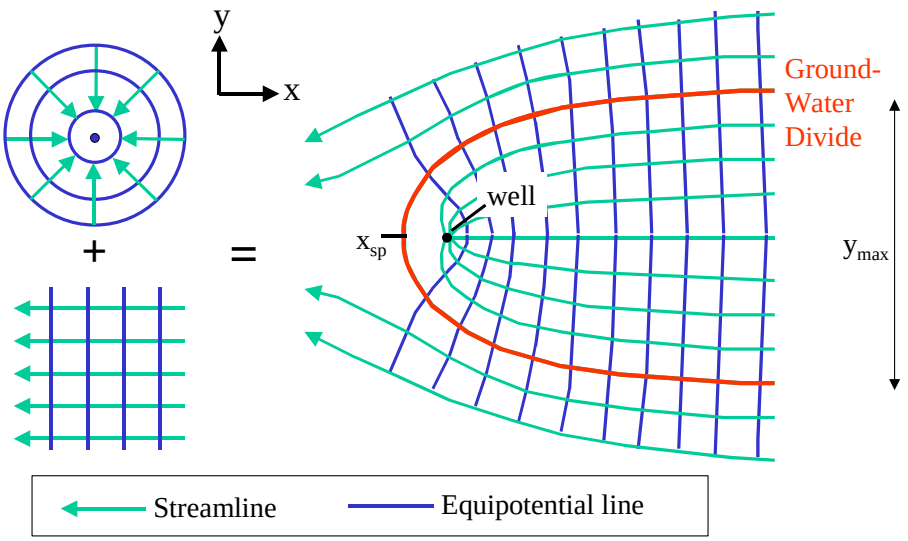

Figure 4. 2-Dimensional superposition of uniform and radial flow, plan view.

For a flow system involving a uniform regional gradient and a discharge well, streamlines in the x-direction are calculated as the sum of uniform and radial flow:

$$\varphi = \underbrace{Kiy}_{\text{Uniform flow}} + \underbrace{\frac{Q}{2\pi b}\tan^{-1}\left(\frac{y}{x}\right)}_{\text{Radial flow}} \tag{7}$$

where *b* is the aquifer thickness and *i* is the regional hydraulic gradient (McWhorter and Sunada, 1977). The streamline for which $\varphi = 0$ serves as the ground-water divide shown in Figure 4; thus, the equation can be rearranged as:

$$-Kiy = \frac{Q}{2\pi b}\tan^{-1}\left(\frac{y}{x}\right) \tag{8}$$

We refer to this as the uniform flow equation, or UFE. The UFE yields a parabolic-shaped outline of the zone contributing recharge to a well, which is known as the zone of contribution (ZOC). Two bounding solutions can be derived from the UFE:

$$x_{sp} = -\frac{Q}{2\pi Kbi} \tag{9}$$

$$y_{\max} = \pm\frac{Q}{Kbi} \tag{10}$$

where y_{max} is the maximum width of the zone as x approaches infinity, and x_{sp} is the down-gradient stagnation point (i.e., the furthest down-gradient point at which flow reverses toward the well).

Note that the ZOC is independent of time. In order to delineate a time-dependent capture zone, another term must be calculated in the analytical solution: the average linear velocity (or 'seepage' velocity). The x and y components of the average linear velocity are defined as:

$$v_x = \frac{q_x}{n} \tag{11}$$

$$v_y = \frac{q_y}{n} \tag{12}$$

This velocity term allows an individual particle of water to be tracked for a given time within the overall flow field (Javandel et al., 1984). It is applied differently among analytical solutions. We describe the techniques used in our selected analytical methods in section 1.2.2.

1.1.2.4 *Simplified Variable Shapes*

The simplified variable shapes (SVS) method is similar to analytical methods in that analytical equations are used to produce two-dimensional delineations. SVS is different

because the analytical equations are used to generate a series of shapes for the entire range of pumping rates and hydrogeologic conditions in the aquifer region. The shapes are then generalized into groups. The aquifer properties and well data required for the delineations depend on which analytical solution is chosen. Typically, data input includes the pumping rate, porosity, hydraulic conductivity, hydraulic gradient, and aquifer thickness. The most suitable shape is applied to each site based on site characteristics, and it is oriented with respect to the direction of ground-water flow and well location (Hansen, 1991).

1.1.2.5 *Hydrogeologic Mapping*

Hydrogeologic mapping is defined by the EPA as an assortment of geologic, geophysical, and dye-tracing techniques used to determine the ZOC (US EPA, 1987). The primary and sometimes only factor determining the wellhead protection area is the identification of flow boundaries, such as ground-water divides, rivers, and geologic contacts. In many cases, hydrogeologic mapping is used as a prelude to analytical solutions or numerical modeling to determine flow direction, aquifer properties, and boundary conditions. The method may be used alone if other methods are unsuitable. For instance, under conditions of conduit flow (e.g., fractured bedrock or karst topography), the assumption of porous flow found in other techniques renders them invalid. Mapping is not useful for delineation if the flow boundaries are outside the study area and would not influence flow to wells in a reasonable period of time. Geologic and water table maps, pump test data, and well logs may serve as data requirements. Unlike fixed radius and SVS methods, mapping necessitates a relatively high level of user expertise in geologic mapping and in identifying boundary conditions.

1.1.2.6 *Numerical Modeling*

Like analytical solutions, numerical methods solve the governing differential equation for ground-water flow (Equation 2). The following is a more complex form (3-D, transient) of the Laplace equation:

$$\frac{\partial}{\partial x}\left(K_X \frac{\partial h}{\partial x}\right)+\frac{\partial}{\partial y}\left(K_Y \frac{\partial h}{\partial y}\right)+\frac{\partial}{\partial z}\left(K_Z \frac{\partial h}{\partial z}\right)\pm N = Ss\frac{\partial h}{\partial t} \qquad (13)$$

where *N* represents source or sink terms; *Ss* is specific storage; and *x, y, z* are the horizontal (x,y) and vertical (z) coordinates. Unlike analytical solutions, however, numerical solutions are approximate. The partial differential equations are replaced with a set of algebraic counterparts, which in turn can be expressed as a matrix equation. A computer code is usually written for the equations so that they can be quickly solved (Anderson and Woessner, 1992). The solutions are discrete points in time and space rather than continuous flow lines. In delineating a capture zone, numerical models are similar to analytical solutions in that they often incorporate particle tracking.

Because a numerical model can discretize flow systems in space and time, it is more capable of representing hydrogeologic processes and variability relative to the other methods. It is therefore capable of generating more accurate results. By the same token, it requires a larger amount of data in order to be credible. It also requires a high degree of expertise, as the user must have a firm grasp of numerical modeling and hydrogeologic principles.

1.1.3 Method Comparison

Of the six EPA-approved methods, CFR, analytical solutions, and numerical models were commonly used in state SWA Programs. We apply and compare them in this study. The three method types have distinctly different levels of sophistication. Table 1 shows a brief comparison of technique capabilities.

Table 1: Comparison of delineation method capabilities

	CFR	ANALYTICAL	NUMERICAL
Dimensions	1	1 to 2	1 to 3
Boundary Conditions	none	stream, barrier	several
Aquifer Material	homogeneous	homogeneous	heterogeneous
Pumping Wells	single	single	multiple
Flow Regime	steady-state (SS)	SS	SS/transient
Flow Direction	horizontal	horizontal	horizontal & vertical

Detailed investigations comparing delineation methods are limited. The EPA and state agencies acknowledge an increasing level of sophistication as one moves from fixed radius techniques to analytical solutions to numerical models. An analytical solution is often recommended to serve as a precursor to numerical modeling rather than as a stand-

alone technique (Javandel et al., 1984); the analytical solution can help to better conceptualize the flow system, which can in turn improve numerical model design and identify data requirements (Gorelick et al., 1993). But despite these acknowledgements and recommendations, quantitative comparisons of the methods are lacking.

However, several studies have examined the sensitivity of capture zones to selected parameters. These studies can be viewed as an indirect method comparison because they identify complex factors that simple methods cannot incorporate. Thus, they point out settings in which applying a simple technique is inappropriate. Recent investigations include USGS reports by Reilly and Pollock (1993, 1995) as well as Franke et al. (1998). They used MODFLOW and designed models of hypothetical systems to examine factors affecting recharge areas to wells. Each system consists of a shallow and unconfined alluvial aquifer. The aquifer receives most of its recharge from precipitation, and so recharge enters the aquifer via infiltration to the water table. The “area contributing recharge” to the well differs from a capture zone or WHPA in that the latter two may originate from regions other than the water table (Figure 5).

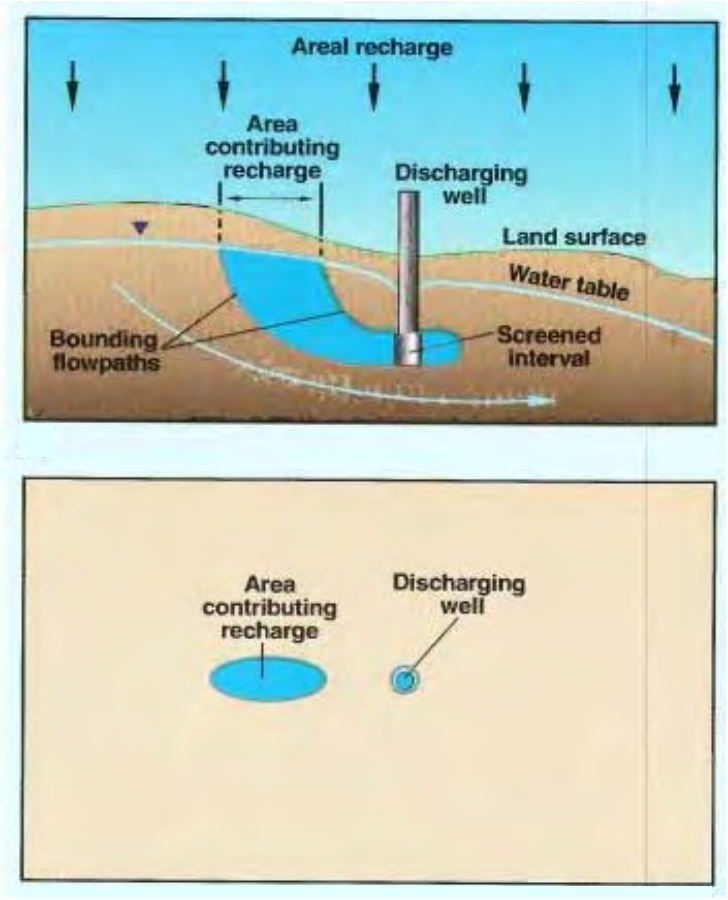

Figure 5: Area contributing recharge to a pumping well (Reilly and Pollock, 1995)

These studies stress the difficulties inherent in determining these areas due to many natural complexities that are hidden from view. Reilly and Pollock (1993) divide influential factors into two categories: 1) those dependent on the ground water system, and 2) those dependent on the well. The first category includes the hydrogeologic framework, stresses and changes in stress, system transmitting properties, and boundary conditions. The latter includes well distribution and the depth of the well's screened interval. In examining temporal changes in stress on well recharge areas, Reilly and Pollock (1995) distinguish short- and long-term changes using the ratio of the mean travel time to the stress period length. If the ratio is much larger than one, the stress is a short-term change; if less than one, it is a long-term change. Short-term cyclic (e.g., seasonal) changes were found to have little impact on sources of recharge, while long-

term cyclic and transient changes did have a large impact. The authors also note a long response time for areas of contribution when affected by long-term stresses. In other words, changes in areas lagged considerably behind changes in stress.

There have also been site-specific case studies. For example, Barlow (1997) compared delineation results of 2-D and 3-D MODFLOW models of simple and complex systems that resembled a stratified-drift aquifer on eastern Cape Cod. Previously applied analytical solutions could not account for such factors as heterogeneity, spatially variable recharge, and partially penetrating wells. Particle tracking within the numerical models revealed that, in simple settings, 2-D simulations seemed sufficient because the capture zones did not differ widely from those of the 3-D model. However, in the complex model, he found that the zones were sensitive to many factors such as those not accounted for in analytical solutions, as well as hydraulic conductivity and the ratio of horizontal to vertical hydraulic conductivity. Certain complexities, namely pond depth, conductance of the pond bottom, and vertical discretization of the model, did not have a significant influence on the delineations. Furthermore, the limitations of particle-tracking on delineation accuracy were also evaluated. It was concluded that uncertainty of boundary conditions, system stresses, and input parameters can decrease reliability of results, in addition to coarse grid discretization and lack of ample data for model calibration.

Knochenmus and Robinson (1996) had similar findings in a study of areas contributing recharge to hypothetical karst carbonate aquifers. In this case, influential factors were categorized based on how they affected the area: those affecting the size of the area included well discharge rates, effective porosity, and transmissivity; those affecting the shape and orientation of the area included carbonate fractures and well distribution. In comparison to delineations using an analytical method, it was found that the analytical method overestimated recharge areas due to its limitations, such as the inability to represent well interference, vertical gradients, and aquifer geometry.

1.2 SELECTED CAPTURE-ZONE DELINEATION METHODS

As stated in the previous section, our study applies and compares commonly-used capture-zone delineation methods. We have selected four: CFR, two analytical solutions, and a numerical model. While CFR is a unique solution, the reader should note that a variety of analytical and numerical methods exist for capture-zone delineation. The three we apply have been chosen due to their popularity among state and local agencies for use in WHP and SWA Programs.

1.2.1 CFR (Calculated Fixed Radius)

The CFR technique is fairly straightforward. The method defines the capture zone as a cylinder around the well screen. This volume is simply the amount of water in the aquifer pore space that is equal to the well's discharge. The data input and assumptions are as specified in section 1.1.2.2.

1.2.2 Analytical Solutions

Several types of analytical solutions can be used to delineate a capture zone. We apply two. The first is used in ADEC's SWA Program (ADEC, 2004), which calculates capture zones based on the UFE and Thiem equation. We therefore refer to it as the UFE-Thiem solution. The second solution is a computer model designed by the EPA to aid in state WHP Programs. It is known as WHPA.

1.2.2.1 UFE (Uniform Flow Equation)-Thiem

Like most analytical solutions, the approach is based on the superposition of a uniform flow field and the radial drawdown distribution (i.e., cone of depression) around a pumping well. The UFE (section 1.1.2.3) is used to delineate a time-independent ZOC. Because we are concerned with specific travel times, the curve must be modified so that it is time-dependent. This method truncates the curve at a distance up-gradient from the well. The distance is solved by applying Darcy's Law and the Thiem equation. The solution is described in the following paragraphs.

The Thiem equation is used to calculate radial flow around a pumping well (Fetter, 1994). The equation is applied to solve for the hydraulic head (h_2) at some distance (r_2) from the well. For unconfined aquifers, the equation is as follows:

$$h_2 = \sqrt{\left[\left(\frac{Q}{K\pi}\right)\ln\left(\frac{r_2}{r_1}\right) + h_1^2\right]} \tag{14}$$

where h_1 is the head at a known distance close to the well (r_1); the head and radius at the well (h_w, r_w) can also be used in this equation. The difference between h_2 and h_1 represents the change in water table elevation with distance from the well.

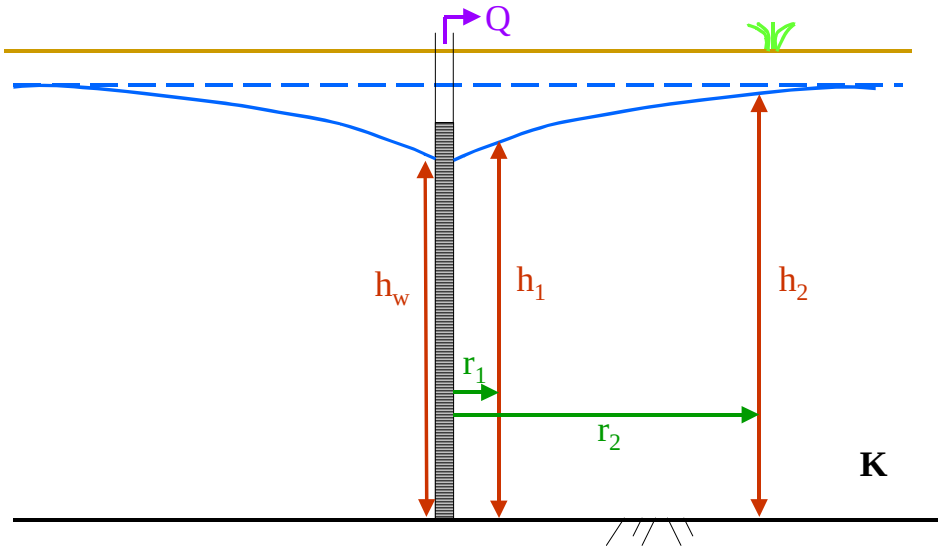

Figure 6. Cross-section of flow to a pumping well. Noted parameters are used in the Thiem equation.

The hydraulic gradient due to pumping (i_p) is measured as:

$$i_p = \frac{h_2 - h_1}{r_2 - r_1} \tag{15}$$

The average linear velocity due to pumping (v_p) is then solved using Darcy's law:

$$v_p = \frac{Ki_p}{n} \tag{16}$$

This is the velocity within the pseudo-steady state cone of depression. The average linear velocity due to the regional gradient outside of the cone of depression (v_i) is calculated in the same manner:

$$v_i = \frac{Ki_{reg}}{n} \tag{17}$$

where i_{reg} is the user-specified regional gradient. Next, ground-water travel time is found using a [time = distance/velocity] relationship. The travel time up-gradient of the well (t_{up}) is calculated as:

$$t_{up} = \frac{(r_2 - r_1)}{(v_p + v_i)} \tag{18}$$

The radius (r_2) is solved iteratively. That is, various r_2 values are used in Equations 14, 15, and 18 until a user-specified t_{up} is achieved (Braumiller, 2000). The final r_2 value is used to truncate the UFE curve, thus establishing a time-dependent capture zone (Figure 7).

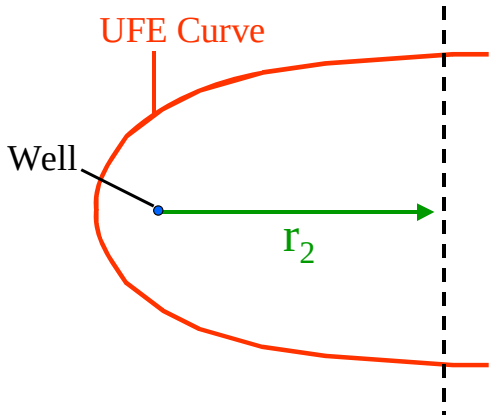

Figure 7. Illustration of the Thiem radius truncating the UFE curve based on a user-specified t_{up}.

The UFE is valid for wells that fully-penetrate a confined aquifer. Often the aquifer is unconfined and the well only partially penetrates it. Thus, certain modifications and assumptions must be made in order to apply the solution.

In unconfined settings, the total thickness of the aquifer (b) is not contributing inflow near the well due to drawdown within the aquifer. Therefore, b is invalid. The term bi (or $b(h_2-h_1)/(r_2-r_1)$ in the bounding solutions of the UFE (Equations 9 and 10) should be replaced with $(h_2^2-h_1^2)/(r_2-r_1)$, which better approximates the product of the saturated thickness and natural gradient. However, the confined equation applies under certain conditions. If the hydraulic head is approximately constant (i.e., only small gradients

exist) and is large relative to the horizontal area of concern, the confined UFE is appropriate (McWhorter and Sunada, 1977).

In 2-D analytical solutions, flow is assumed to enter a well horizontally and from the full aquifer thickness. When a well partially penetrates the aquifer, however, flow arrives from only part of the aquifer thickness and a vertical component is added near the well. Anisotropy may be influential if the vertical hydraulic conductivity (K_v) differs significantly from the horizontal hydraulic conductivity (K_h). Effects of partial penetration are considered influential over a horizontal distance equal to$1.5b\sqrt{K_h/K_v}$ (Hantush, 1961).

To account for effects of partial penetration near the well, an effective aquifer thickness, B_{eff}, replaces b in the UFE:

$$B_{eff} = \frac{(b+l)r_{pp}}{2r_2} + \frac{(r_2 - r_{pp})b}{r_2} \qquad \text{if } r_{pp}<r_2 \qquad (19)$$

where l is the well-screen length and r_{pp} is the distance past which the effects of partial penetration become negligible ($1.5b\sqrt{K_h/K_v}$).B_{eff} calculates the aquifer thickness as a weighted average of b and l. For cases where $r_{pp} < r_2$, between the well and r_{pp}, the average aquifer thickness is the arithmetic average of the total aquifer thickness (b) and the well screen (l). This average is multiplied by the ratio of the distance (r_{pp}) to the total distance (r_2), thus yielding the first half of Equation 19. At the distance where partial penetration effects become negligible ($r>r_{pp}$), flow to the well is derived from the total aquifer thickness (Figure 8). Therefore, b is multiplied by the ratio of (r_2-r_{pp}) to r_2, which yields the second half of Equation 19 (Braumiller, 2004).

If $r_2 < r_{pp}$, and the effects of partial penetration do impact flow to the well, B_{eff} is computed as:

$$B_{eff} = l + \frac{(b-l)r_2}{r_{pp}} \qquad \text{if } r_{pp}>r_2 \qquad (20)$$

In this case, B_{eff} is equal to the well screen plus the section of remaining thickness (b-l) that is proportional to r_2/r_{pp}.

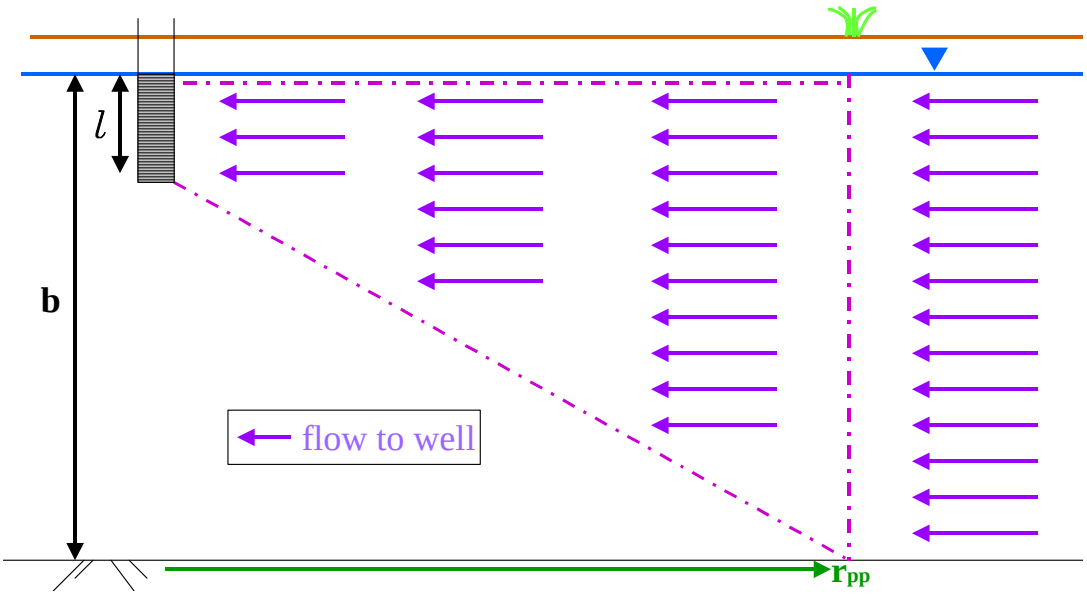

Figure 8. Diagram of measurements used to calculate B_{eff} in cases of partial penetration.

ADEC acknowledges that the method is not capable of producing a capture zone with complete accuracy due to simplifying assumptions. To avoid underestimating the actual capture zone, they take several measures to produce a more conservative delineation (Rygh, 2003-2004). One example is a 'safety factor' that is applied to the zone's bounding parameters (e.g., x_{sp}, y_{max}, section 1.1.2.3). Each parameter is multiplied by a factor ranging from 1.5 to 2.5 (Braumiller, 2000). The resulting SWA area is significantly larger than the original delineation.

In our study, we apply only the analytical solution described above. Therefore, our delineations are significantly smaller than those that would result from using ADEC's full methodology. This is of particular importance for our field case on Fort Wainwright; our results should not be equated with ADEC's delineation of the same well.

1.2.2.2 WHPA (Wellhead Protection Area)

WHPA is an outgrowth of the WHP Program (section 1.1.1). It was designed by the EPA to aid state agencies with the delineation of Wellhead Protection Areas (WHPAs), hence the name. To date, many states have applied the method in their WHP and SWA Programs.

WHPA is a modular analytical code. Of the four that exist, we apply the most commonly used module to delineate capture zones. It is known as the Multiple-Well Capture Zone Module (MWCAP) (Blandford and Huyakorn, 1991). MWCAP relies on the same principles of superposition as the previous analytical solution (section 1.2.2.1), in which the UFE defines the flow field. An added feature is the capability to model stream and barrier boundaries using image-well theory. Both boundary types are simulated as an infinite line that fully penetrates the aquifer. The user specifies the line's orientation and perpendicular distance from the well. Due to the two-dimensional steady-state nature of the solution, stream boundaries are assumed to always act as sources rather than sinks. Barrier boundaries will be discussed further in sections 2.1.4 and 2.2.4.

WHPA also differs from the previous solution in the way it determines capture zone boundaries. Rather than truncate the UFE curve at a calculated up-gradient distance, MWCAP uses particle tracking. Particle tracking traces the movement of imaginary particles within a ground-water flow field (Anderson and Woessner, 1992). The path of each particle forms a pathline, which is equivalent to a streamline in the case of 2-D steady-state flow. The term 'particle' is used for conceptual purposes; each is infinitely small and represents a molecule of water or conservative tracer.

Streamlines are traced by computing the average linear velocity distribution. Particles are tracked along streamlines by finding the distance traversed in a given time. The differential equation is as follows:

$$\frac{dx}{dt} = v_x \tag{21}$$

The equation is solved through integration. WHPA uses Euler integration to delineate a particle path from one point (x_i) to another (x_{i+1}) by approximating dt by a finite time step (Δt) and dx by a finite length increment (Δx):

$$x_{i+1} = x_i + \Delta x = x_i + v_x \Delta t \quad (22)$$

Equations 21 and 22 are applied in the y direction as well. Tracking continues until the particle either reaches a discharge point or the user-specified TOT is reached (Blandford and Huyakorn, 1991). Figure 9 illustrates a typical WHPA delineation.

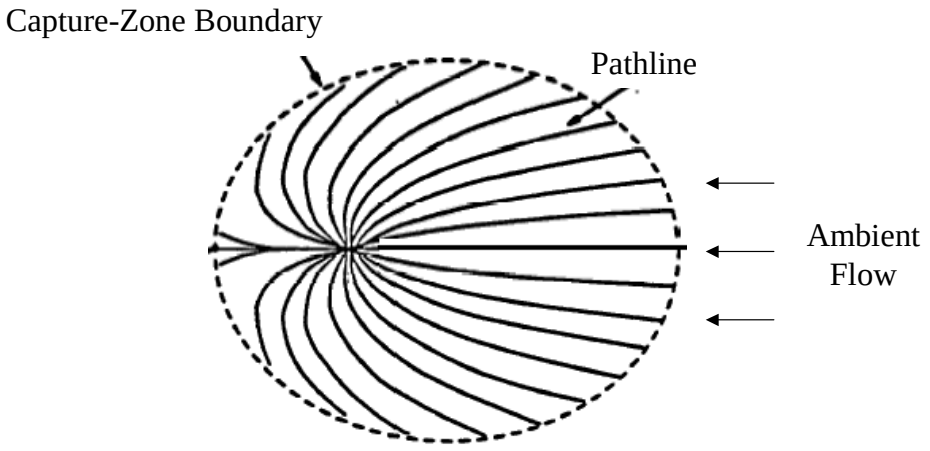

Figure 9. Example of WHPA capture-zone delineation (Modified from Blandford and Huyakorn, 1991).

1.2.3 Numerical Model

Section 1.1.2.6 provides a brief introduction to numerical modeling. We are using MODFLOW-2000, a USGS three-dimensional ground-water flow model (McDonald and Harbaugh, 1988). The model code is written in FORTRAN and divides input data into modules known as packages. The core packages (i.e., those common to all models) contain information on initial and boundary conditions, spatial and temporal discretization, the matrix solver, and hydraulic properties of the aquifer. Optional packages incorporate data on any sources or stresses to the system, such as wells, surface water, and recharge. Pre-processors are often used to assemble the input data. A USGS pre-processor, MFI2K, is used in this study.

Selection of boundary conditions is a key step in model design because they significantly control the flow pattern. A boundary condition is a mathematical statement specifing the head or flux at the boundaries of the model domain (Anderson and

Woessner, 1992). Three types of mathematical conditions represent boundaries in a ground-water flow model: specified-head, specified-flow, and head-dependent flow. Hydraulic boundaries may coincide with physical boundaries such as impermeable rock. Elsewhere, invisible boundaries, known as hydraulic boundaries, define a hydrologic flow condition (e.g., drainage divides). If there are no natural flow boundaries within the study area, artificial boundaries can be induced, or the model extents must be distant enough to not be impacted by stresses simulated in the system.

MODFLOW is capable of temporally and spatially discretizing a ground-water flow model. Our simulations are all steady-state (i.e., constant head and storage with time), and so temporal discretization is not discussed here. Spatially, the aquifer system is discretized into rectangular cells that form a three-dimensional grid. The grid consists of horizontal rows and columns and vertical layers. Each cell is assumed to have uniform properties. According to MODFLOW's block-centered finite-difference method, the hydraulic-head node lies at the center of the cell. As noted in section 1.1.2.6, a series of algebraic equations is created from the governing differential equation. Their solution is the array of nodal head values that simultaneously satisfies all cells. The equations are usually solved through an iterative process. That is, they are approximated and solved repeatedly until the solution converges to the original system of equations. Each iteration generates an intermediate solution that updates the modified equations for the next iteration. Convergence is measured by checking that the maximum head change between iterations is less than a user-specified limit (USGS, 2003). Once the convergence criterion has been met and all heads are computed, MODFLOW calculates the derivatives to determine cell-by-cell flow terms.

Calibration typically follows the first error-free execution of a numerical model. The goal is to simulate heads and flows that closely resemble field observations (Anderson and Woessner, 1992). During the process, parameter and stress values that approximate field heads and flows are determined. The process is known as solving the inverse problem. That is, head information is used to solve for parameter and stress values, where as parameter and stress values are used to calculate heads in the forward problem.

Calibration is performed by either trial-and-error or an automated estimation code. MODFLOW also provides a sensitivity analysis package to determine the effect of parameter uncertainty on the model.

In order to delineate capture zones, we use MODPATH (referred to in figures and tables as MPATH), a particle-tracking program within MODFLOW. The code is semi-analytical. In a solution created by Pollock (1994), a linear interpolation for the seepage velocity is used to find particle travel paths and times. Velocity components between cells are determined by the head distribution produced by MODFLOW. In the x direction, the average linear velocity (v_x) is computed by dividing the volumetric flow rate through a cell face (Q_x) by the face's cross-sectional area ($\Delta y \Delta z$) and the porosity of the cell material (n):

$$v_x = \frac{Q_x}{n\Delta y \Delta z} \tag{23}$$

The flow rate (Q_x) is calculated from the head distribution at cell nodes (Pollock, 1994). This formula is applied in the y direction as well. The particle will exit the cell face that requires the shortest travel time. Figure 10 provides an illustration. Within cells, an interpolation scheme is required to calculate velocities since head values are known only at discrete points (cell nodes) in the grid. This intra-cell velocity distribution is solved analytically as in the WHPA code (section 1.2.2.2).

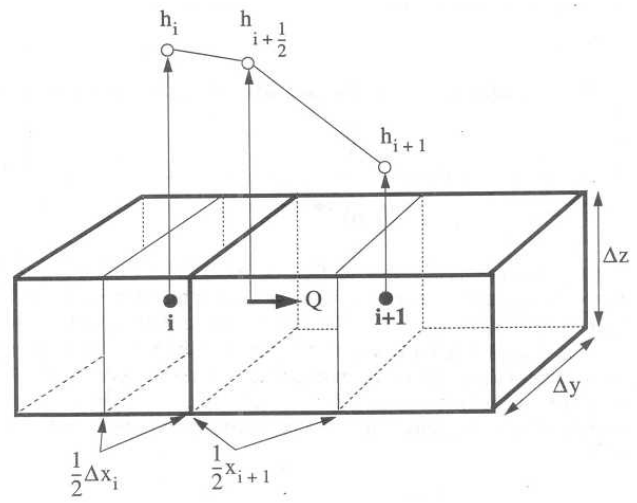

Figure 10: Block-centered flow in a finite-difference grid (Pollock, 1994). Particles are tracked in MODPATH according to the head gradient.

We run MODPATH in backward-tracking mode, in which particles begin at the well's cell and trace flow paths in reverse. For steady-state simulations, MODPATH offers two output modes: pathline and endpoint. A pathline analysis tracks the coordinates along the path of each particle by recording the location of each cell through which it passes. In contrast, an endpoint analysis records only the end locations; in backward-tracking mode, the end locations are where particles begin.

1.2.4 Plotting Techniques

We plot the capture-zone delineations in AutoCAD. The plots depict the capture zones in 2-D plan view; as such, we refer to them as 'capture areas'. For CFR, a simple circle is drawn. For UFE-Thiem, we use the UFE (Equation 2, section 1.1.2.3) to compute points along the ZOC boundary. An open curve is drawn in AutoCAD that traces these points. The curve is then truncated at the radius that was calculated from the Thiem equation. The WHPA delineation is plotted in a similar fashion: the WHPA model outputs a series of points for the capture-zone boundary. The points are read into AutoCAD to draw a closed curve. Likewise, for the numerical delineation, we plot the pathlines and endpoints produced by MODPATH and trace the capture-area limits.

2 SYNTHETIC CASE STUDIES

Section 2 focuses on capture-zone delineations of wells in hypothetical case studies. Hydrogeologic complexity increases with each case. Our objectives were as follows:

1) for each case, compare differences in the size and shape among the four capture areas; and
2) identify the method assumptions that create these differences

For Case 1, we designed a conceptual model representing an unrealistically simple aquifer. We begin by reviewing the conceptual model. We define boundary conditions, hydraulic properties, and pumping conditions. We also outline MODFLOW specifications. We cumulatively add complexity to the hydrologic system in Cases 2-4. The four delineation methods are applied to each case, and resulting capture zones are compared. Finally, we examine the effects of simplifying assumptions on each method's results.

2.1 CASE DESCRIPTIONS

2.1.1 Case 1: Simple

We first build a conceptual model of our aquifer. This is one of the first steps to understanding the ground-water flow system. The aim of a conceptual model is often to match the field problem in order to design a mathematical model that accurately predicts system behavior (section 3.3.2). Since our case studies are synthetic, a field system does not exist. However, our present goal is not to predict flow within a field problem, but rather to analyze flow and how it is impacted by system modifications.

Case 1 is a very simple representation of an alluvial floodplain (Figure 11). It can be likened to a homogeneous sandbox. The aquifer is unconfined and isotropic. The domain is 10x20 miles (mi) in area and 510 feet (ft) thick. East-West trending mountain ranges form ground-water divides along the northern and southern limits. Reservoirs exist at both the eastern and western boundaries of the domain. Beneath the aquifer lies impermeable bedrock. The water table slopes to the west at 4 feet/mile. We assume recharge from precipitation is negligible. There is one water-supply well, located in the

center of the model. It is screened between 160 and 180 feet below ground surface (fbgs), with a pumping rate of 2500 gallons per minute (gpm).

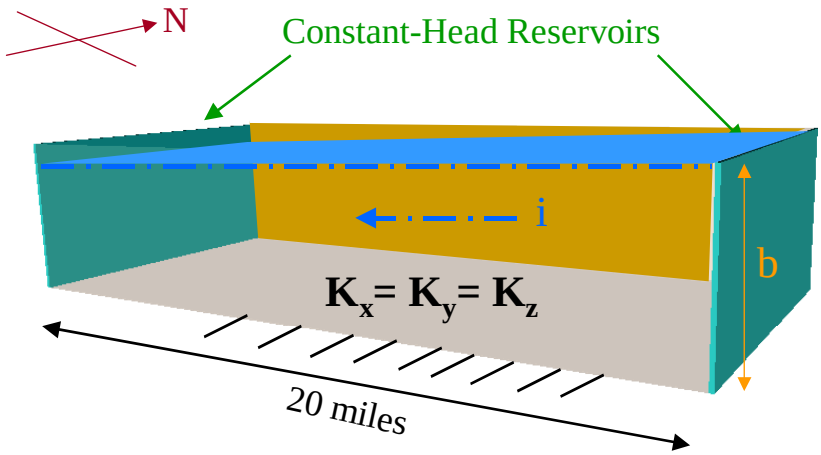

Figure 11. Case 1 conceptual model.

Table 2 contains input parameters required by each method, while Table 3 lists parameter values for each case. Note in Table 3 that one parameter value is changed per case (highlighted in red) and is held constant for the following cases. Also note that ten-year capture zones are delineated in all cases. We selected a ten-year time frame due to its commonality among state SWA Programs. Many SWA Programs delineate multiple capture zones with different travel times, which range from months to 20 years.

Table 2: Comparison of case-study parameters for selected delineation methods.

Case Parameters	symbol	CFR	WHPA	UFE-Thiem	MPATH
well discharge	Q	X	X	X	X
horizontal hydraulic conductivity	K_h		X	X	X
regional hydraulic gradient	I		X	X	
aquifer thickness	b		X	X	X
time of travel	TOT	X	X	X	X
flow direction	α		X	X	
vertical hydraulic conductivity	K_v			X	X
porosity	n	X	X	X	X
well-screen thickness	*l*	X		X	
head at well	h_w			X	
well radius	r_w			X	
MODFLOW grid discretization					X
MODFLOW cell-by-cell flows & heads					X

Table 3: Case-Study Input Parameters. Modifications to Case 1 are highlighted in red.

Case Parameters	Symbol	Unit	Case 1	Case 2	Case 3	Case 4
well discharge	Q	gpm	2500	833 X 3	833 X 3	833 X 3
horizontal hydraulic conductivity	K_h	ft/d	200	200	200	200
	K_{low}	ft/d	--	--	--	2
regional hydraulic gradient	I	ft/mi	4	4	4	4
aquifer thickness	b	ft	510	510	510	510
time of travel	TOT	yr	10	10	10	10
flow direction	α	degrees	0	0	0	0
vertical hydraulic conductivity	K_v	ft/d	200	200	2	2
porosity	n	--	0.3	0.3	0.3	0.3
well-screen thickness	*l*	ft	20	20	20	20
average head at well(s)[2]	h_w	ft	453.1	456.3	456.9	453.1
well radius	r_w	ft	1	1	1	1

[1]input for WHPA; due West is set to 0 degrees
[2]input for UFE-Thiem solution; head at the well's cell in MODFLOW is used as h_w

2.1.1.1 Numerical Model Specifications

Our MODFLOW model was designed to best represent the conceptual aquifer. The domain is 10x20 miles and 510 feet thick. A pumping well was placed in the center of the model grid. The grid is divided vertically into 5 layers (Figure 12); the layer containing the well is 20 feet thick to represent the screened interval. The grid is horizontally discretized into 123 rows and 233 columns, with most cells 500x500 feet. However, the dimensions of a cluster of cells surrounding the well were fined (125x125 feet), with the goal of obtaining a finer resolution of the head distribution and flow field around the well. Figure 12 illustrates the entire grid and Figure 13 shows a close-up view of the finer cells around the well.

Physical and hydraulic boundaries must be represented mathematically in the model (section 1.2.3). To represent the reservoirs at the model's eastern and western limits, we assign fully-penetrating, specified-head boundaries. The eastern- and western-most columns are respectively set to 500 and 420 feet above sea level (asl) to ensure a 4 feet/mile hydraulic gradient. The rest of the model boundaries are specified-flow. For instance, the bedrock underlying the aquifer is assumed impermeable and considered a no-flow boundary. Likewise, the ground-water divides to the north and south are set as no-flow boundaries. Lastly, the top of the model represents the interface between the vadose and saturated zones, to which we could potentially apply recharge. However, because we are assuming recharge is negligible, the top surface is also a no-flow boundary.

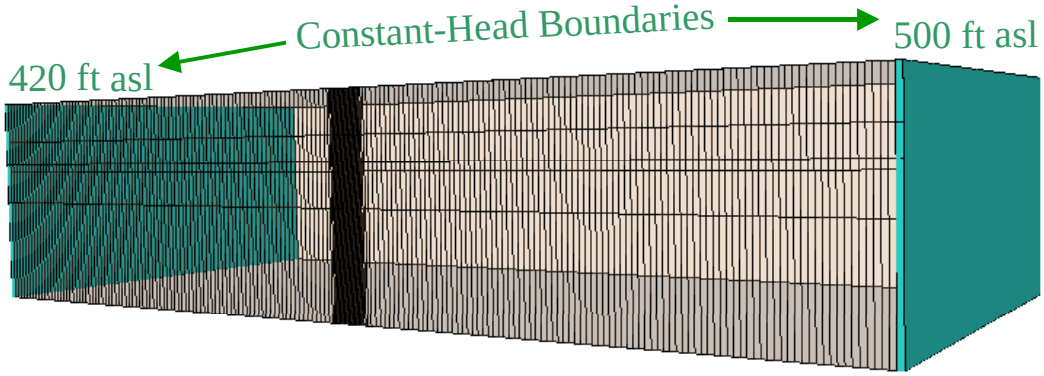

Figure 12. Numerical model of Case 1. Vertical Exaggeration 20X.

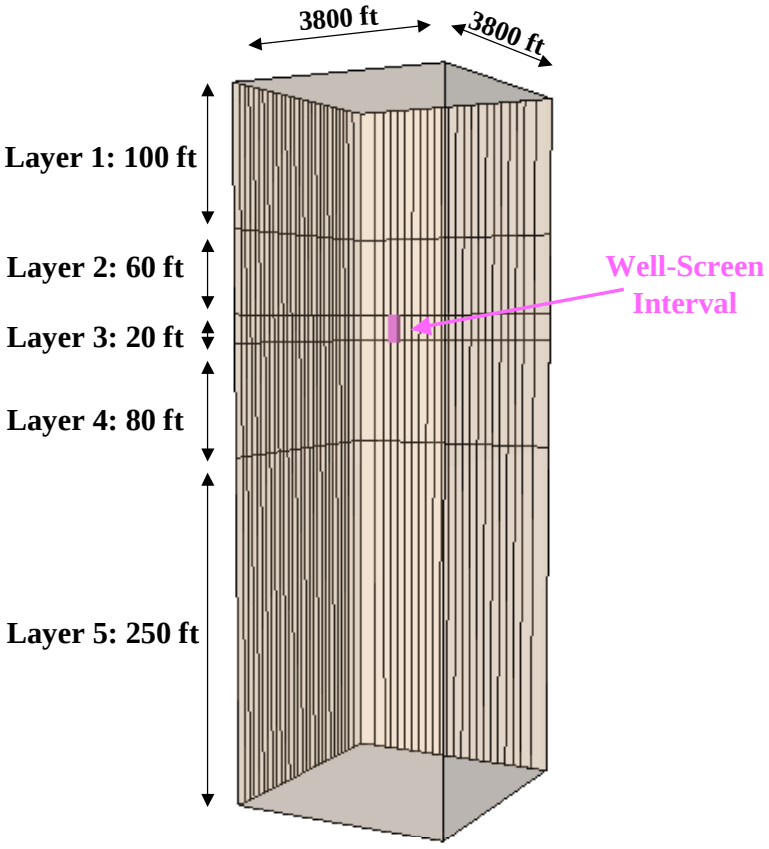

Figure 13. Close-up of well vicinity. Vertical exaggeration 20X.

Due to the simplicity of Case 1, relatively few method assumptions are violated. For example, the assumptions of homogeneity and steady-state flow are valid because such conditions exist within our conceptual model. Table 4 lists the assumptions of each method that are violated by the Case 1 conceptual design. Note that UFE-Thiem does not assume a fully-penetrating well (as described in section 1.2.2.1), and that the numerical model makes no assumptions that conflict with the conceptual model.

Table 4. Invalid assumptions in Case 1.

Assumption	CFR	UFE-Thiem	WHPA	MPATH
Fully-penetrating well	X		X	
Horizontally infinite aquifer	X	X	X	
1- or 2-Dimensional flow	1	2	2	

2.1.2 Case 2: Multiple Wells

The second case features multiple wells in close proximity (i.e., within 2/3 mile of each other). The original well is removed and replaced with three wells. The cumulative pumping rate of these wells equals that of the original well. Figure 14 and Figure 15 show well locations in the MODFLOW grid for Case 1 and Case 2, respectively. In cross-section, they are located at the same depth (160-180 fbgs). Table 3 lists input parameters for each of the delineation methods.

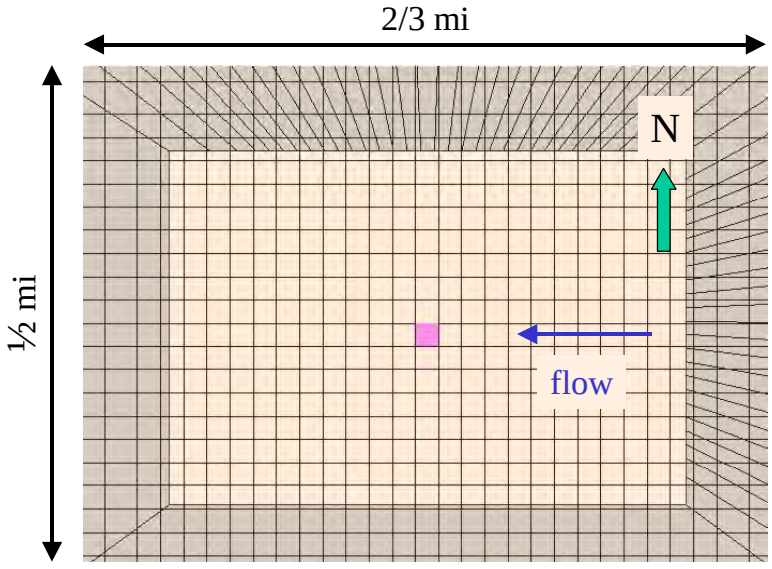

Figure 14. Close-up plan view of well in MODFLOW grid for Case 1.

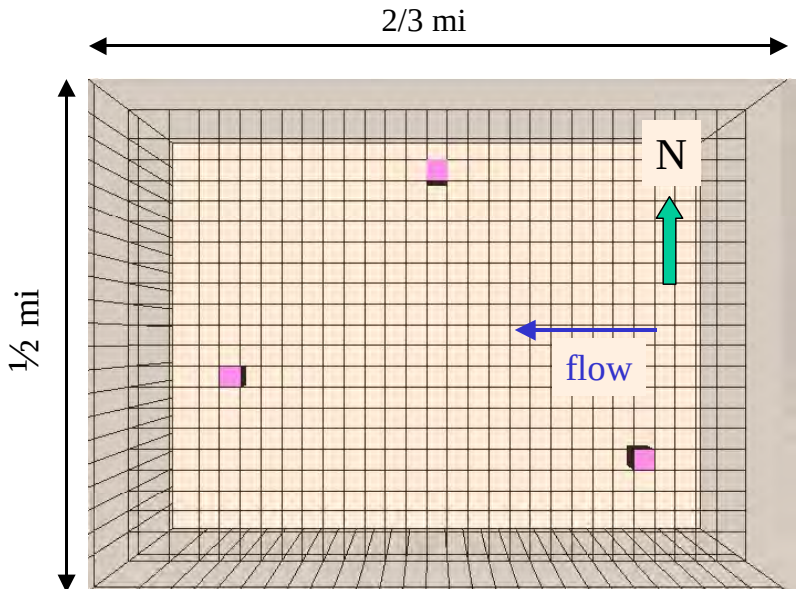

Figure 15. Close-up plan view of wells in MODFLOW grid for Case 2.

Table 5 lists assumptions that are not valid for our Case 2 conceptual model. Note that MODPATH is the only method that can account for well interference.

Table 5. Invalid assumptions in Case 2.

Assumption	CFR	UFE-Thiem	WHPA	MPATH
Fully-penetrating well	X		X	
Horizontally infinite aquifer	X	X	X	
1- or 2-Dimensional flow	1	2	2	
Negligible well interference	X	X	X	

2.1.3 Case 3: Anisotropy

Case 3 modifies Case 2 by adding vertical anisotropy. The vertical hydraulic conductivity (K_v) is set to one-hundreth of the horizontal hydraulic conductivity (K_h). With K_h equal to 200 feet/day, K_v becomes 2 feet/day. Table 3 contains input parameters for Case 3.

Table 6 lists simplifying assumptions that are violated in Case 3. As the table indicates, anisotropy cannot be accounted for in CFR and WHPA. In the UFE-Thiem solution, the anisotropy ratio is used to find the maximum radius of influence of partial

penetration (r_{pp}); r_{pp} is then factored into the effective aquifer thickness, or B_{eff} (section 1.2.2.1), which is inversely proportional to the capture zone bounding parameters (x_{sp}, and y_{max}). In MODFLOW, vertical anisotropy is directly simulated. Vertical anisotropy affects inter-layer flow only. That is, vertical flow within a layer is a function of K_h, while vertical flow between layers is a function of K_v.

Table 6. Invalid assumptions in Case 3.

Assumption	CFR	UFE-Thiem	WHPA	MPATH
Fully-penetrating well	X		X	
Horizontally infinite aquifer	X	X	X	
1- or 2-Dimensional flow	1	2	2	
Negligible well interference	X	X	X	
Isotropy	X		X	

2.1.4 Case 4: Heterogeneity

Lastly, Case 4 includes heterogeneity. A volume of lower hydraulic conductivity (low-K) is added near the three pumping wells (Figure 16). The horizontal hydraulic conductivity of this volume (K_{low}) is two orders of magnitude less than the original value (K_h). Conceptually, the volume represents a less-permeable formation within the alluvial aquifer, possibly an igneous intrusion. It meets the aquifer floor at an angle and extends through the entire aquifer thickness. It spans approximately one mile in diameter.

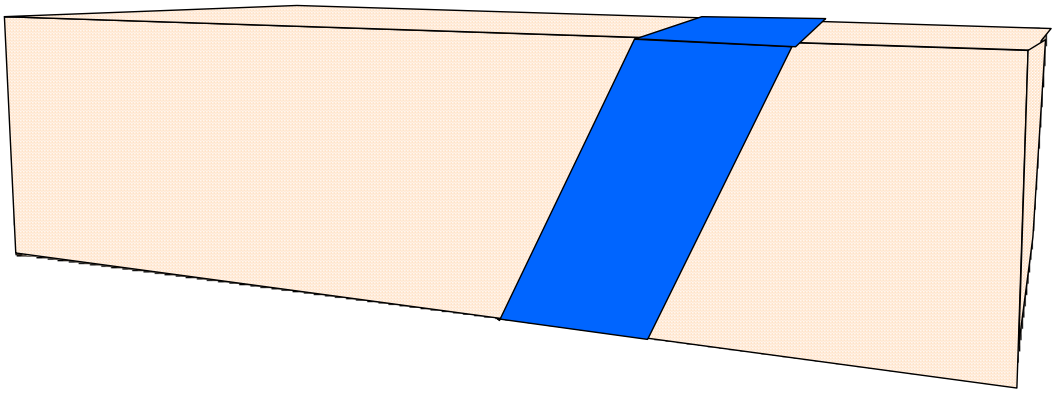

Figure 16. Cropped cross-section of Case 4 showing low-K zone.

Since heterogeneity cannot be incorporated into CFR or UFE-Thiem, their solutions are identical to Case 3. In WHPA, heterogeneity likewise cannot be represented within

the aquifer. However, as noted in section 1.2.2.2, it is possible to simulate a 2-D flow barrier. The barrier is simulated as an infinite line. We place a line in the model where the block is nearest the wells at land surface. The line lies 500 feet from the nearest well and runs North to South (Figure 17).

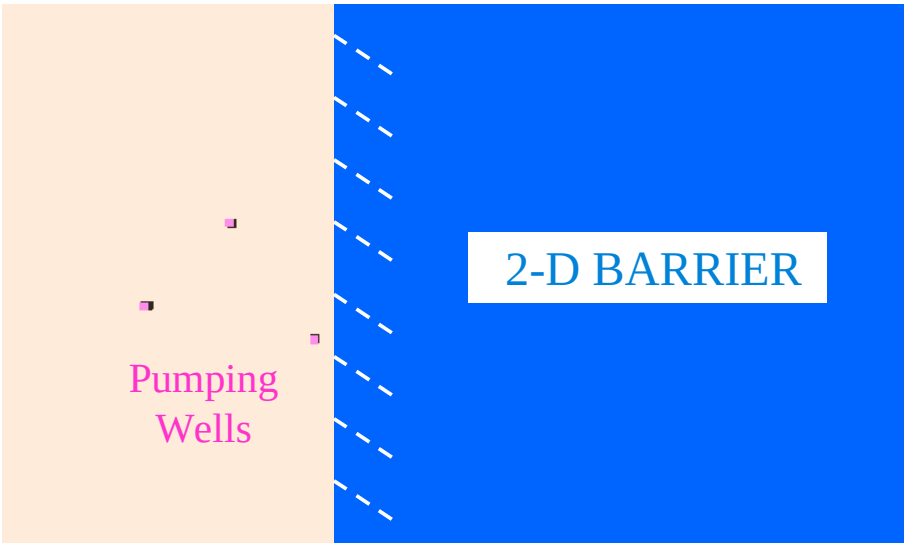

Figure 17. Plan view of Case 4 well vicinity. The low-K zone is shown as it is represented in WHPA.

MODFLOW allows a more detailed representation of the low-K zone. We insert a block of low-K cells to represent the formation. As shown in Figure 18, the low-K cells move westward with depth until they are beneath the well field.

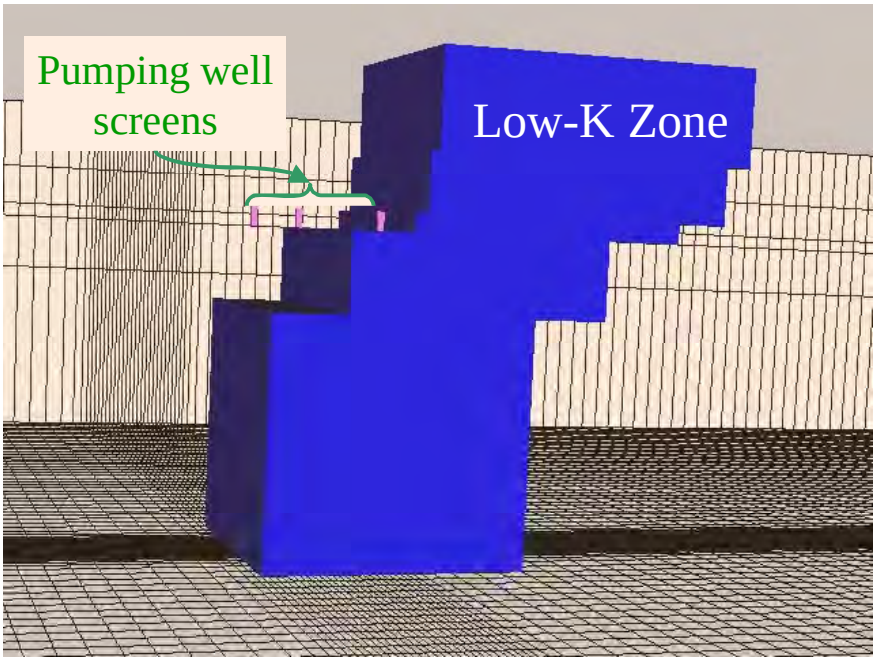

Figure 18. Low-K zone as simulated in MODFLOW.

Table 7 lists the assumptions that are not valid in Case 4. Homogeneity has been added to the list, and MODPATH is the only method that does not assume a homogeneous aquifer. Note that WHPA assumes homogeneity despite its ability to represent a barrier. Because it is a 2-D no-flow boundary condition, it does not represent homogeneity; rather, it sets a finite limit to the aquifer. Thus, WHPA no longer assumes a horizontally finite aquifer.

Table 7. Invalid assumptions in Case 4.

Assumption	CFR	UFE-Thiem	WHPA	MPATH
Fully-penetrating well	X		X	
Horizontally infinite aquifer	X	X		
1- or 2-Dimensional flow	1	2	2	
Negligible well interference	X	X	X	
Isotropy	X		X	
Homogeneity	X	X	X	

2.2 CASE-STUDY DELINEATION RESULTS AND COMPARISONS

This section presents our capture-zone delineation results and compares them. Since three of the four methods are not 3-dimensional, we compare capture zones in plan view,

which we refer to as 'capture areas.' Table 8 lists the capture areas for all cases. It also shows how the total area-per-method was calculated in cases with multiple wells (Cases 2-4): the overlapping areas were subtracted from the cumulative area to obtain a net capture area. We use these net areas in our comparisons.

Table 8. Delineation areas for all case studies. Units are in square miles.

	Well1	Well2	Well3	Sum of Areas	Overlap[1]	% Overlap	Total Area (Sum-Overlap)
CASE 1							
CFR	**10.50**	--	--	--	--	--	--
UFE-Thiem	**1.05**	--	--	--	--	--	--
WHPA	**0.41**	--	--	--	--	--	--
MPATH	**0.40**	--	--	--	--	--	--
CASE 2							
CFR	**3.50**	**3.50**	**3.50**	**10.50**	**5.66**	**53.92%**	**4.84**
UFE-Thiem	**0.24**	**0.24**	**0.24**	**0.73**	**0.12**	**16.26%**	**0.61**
WHPA	**0.14**	**0.14**	**0.14**	**0.41**	**0.04**	**8.77%**	**0.37**
MPATH	**0.15**	**0.15**	**0.15**	**0.45**	**0.00**	**0.00%**	**0.45**
CASE 3							
CFR	**3.50**	**3.50**	**3.50**	**10.50**	**5.66**	**53.92%**	**4.84**
UFE-Thiem	**0.42**	**0.42**	**0.42**	**1.25**	**0.33**	**26.29%**	**0.92**
WHPA	**0.14**	**0.14**	**0.14**	**0.41**	**0.04**	**8.77%**	**0.37**
MPATH	**0.30**	**0.37**	**0.33**	**1.00**	**0.08**	**7.53%**	**0.92**
CASE 4							
CFR	**3.50**	**3.50**	**3.50**	**10.50**	**5.66**	**53.92%**	**4.84**
UFE-Thiem	**0.42**	**0.42**	**0.42**	**1.25**	**0.33**	**26.29%**	**0.92**
WHPA	**0.11**	**0.14**	**0.04**	**0.29**	**0.02**	**5.30%**	**0.27**
MPATH	**0.36**	**0.37**	**0.39**	**1.12**	**0.05**	**4.17%**	**1.07**

[1]Signifies overlap of the 3 wells' capture areas within a single method

In the subsequent analyses, we assume the MODPATH delineations most closely represent the true capture area. We make this assumption in order to compare the relative accuracy of the other methods. For instance, we break down each method's area into three parts:

1) the percent shared with the MODPATH delineation, calculated as:

$$SHARED = \frac{common\_area}{method\_area} \times 100 \tag{24}$$

where *common_area* is the area shared by MODPATH and the simpler method (CFR, UFE-Thiem, or WHPA), and *method_area* is the total area of the simpler method;

2) the percent outside of MODPATH's area, which we refer to as the 'extra' area, calculated as:

$$EXTRA = (1 - SHARED) \times 100 \quad (25)$$

3) the percent of the MODPATH delineation outside of the simpler method's area, which we call the 'missed' area, calculated as:

$$MISSED = \frac{MPATH - common\_area}{MPATH} \times 100 \quad (26)$$

where *MPATH* is the total area of the MODPATH delineation.

Note that 1) and 2) comprise 100% of the simpler method's area; the third component is a measure of MODPATH's area. In the comparison charts, it is denoted as a negative percentage. Figure 19 illustrates the area divisions. After analyzing the results by case, we then review the cases by method to better examine the effects of complexity on each method's delineation.

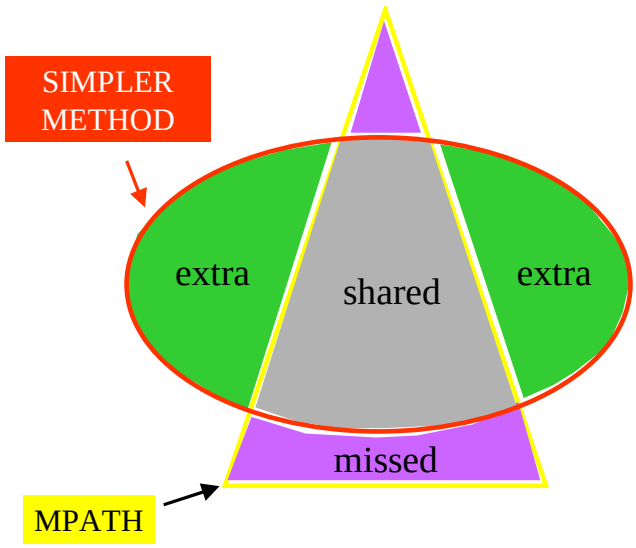

Figure 19. Illustration of percent-area divisions in our delineation comparisons.

2.2.1 Case 1

As stated in section 2.1.1, Case 1 consists of a single well in a homogeneous and isotropic aquifer. Figure 20 shows the four delineations in plan view. Figure 21 displays the total area per method.

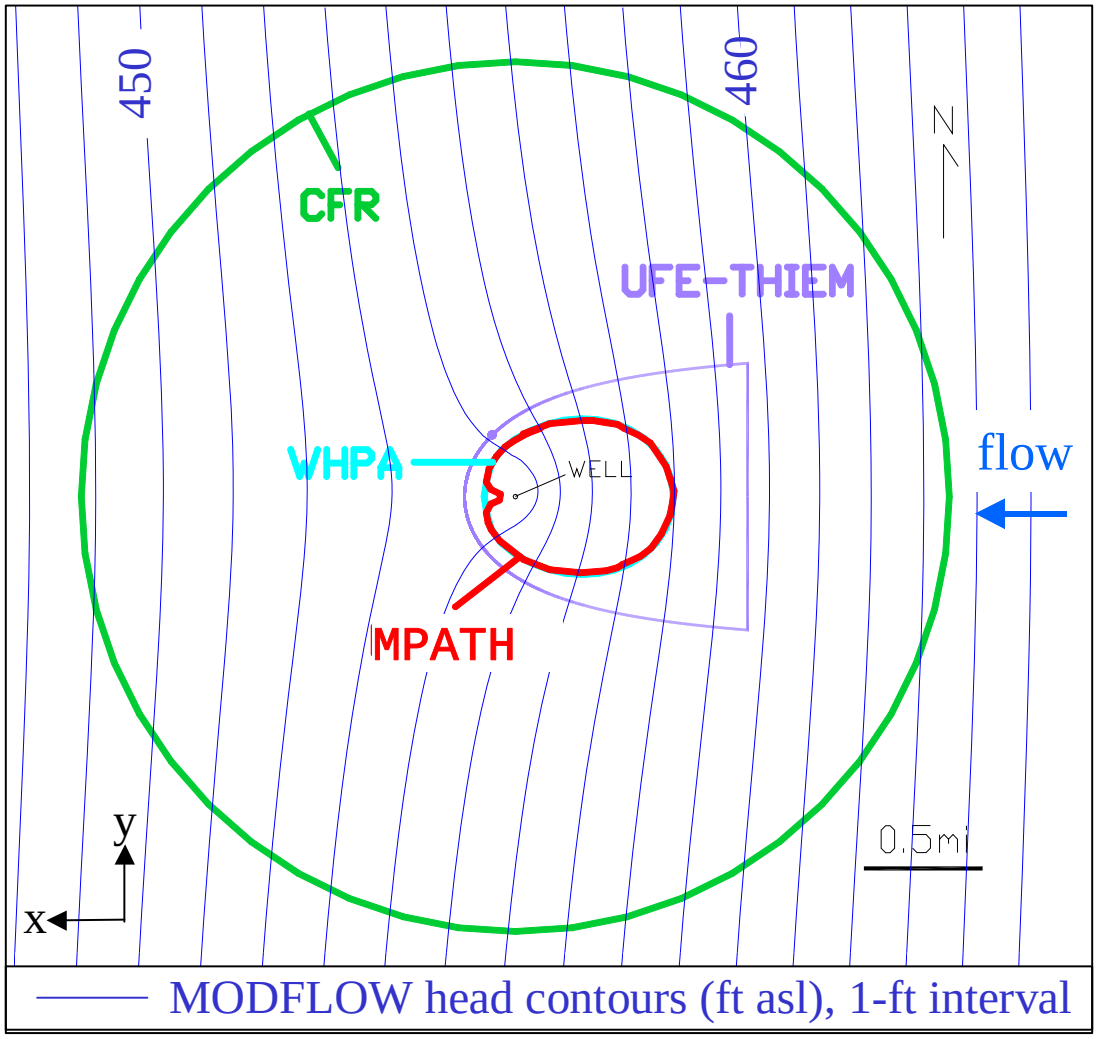

Figure 20. Case 1 capture areas, plan view.

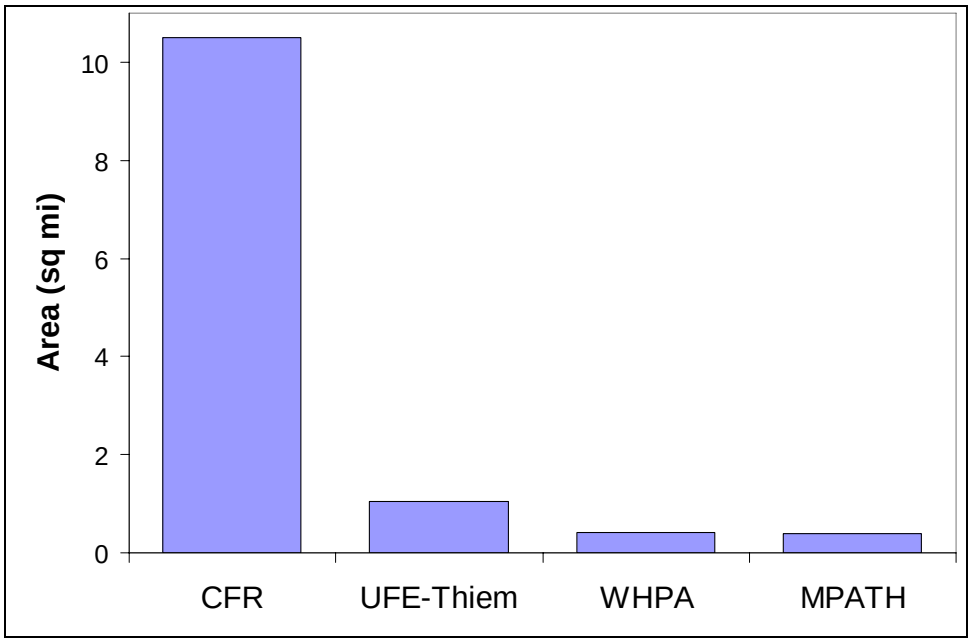

Figure 21. Total capture area per method in Case 1.

Figure 20 illustrates that the CFR delineation is a gross overestimation of the capture area. Its delineation is more than an order of magnitude larger than MODPATH results. This is primarily due to CFR's assumption of no regional gradient. Its circular shape encompasses a large amount of area that is not up-gradient of the well.

Although less dramatic, the UFE-Thiem overestimate is also significant. Figure 22 shows that 62% of its area is considered extra; that is, more than half lies outside of the MODPATH delineation. This comparison indicates that the method is conservative under the simple Case 1 conditions.

In contrast, the WHPA area matches that of MODPATH almost exactly. Figure 22 shows over 97% of its capture area is shared with MODPATH, and none of the MODPATH area is missed. This demonstrates WHPA's ability to produce accurate results in a case where nearly all of its simplifying assumptions are valid.

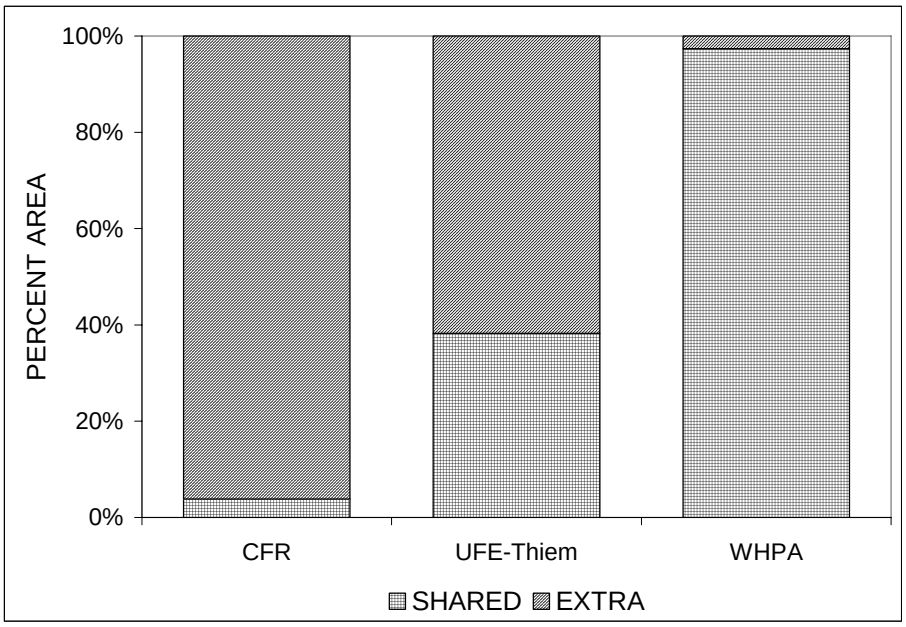

Figure 22. Comparison of CFR, UFE-Thiem, and WHPA delineations to MODPATH results in Case 1.

2.2.2 Case 2

In Case 2, the single well is replaced with three distributed wells. The pumping rate of each well is 1/3 of the Case 1 well. Figure 23 shows the capture areas of the four methods. In Figure 24, the combined areas of the three wells are outlined to show the net area covered by each method.

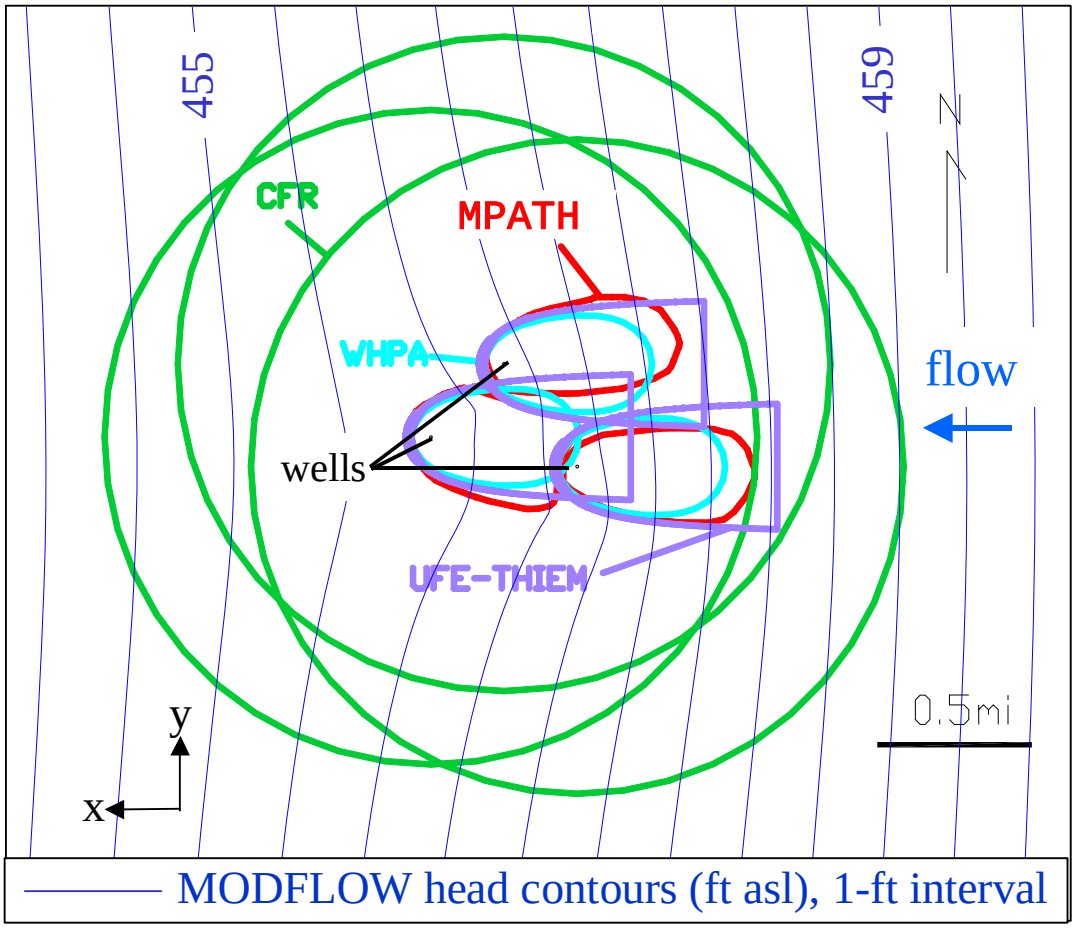

Figure 23. Case 2 capture areas, plan view.

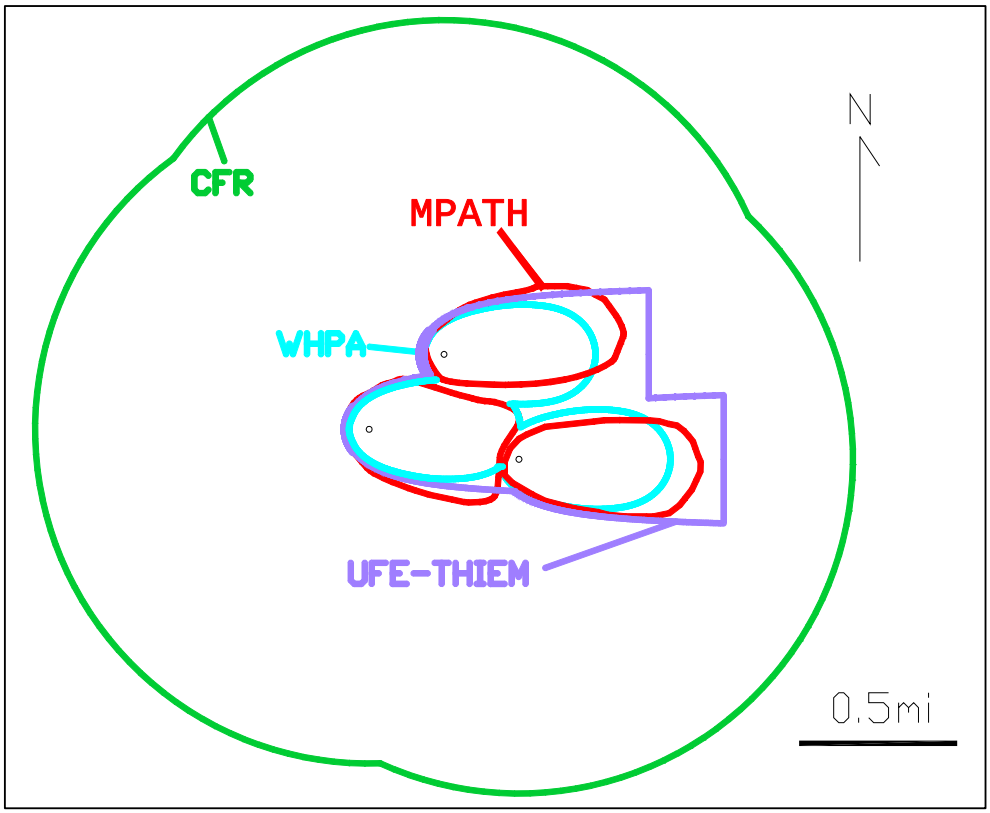

Figure 24. Outline of net capture areas for Case 2.

Note the slight lateral movement of capture-zone boundaries in the MODPATH delineation, whereas the WHPA and UFE zones remain parallel with the flow direction (East-West). This illustrates MODPATH's ability to account for well interference. Multiple discharging wells in close proximity cause the wells to draw recharge from the same aquifer volume. If a well's radius of influence intersects that of another well, the net drawdown between the wells is greater than if they were operating independently (Figure 25). As a result, each well's cone of depression expands away from the shared recharge volume. MODPATH's delineation shows the capture area location moving out laterally and extending farther up-gradient in comparison to the other delineations, in which well interference is assumed negligible. The effect of well interference is also demonstrated in the percent of overlap between the three capture areas for each method (Table 8): the percent is lowest for MODPATH in all cases.

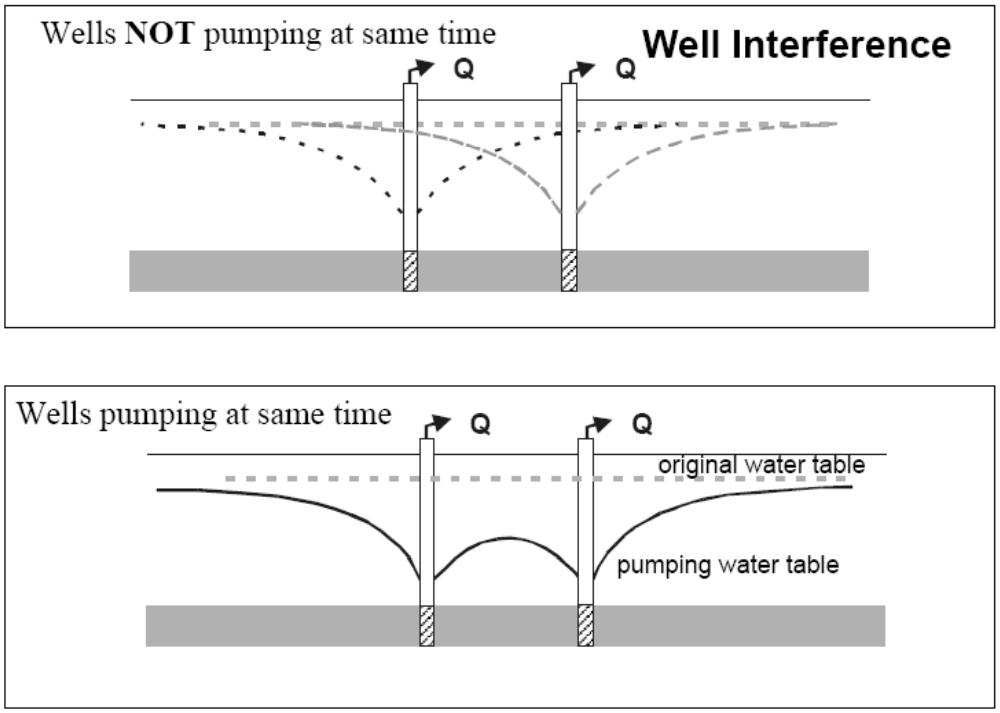

Figure 25. Simple illustration of well interference (Krohelski, 2003).

Figure 26 displays the total area per method, while Figure 27 divides each method's area coverage into three parts as described earlier in this section. The total-area comparison shows that MODPATH is now between UFE-Thiem and WHPA; CFR is again more than an order of magnitude larger since it does not account for the natural flow gradient. CFR does have a slightly higher percent-shared area (9.3% vs. 3.8%) than in Case 1. This increase occurs partly because MODPATH's area increased slightly (0.40 to 0.45 square miles). However, the main cause of the increase is the substantial decrease in CFR's net area (10.5 to 4.84 square miles) due to overlap of the three circles.

The UFE-Thiem capture area is also more similar in size to MODPATH results. This is partially due to why CFR increased in similarity: much of the capture areas of the three wells overlap, and so the net area is less conservative. However, unlike CFR, the UFE-Thiem delineation is significantly more comparable to MODPATH's delineation than in Case 1: its percent-shared area increases from 38% to 71%. Note in Figure 24 that the

UFE-Thiem and MODPATH shapes also increase in similarity: both are more elongate (i.e., greater length-to-width ratio) than in Case 1.

Note UFE-Thiem's small percent-missed area (4.5%) in Figure 27. The delineation overlay shows that the missed MODPATH area falls outside of the lateral boundaries of the UFE-Thiem delineation. This missed area is due to UFE-Thiem's inability to account for the lateral shift in flow direction caused by well interference, and so it fails to produce a capture area that shifts in location. Thus, although more conservative than our other analytical solution (WHPA), it is not conservative enough to encapsulate the entire MODPATH capture area.

In contrast to the first two methods, WHPA is now significantly less similar to MODPATH. Because the two delineations were nearly identical in the previous case, we can attribute their differences to the presence of multiple wells. That is, WHPA does not match MODPATH's up-gradient expansion or lateral shift in location because it does not account for well interference. Consequently, it overestimates in the central region between MODPATH's capture areas, and it underestimates the MODPATH area's lateral and up-gradient extents. Because it is less conservative than the UFE-Thiem method, WHPA's percent-extra area is smaller (5% versus UFE-Thiem's 29%) and its percent-missed area is greater (22% versus 4.5%).

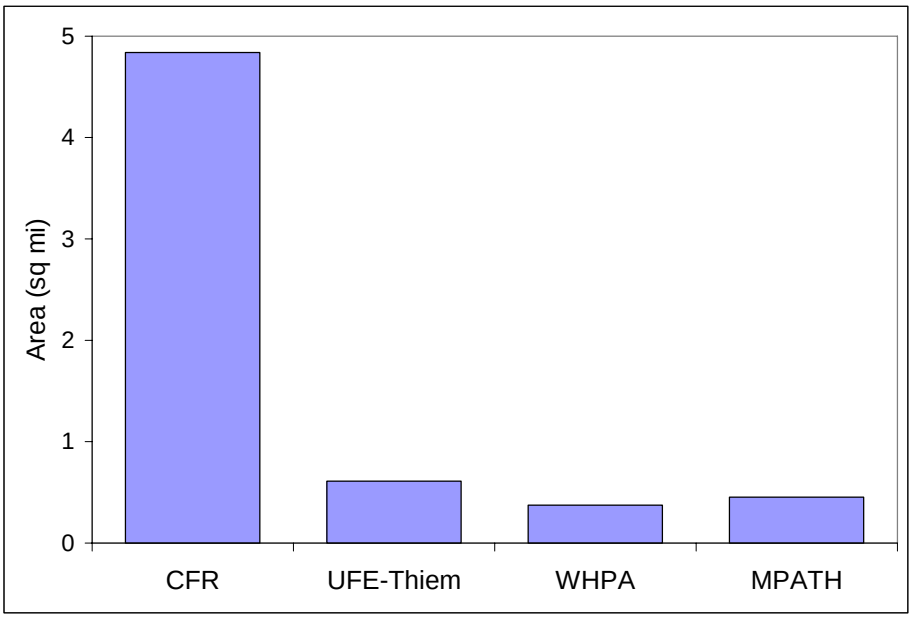

Figure 26. Total area per method in Case 2.

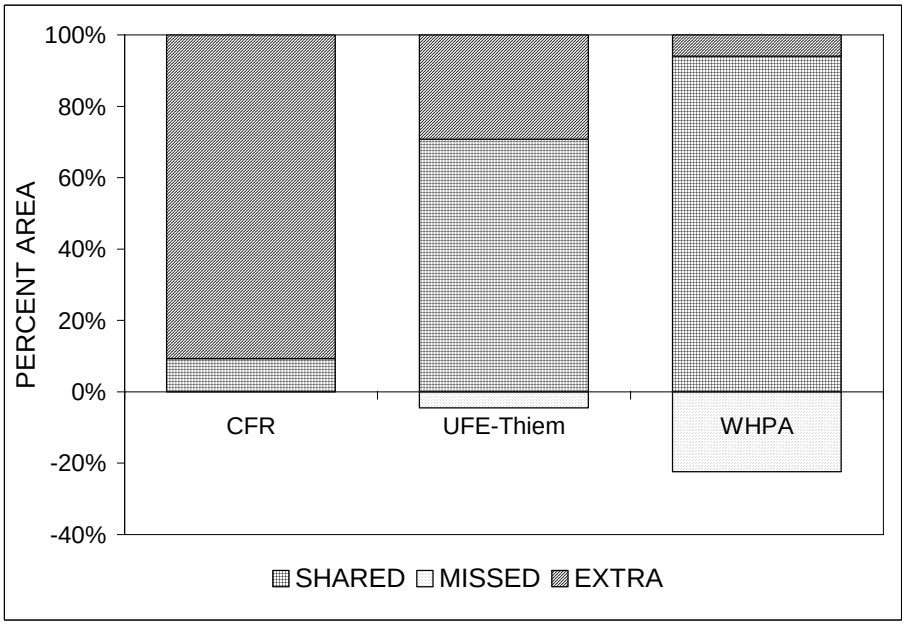

Figure 27. Comparison of CFR, UFE-Thiem, and WHPA delineations to MODPATH results in Case 2.

2.2.3 Case 3

Case 3 adds anisotropy. The vertical hydraulic conductivity is decreased by two orders of magnitude to 2 feet/day in our conceptual model. Figure 28 shows the delineations, while Figure 29 outlines the net areas of each method.

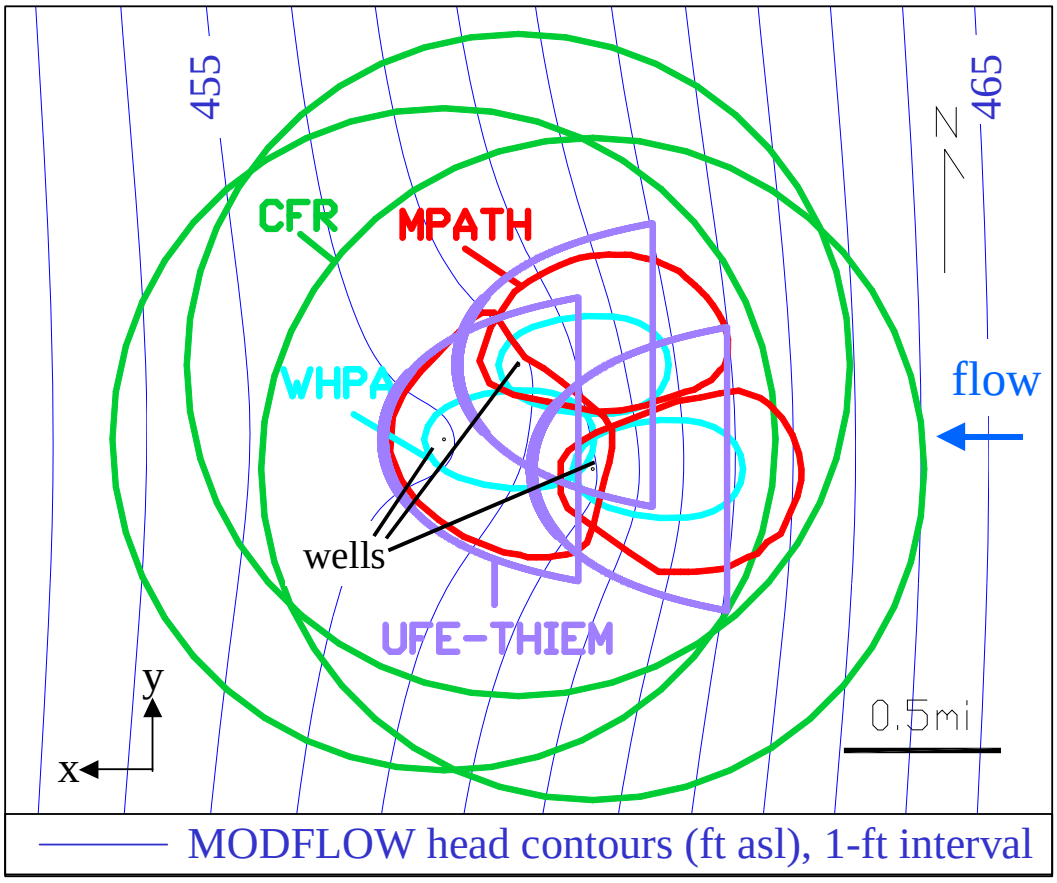

Figure 28. Case 3 capture areas, plan view.

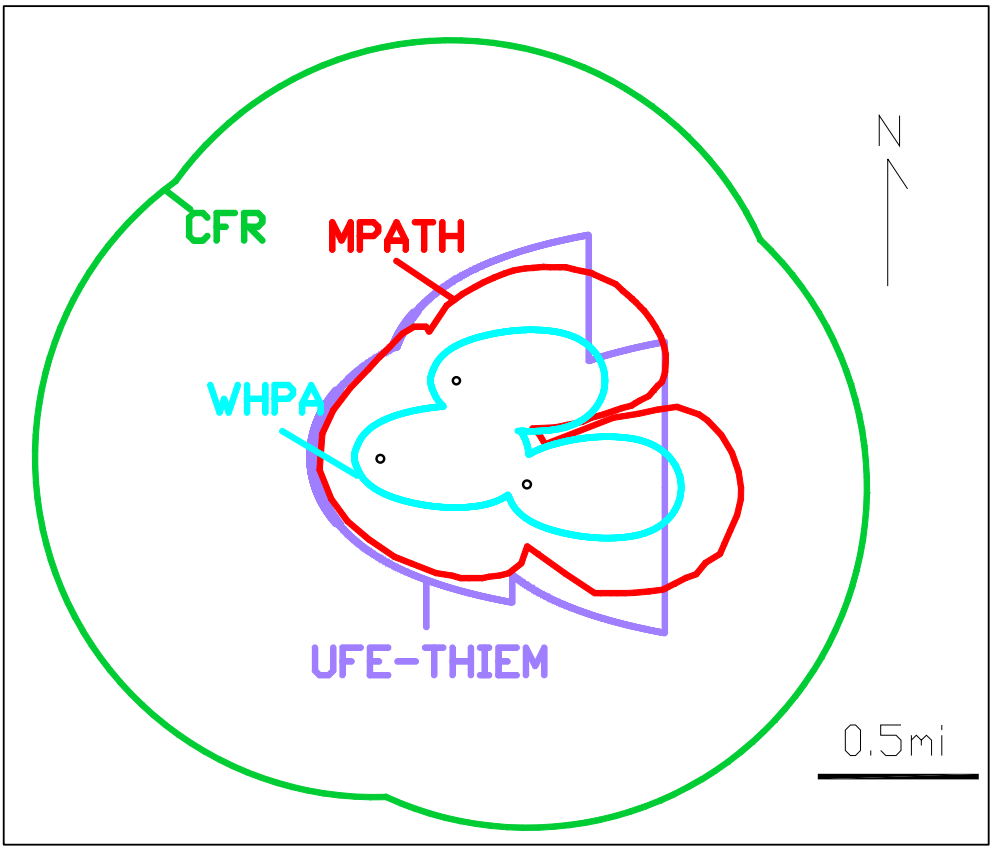

Figure 29. Outline of net capture areas for Case 3.

The MODPATH delineation has enlarged considerably relative to Case 2; Table 8 shows its net area has more than doubled (0.45 to 0.92 square miles). Note that the delineation has both widened and lengthened up-gradient of the wells. Vertical anisotropy produces this change. By lowering the hydraulic conductivity in the vertical direction, flow now moves faster in the horizontal direction. Faster flow means a farther travel distance in a given time interval. Thus, although the volume of recharge is equal to that of Case 2, the capture zone now spans less distance vertically and more horizontally.

Figure 32 and Figure 33 show that MODPATH particles simulate this flow behavior. Note that the well's recharge in Case 3 is being drawn from a narrower portion of the aquifer thickness. As noted in section 1.2.3, MODPATH, particles follow the path of least resistance. That is, within a grid cell, particles exit the cell-face that requires the

shortest travel time. Hence, they are directed more toward horizontal cell faces when vertical flow is slower.

The CFR delineation remains the same as in Case 2, and once again, it encompasses the MODPATH area. Its percent-shared area has increased (9.3% to 19.1%) in proportion to the MODPATH area enlargement. Comparing Figure 26 with Figure 30 illustrates this point.

The UFE-Thiem area is noticeably different from Case 2. Its total net area has increased by 33%. This increase is primarily caused by a wider capture area. The capture area widens because anisotropy is partially accounted for in the UFE-Thiem solution. Recall from section 1.2.2.1 that an anisotropy ratio is used in calculating of B_{eff}, the effective aquifer thickness, which is used in the UFE. Decreasing the vertical hydraulic conductivity decreases B_{eff}. Since B_{eff} is inversely proportional to the UFE bounding parameters (e.g., x_{sp} and y_{max}, Equations 9 and 10), the parameters increase. As a result, the capture area's width and down-gradient distance increase. However, because there is no anisotropy term in the Thiem equation, the up-gradient distance of the capture area remains the same as in Case 2.

We see that UFE-Thiem results are most similar to those of MODPATH because UFE-Thiem partially accounts for anisotropy. Now 86% of its area coincides with MODPATH (Figure 31). However, the MODPATH area it misses increases from 5% to 15%. It misses the up-gradient extent of the MODPATH capture area because the Thiem radius does not lengthen.

Like CFR, WHPA's delineation remains the same as in Case 2. Its area now lies entirely within the MODPATH delineation, and its percent-area missed more than doubles to 60% (Figure 31). This dramatically increases WHPA's level of underestimation.

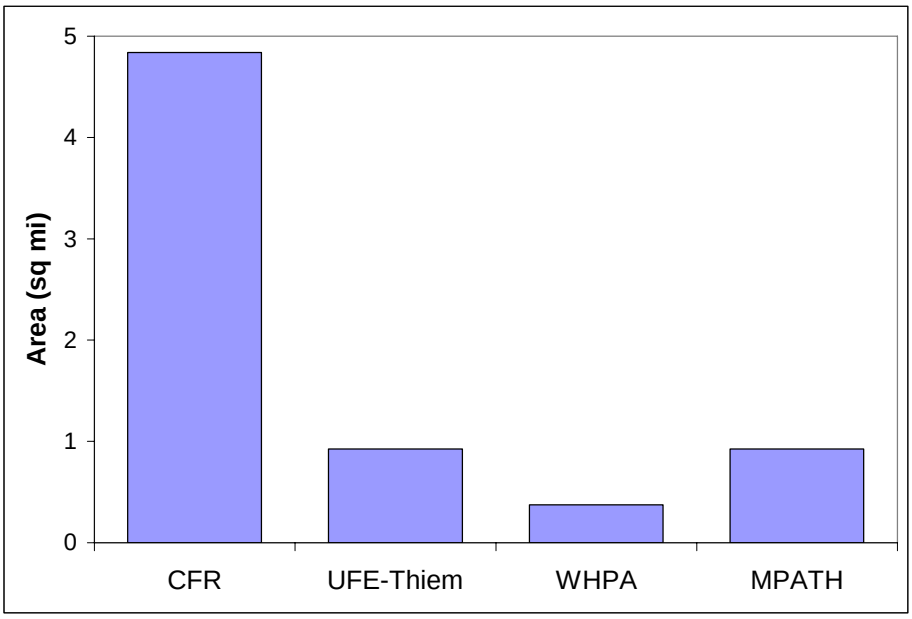

Figure 30. Total area per method in Case 3.

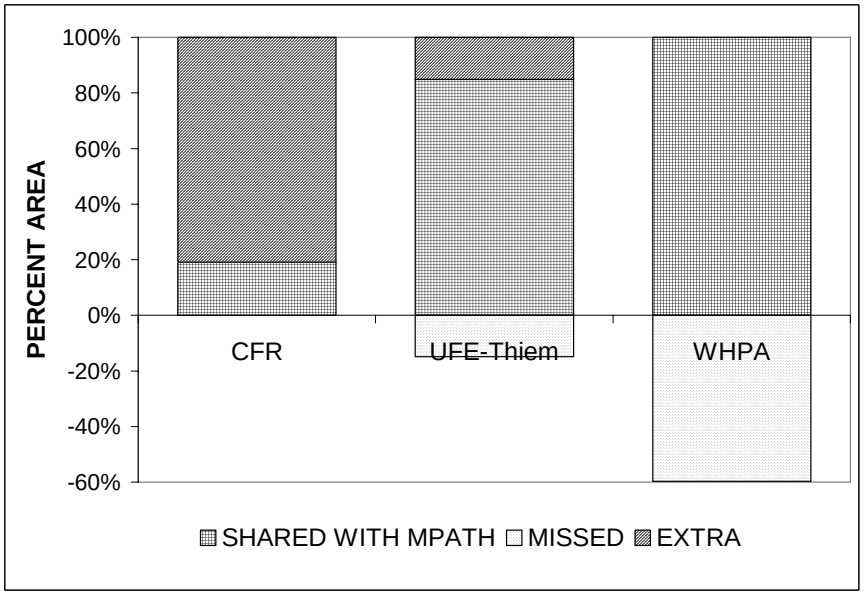

Figure 31. Comparison of CFR, UFE-Thiem, and WHPA delineations to MODPATH results in Case 3.

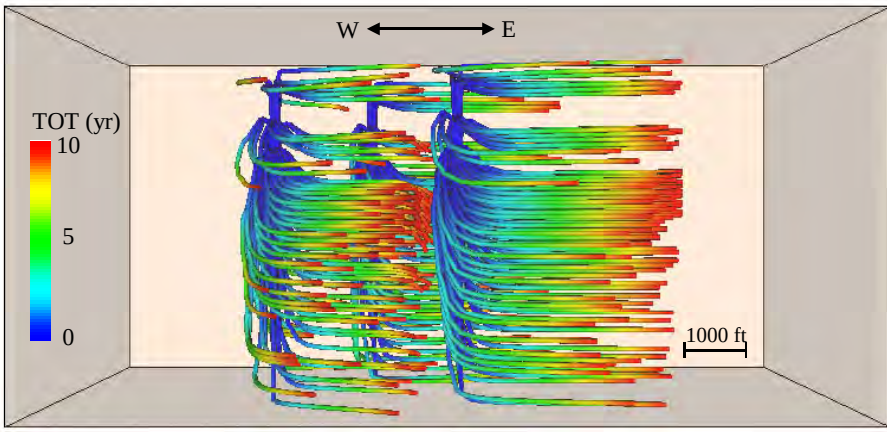

Figure 32. Cross-section of MODPATH pathlines in Case 2.

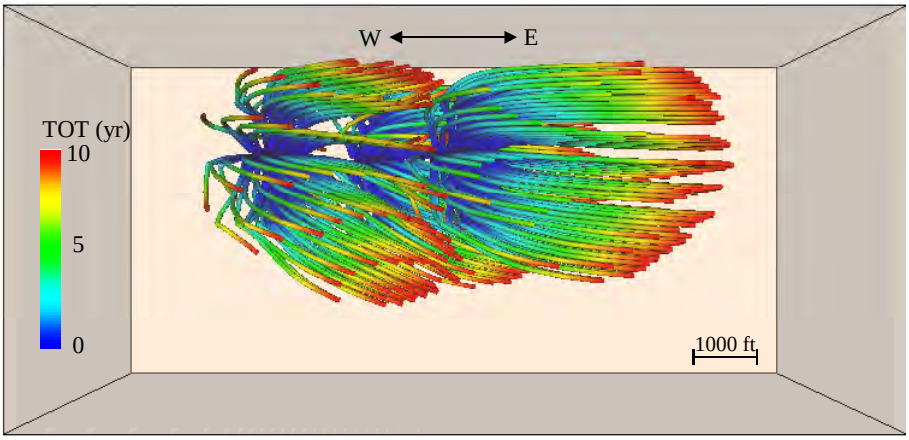

Figure 33. Cross-section of MODPATH pathlines in Case 3.

2.2.4 Case 4

Case 4 adds heterogeneity. A low hydraulic conductivity zone was placed immediately up-gradient of the well field (Figure 16). Its horizontal hydraulic conductivity is two orders of magnitude lower than the rest of the aquifer. Figure 34 shows the delineations, while Figure 35 outlines the net areas of each method.

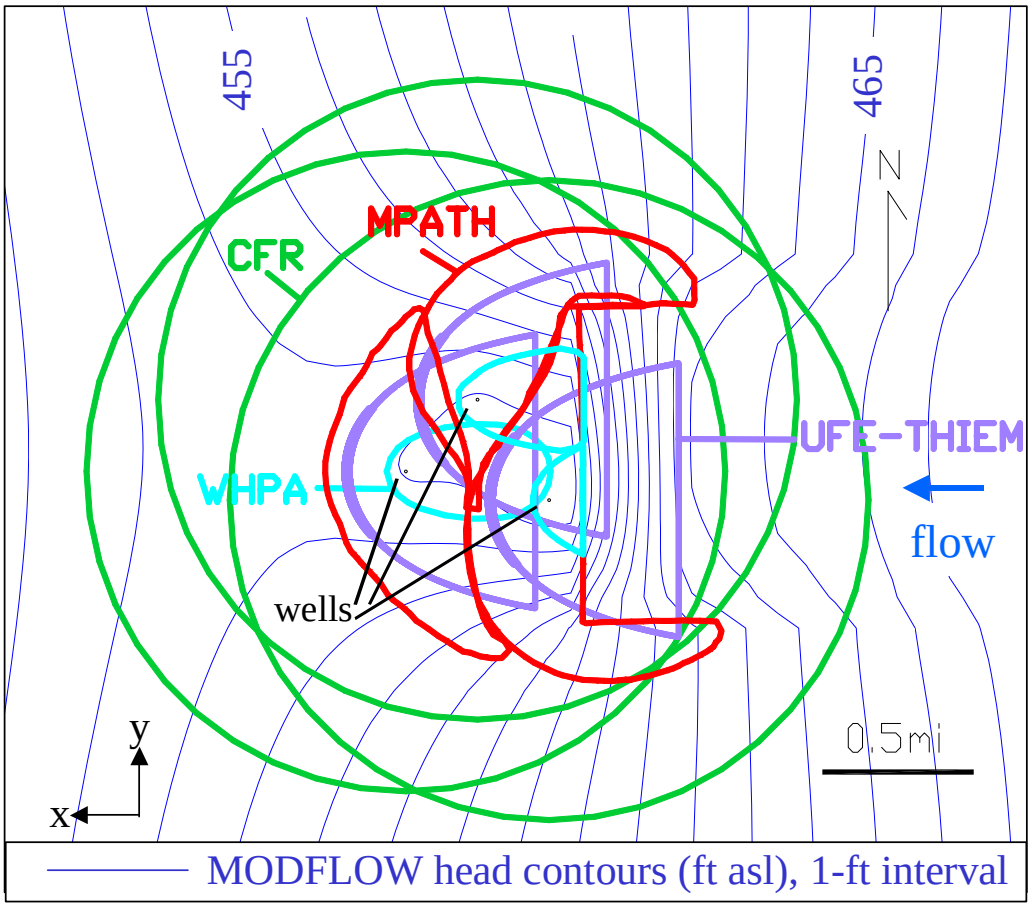

Figure 34. Case 4 capture areas, plan view.

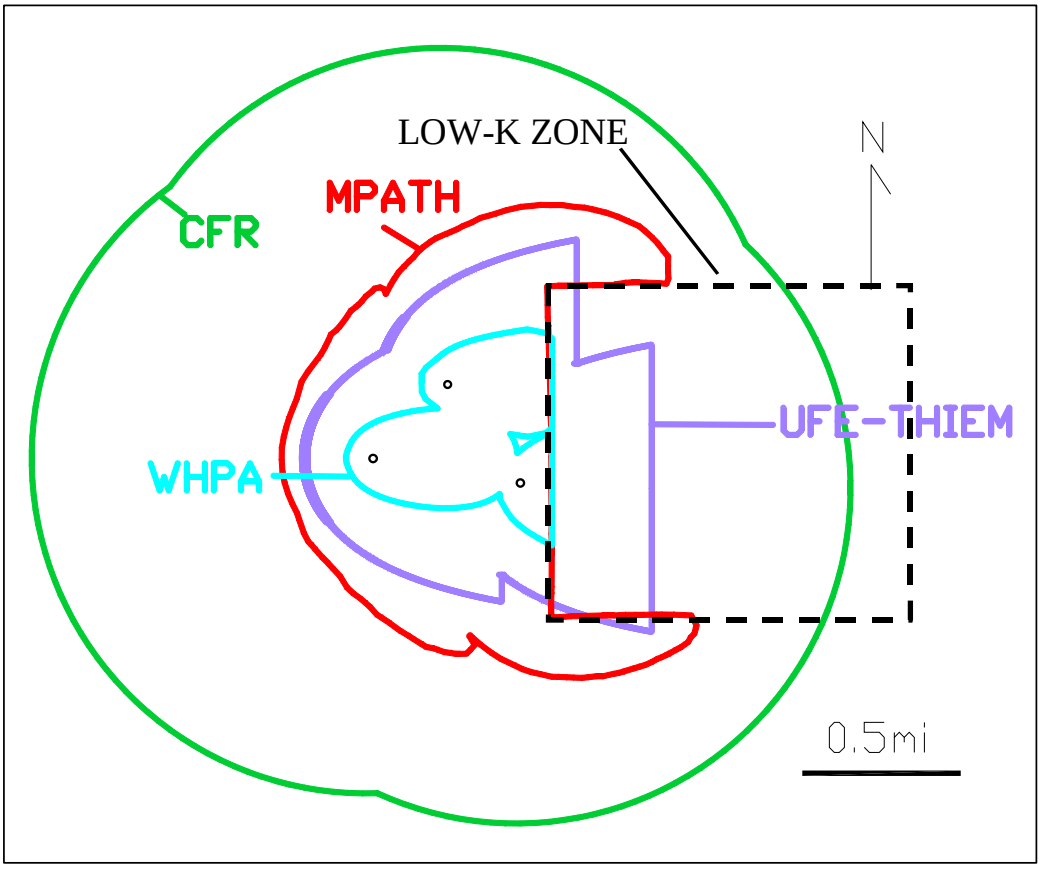

Figure 35. Outline of net capture areas for Case 4.

The MODPATH net capture area in Figure 35 clearly outlines the low-K zone, which creates a very irregular shape. The shaping indicates that much of the flow is diverted around the low-K block in the MODFLOW simulation. This flow pattern is caused by the same mechanism discussed in Case 3: ground water travels faster (and therefore farther) in regions of relatively high hydraulic conductivity. The low-K zone affects the size as well as shape of the capture area: it has increased by approximately 14% (Figure 36).

The CFR delineation is equal to the previous two cases. Its percent-shared area has increased to 22%. Like CFR, the UFE-Thiem solution assumes homogeneity and does not change from Case 3. Due to the enlarged MODPATH delineation, UFE-Thiem now misses over 40% of MODPATH's area. Its percent-extra area also increases (14% to 31%) since much of its up-gradient extent overlaps with the low-K zone.

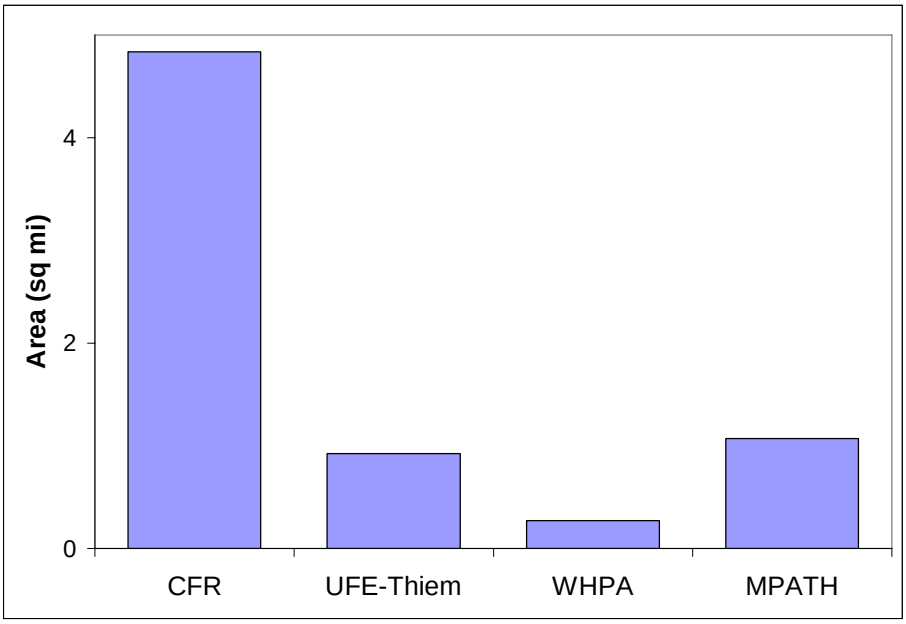

Figure 36. Total area per method in Case 4.

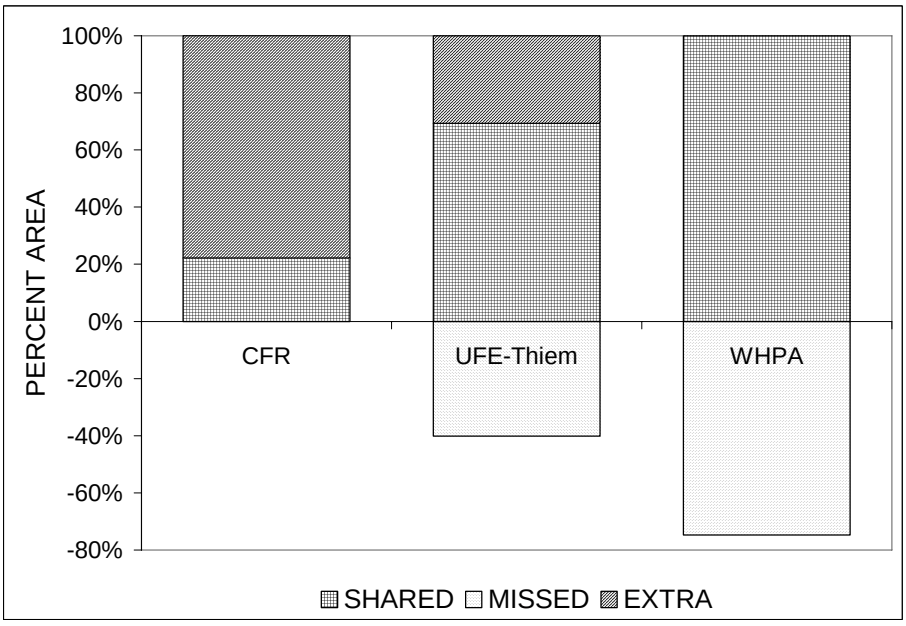

Figure 37. Comparison of CFR, UFE-Thiem, and WHPA delineations to MODPATH results in Case 4.

WHPA's delineation changes due to its simulation of a barrier boundary (section 2.1.4). The resulting capture area is now more comparable in shape to MODPATH; two

of the three well's capture areas are cut short at the barrier and extend laterally. However, the capture areas are much smaller in size in comparison to MODPATH results. The WHPA delineation now misses 75% of MODPATH's capture area (Figure 37). The net WHPA area decreases from Case 3 to Case 4 because the lateral expansion near the barrier does not compensate for the distance lost in the up-gradient direction.

The small capture area is due to the way WHPA simulates a barrier-boundary. The barrier is simulated in WHPA using the method of images. This method places an imaginary discharge well on the other side of the boundary that is a mirror image of the real well; Figure 38 shows the design in plan view. This results in additive drawdown as in the case of well interference (Figure 25), and so the barrier serves as an impermeable (i.e., no-flow) boundary.

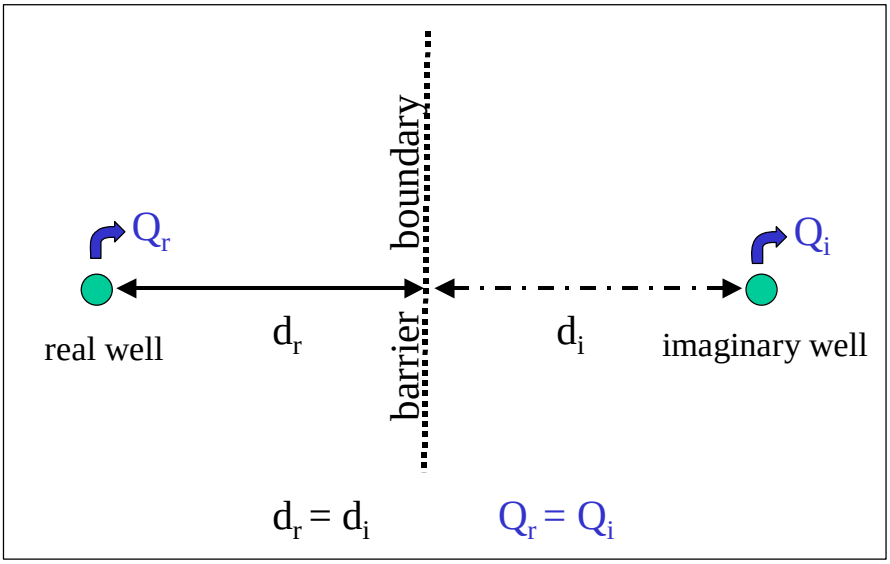

Figure 38. Image well theory as applied to a 2-D barrier boundary, plan view.

However, image well theory applies only to the radial flow component of the velocity potential. Recall from section 1.1.2.3 that analytical solutions follow the principal of superposition, in which uniform and radial flow combine to form a well's flow field (Equation 7). Thus, the barrier acts as a semi-permeable rather than impermeable boundary, as the flow due to the natural gradient is assumed to pass across it. The capture area therefore does not expand significantly in other directions because recharge is still

being derived from the up-gradient direction. WHPA's inability to simulate a no-flow barrier is another example of its simplistic nature.

A comparison of streamline configurations illustrates the different effects of an impermeable and semi-permeable boundary. Figure 39 overlays WHPA streamlines for a case with uniform and radial flow components (blue) and a case with radial flow only (red). Note the red streamlines are longer; the capture area increases in order to obtain the amount of recharge that is no longer provided up-gradient of the barrier boundary. Also note that the blue streamlines (representing uniform and radial flow) meet the barrier at an angle. The angle of the streamlines depends on the magnitude of the uniform-flow velocity component; that is, as the uniform-flow velocity increases, the more perpendicular the flow lines will become to the barrier. Conversely, the blue streamlines will become more radial as the uniform-flow velocity decreases. If the term cancels out altogether (e.g., if the natural gradient is set to zero), the barrier acts as a no-flow boundary since flow to the well is due to pumping only. The blue streamlines will therefore converge on the red.

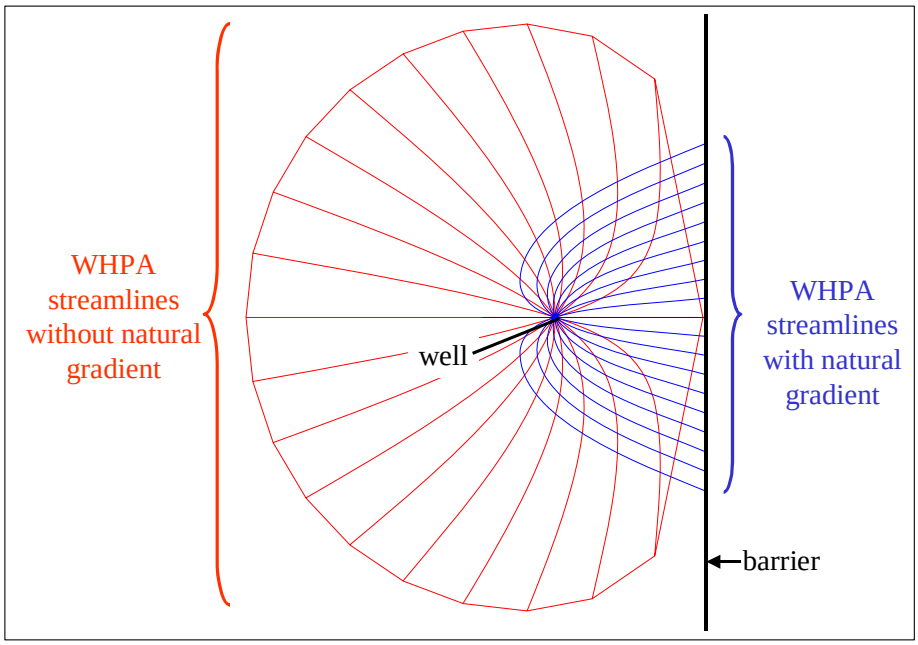

Figure 39. Comparison of WHPA-generated streamlines with and without a natural hydraulic gradient.

2.2.5 Case-Study Summary

In the following sections, we review results of the three simpler methods through all four cases. We test our hypothesis for each method in chapter 5, after presenting the results of our field case. Implications of results for method applicability are included in chapter 5 as well.

2.2.5.1 CFR

Figure 40 shows the CFR area break-down for cases 1-4. Note that CFR was the only delineation that encompassed the MODPATH delineation in all cases (i.e., its percent-missed area was always equal to zero). Furthermore, most of its capture area was unneeded in all cases, with its percent-extra area ranging from 77% to 96%. Thus, it was by far the most conservative method. Also note that the percent area shared with MODPATH increased in each case. The reader might interpret this to mean that CFR improves in accuracy with hydrogeologic complexity. In reality, however, the capture areas were simply smaller relative to MODPATH's areas.

This raises an important point regarding our methodology: our synthetic cases studies are unique systems; adding different complexities could potentially produce very different results. For example, a case involving a losing stream near a pumping well will *decrease* its capture area, making CFR *less* similar to MODPATH results. Thus, it is incorrect to conclude that CFR will always better represent capture areas as system complexity increases.

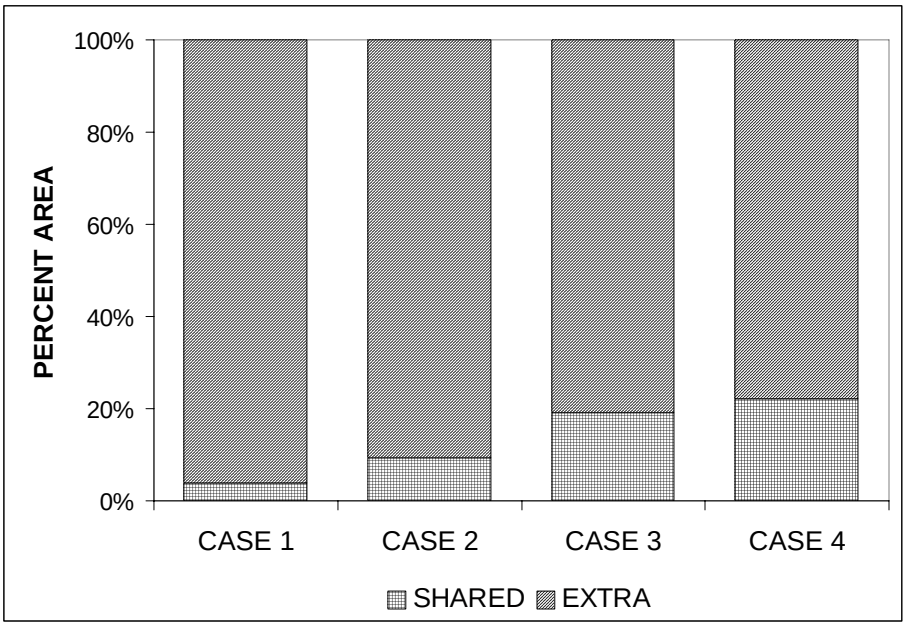

Figure 40. Comparison of CFR-area to MODPATH for cases 1-4.

2.2.5.2 *UFE-Thiem*

Figure 41 shows the UFE-Thiem area break-down for cases 1-4. Note that the percent shared with MODPATH increased through Case 3, although the percent of MODPATH it missed also increased. The last case had an especially high amount of inaccuracy due to the method's inability to account for heterogeneity.

Our first and simplest case illustrated UFE-Thiem is somewhat conservative, with over half of its area outside of the MODPATH delineation. However, its conservative nature made it more comparable in Case 2, where it could not account for complexity and the MODPATH area enlarged; this is similar to CFR results except that UFE-Thiem was much more comparable in shape and size to MODPATH. Furthermore, Case 3 showed that its ability to represent anisotropy (at least partially) rendered a capture area that was most comparable to MODPATH.

In summary, UFE-Thiem most closely resembled MODPATH in our case studies because it made fewer assumptions than CFR and WHPA, and its level of conservativeness lies somewhere between CFR and WHPA. However, the increasing amount of MODPATH area missed by UFE-Thiem must not be overlooked.

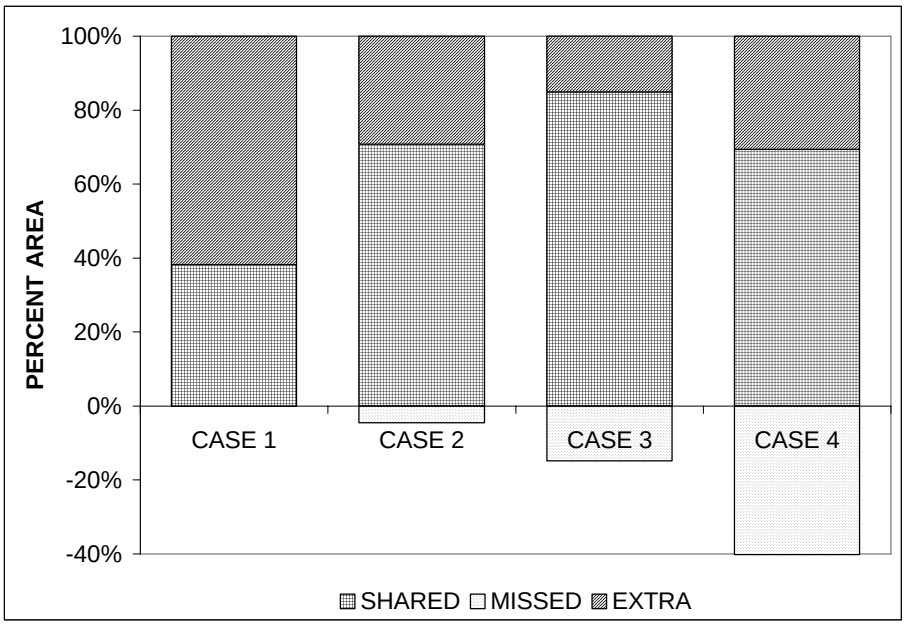

Figure 41. Comparison of UFE-Thiem-area to MODPATH for cases 1-4.

2.2.5.3 *WHPA*

Figure 42 shows the WHPA area break-down for cases 1-4. Note the shared area was consistently at or near 100% in all cases; this signifies that the MODPATH capture areas encompassed those of WHPA. WHPA's percent-missed area was similar to UFE-Thiem in that it increased in each case. Thus, its results increasingly differed from MODPATH with added complexity.

Also note that WHPA's percent-missed area was more pronounced than the UFE-Thiem results. This is partly due to WHPA's less conservative nature. The larger percent-missed area is also due to the increase in invalid assumptions that WHPA made relative to UFE-Thiem. For instance, Case 3 showed their difference in percent-missed area (62% WHPA vs. 15% UFE-Thiem) because UFE-Thiem can partially account for anisotropy. Case 4 illustrated another disadvantage to WHPA's simple design: it does not accurately represent a flow barrier due to the design of its velocity calculations.

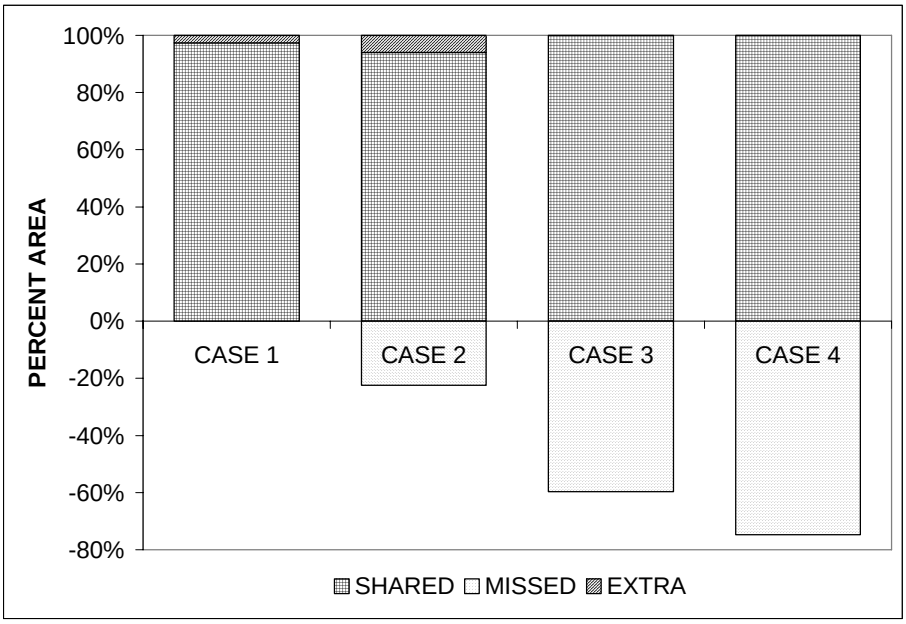

Figure 42. Comparison of WHPA-area to MODPATH for cases 1-4.

3 FIELD CASE BACKGROUND

3.1 DESCRIPTION OF STUDY AREA

3.1.1 Location

Fort Wainwright is a military post in Interior Alaska, located immediately east of Fairbanks (Figure 43). It is approximately 100 miles south of the Arctic Circle and lies within the 44,500 square-mile Tanana Basin. The post occupies 1430 square miles of land on which approximately 15,000 residents live. Most of the area is comprised of the floodplain in the Tanana-Kuskokwim Lowlands (Anderson, 1970), with Birch Hill forming the northern border. The Chena River enters the floodplain east of Fort Wainwright and meanders west through the center of the installation before merging with the Tanana River about six miles southwest of Fairbanks. The Tanana River runs in a northwesterly direction approximately three miles south of the study area.

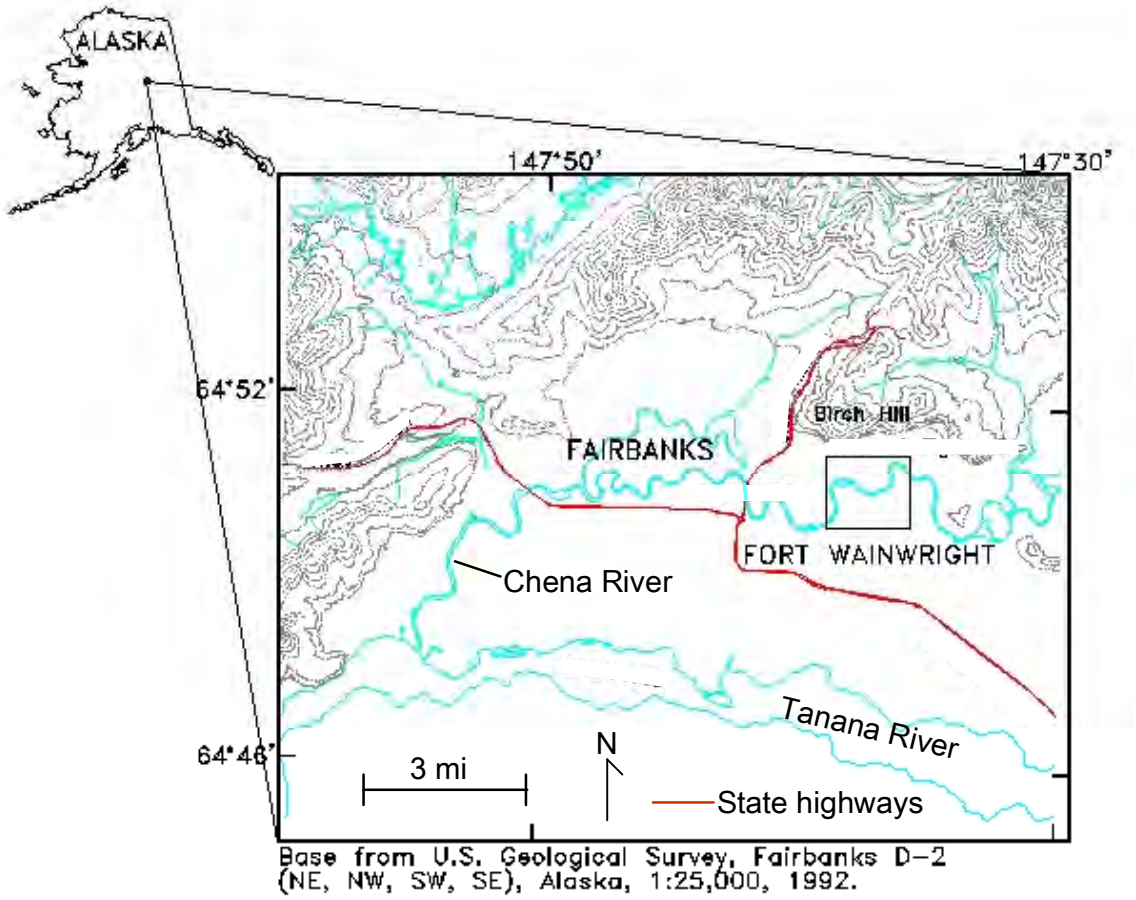

Figure 43. Map of the Fairbanks and Fort Wainwright area (Adapted from Wegner, 1997).

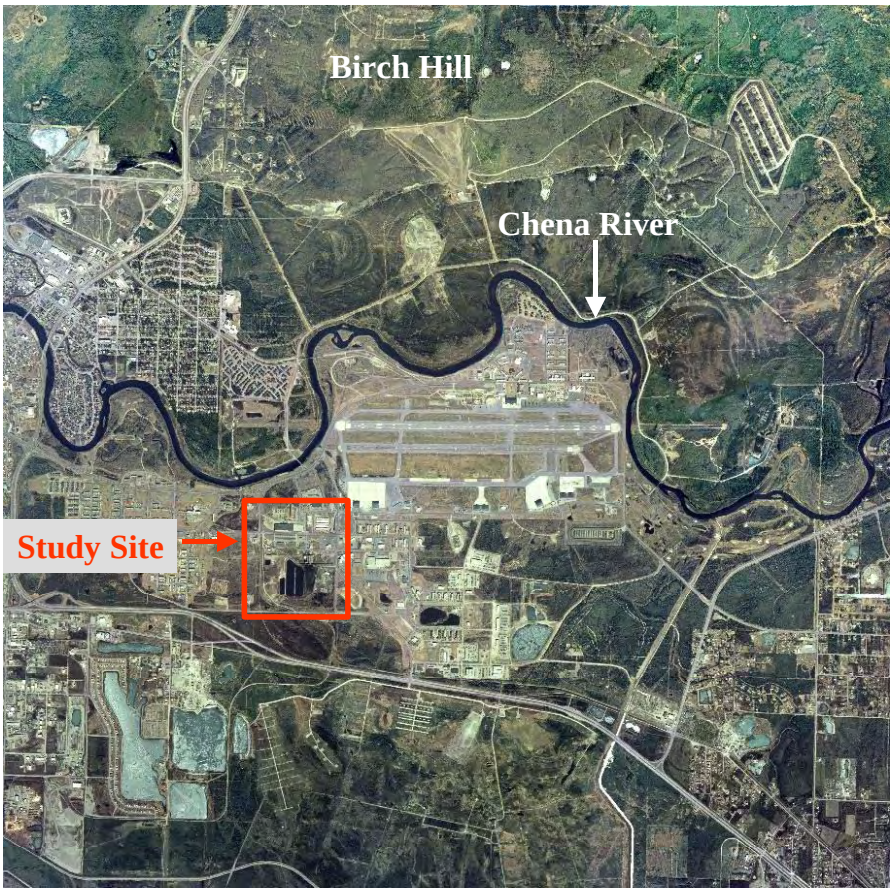

Figure 44. Aerial photo of Fort Wainwright.

The main drinking water-supply wells, WS 3559 A and B, are near the center of the post, approximately 0.5 miles south of the nearest bend in the Chena River (Figure 44). The wells are located in a small building northeast of a water treatment facility (WTF) (Figure 45). The post's power plant lies about a mile southeast of the wells. Both the plant and WTF have adjacent discharge ponds. These ponds are man-made and unlined. The power plant uses the water in its pond for cooling purposes; section 3.3.4.3 provides further detail. A smaller pond directly south of the WTF is used to backflush filters in the facility (ASCI/NANA, 2001). The WTF pond is lined with sediments that are considerably finer than the alluvial aquifer. We assume that its interaction with the ambient ground water is negligible and do not include it in our site analysis.

WS 3559 A and B pump alternately at an average rate of 1100 gpm. Due to their alternating operation, we will consider them as single well for the purposes of our study; we hereafter refer to them as one well. WS 3559 has been operating since 1988. Prior to its operation, WS 3565 served as the primary water-supply well from 1969 to 1988. The first primary water-supply well on post was WS 3563, which operated from the mid-1950's until 1969. Both WS 3565 and 3563 now serve as back-up wells. Several other wells on post are also used for back-up support or fire protection. However, little information is available on their pump rates and frequency of use. Appendix A provides a table of existing pumping records.

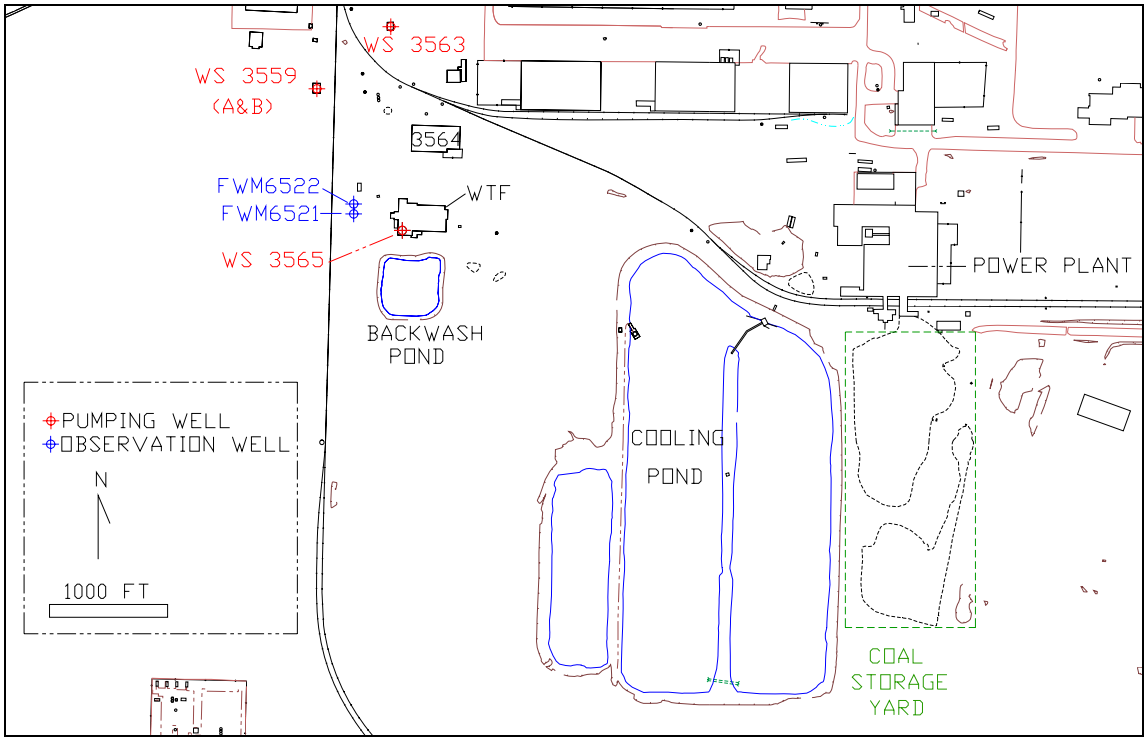

Figure 45: Study site with relevant features marked.

3.1.2 Climate

Interior Alaska has a continental climate. The Brooks Range to the north and Alaska Range to the south block maritime influences. As a result, Fairbanks experiences a wide temperature variation from winter to summer. The average daily minimum is 16.3°F,

while the average daily high is 37.0°F for the period of 1904-2004 (National Weather Service, 2005). The climate can be described as low in wind, humidity, and precipitation. The average annual precipitation is 11.09 inches, with 7.05 inches as summer rainfall. The average annual snowfall is 62.7 inches (4.04 in snow-water equivalent)(National Weather Service, 2005). The amount of snowfall tends to vary with elevation (Anderson, 1970; Youcha, 2003), with higher elevations receiving more precipitation. Snowfall is also temporally variable; for example, Fairbanks received 36.4 inches in the winter of 1969-1970 and 145.7 inches the following year (Plumb and Lilly, 1996). Evapotranspiration (ET) is more difficult than precipitation to quantify. Dingman (1973) estimated ET rates ranging from 40% to 78% of precipitation rates in watersheds throughout Alaska. The calculations were based on the assumptions that there was no change in ground-water or surface-water storage. In a small watershed about 10 miles north of Fort Wainwright, in Fox, Alaska, Dingman estimated 6 inches/year was lost to evapotranspiration (Nelson, 1978). In a study of two watersheds approximately 15 miles west of the post, Gieck (1986) found ET rates at both sites to be about 90% of precipitation rates. Although the Interior is classified as semiarid to arid, an abundance of water exists in lakes and wet muskeg. This is due to permafrost inhibiting drainage, short summer seasons, and lack of ET in winter.

3.1.3 Ecology

Fort Wainwright is part of a boreal forest ecosystem (Anderson, 1970). Trees and shrubs are found in undeveloped areas. The main coniferous species is black spruce, while deciduous include birch, aspen, alder, and willow. Most of the site is developed, with only grasses, herbs, and a few aspen and willow remaining. Several small wetlands exist, which are classified as such based on vegetation type rather than hydrology or habitat value (CH2MHILL, 1996a).

3.2 GEOLOGIC FRAMEWORK

3.2.1 Regional Geology

The three main landscape features within the Tanana Basin are the Yukon-Tanana Uplands to the north and east, the Alaska Range to the south, and the Tanana-Kuskokwim Lowlands through the central region. The Uplands are a northwest-trending series of rounded ridges 2,000-3,000 feet in altitude; scattered mountain groups rise to between 5,000 and 6,000 feet. Sloping to the northwest at 5 feet/mile, the Lowlands are filled with glaciofluvial sedimentary deposits and alluvial fans that form an apron over much of the southern Tanana Valley (Nelson, 1978). These sediments were derived from erosion of the Alaska Range.

The oldest rocks within the basin are a metamorphic complex of sedimentary origin, known as the Yukon-Tanana Metamorphic Terrane (Newberry et al., 1996). Once believed to be of Precambrian age, they are now dated to the Jurassic era. The terrane was intruded by granitic rocks, such as granite and quartz diorite, during the Mesozoic. Little evidence exists regarding events of the Tertiary period, other than the re-folding and deep weathering of the metamorphic complex, as well as local lava flows that resulted in basalt forming a minor portion of the basin bedrock.

The Cenezoic is characterized by climate change; temperatures during this time have been both colder and warmer than those today. The Pliocene and Pleistocene saw heavy sediment deposition, including the Fox and Cripple Creek Gravels that overlie bedrock in upland valley bottoms. These gravels are in turn covered by solifluction materials, which are moisture-rich soils that are underlain by permafrost and have slowly moved downhill. In later Quaternary time, eolian silt was carried from the floodplain and glacial outwash south of the Tanana and blanketed the uplands. Some of this silt, known as reworked loess, was then transported to valley bottoms where it now covers creek gravels as well as bedrock. Thicknesses range from 1 to 100 feet (Péwé et al., 1976).

Climate fluctuations continued into recent time. During the glacial maxima of the Pliocene and Pleistocene, the depositional environment of the Tanana floodplain was at a

higher energy level than today. Streams issuing from the Alaska Range were heavily loaded with sediment and deposited large amounts of silt, sand, and gravel in the Tanana Valley. Alluvial fans that extended north from the Alaska Range forced the Tanana to flow in the northern portion of the lowlands. The fans also formed large lakes by damming up non-glacial tributaries in the valley (Anderson, 1970). Some of the deposited sediment would subsequently be eroded. From Illinoian to present-day, the deposition-erosion cycle has repeated multiple times. A cycle of permafrost formation and degradation, mostly within bedrock and organic silts, has continued as well. Further detail on Quaternary events that shaped the present landscape is lacking.

3.2.2 Sub-Regional Geology: The Fairbanks Floodplain

3.2.2.1 Bedrock

Underlying the alluvial deposits in the floodplain are rocks of the Birch Hill Sequence, which is part of the greater Yukon-Tanana Metamorphic Terrane. Depth to the sequence decreases as one heads north on Fort Wainwright, until outcrops begin to appear at the southern edge of Birch Hill. The sequence consists of fine-grained quartzite, slate, and phyllite, and contains thin (< 1 meter) layers of feldspathic tuff (Newberry et al., 1996). Also present are marble and calcareous schist. The schist is locally intruded by granitic rocks, primarily granite and quartz diorite. The formation exhibits fracturing and weathering in some areas, as can be seen in core samples taken from Birch Hill (Figure 46). Basalt also occurs in outcrops east and south of Fort Wainwright (Péwé et al., 1976).

Figure 46: Core samples of the Birch Hill Sequence (photo by Emily Youcha, 2002).

3.2.2.2 *Quaternary Deposits*

The Chena Alluvium is the predominant surficial formation of the Fairbanks floodplain. Contrary to the name, the alluvium was deposited by the braided Tanana River rather than the meandering Chena River. The alluvium is therefore comprised of braided-river deposits. During the Pleistocene and Holocene, the Tanana deposited glacial outwash from the Alaska Range. These unconsolidated sediments are described as sand and gravel with silt lenses. The gravel clasts consist mostly of quartz and gneiss and range from ¼ to three inches in size. The alluvium is underlain by bedrock and locally overlain by as much as 15 feet of gray silt. The sand and gravel are arranged in thin (20 feet maximum), well-stratified, alternating and laterally-discontinuous layers (Péwé et al., 1976).The alluvium as a whole ranges from 10 to over 600 feet in depth. In observing "every gradation and combination of fine and coarse material," Cederstrom (1963) noted

heterogeneity as its outstanding characteristic. Figure 47 shows the sediment variation within a shallow excavation.

The silts found locally overlying and within the Chena Alluvium are swale and slough deposits. Their angular to sub-rounded grains contain quartz, feldspar and mica. They contain clay (10-30%) and organic matter, and have high ice content in frozen areas. The swale and slough deposits exhibit poor drainage and permeability. Another silt formation occurs on the south slopes of upland hills. It is known as the Fairbanks Loess, part of the reworked loess discussed in section 3.2.1. It consists of massive, homogeneous eolian silt (Newberry et al., 1996), and contains less clay (<10%) than the swale and slough deposits.

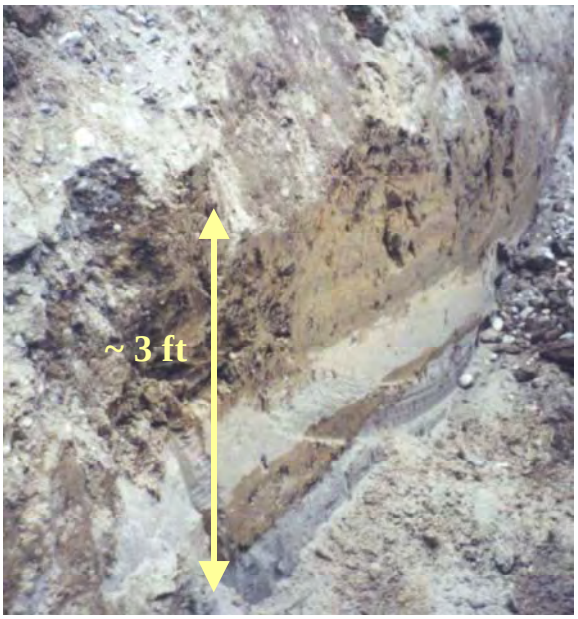

Figure 47: Shallow excavation on Fort Wainwright (photo by author, 2002).

Figure 48 illustrates the geologic units of the floodplain on Fort Wainwright. The Chena Alluvium is clearly the main formation of the floodplain, while the swale and slough deposits are embedded within it. Likewise, the Birch Hill Sequence is the dominant unit of the uplands in this area, while the thin blanket of reworked loess is a relatively minor feature. The gray feature is permafrost and is discussed in the next section.

3.2.2.3 Permafrost

Permafrost is defined as soil or rock that remains frozen for at least 2 years. It can contain varying levels of ice content. The Fairbanks area lies within a zone of discontinuous permafrost. Péwé and Bell (1975) mapped the permafrost distribution of the Fairbanks area in 1974 and 1975. In the uplands, it is most often found on north-facing slopes, lower south-facing slopes and valley bottoms, while it is usually absent from ridgetops as well as west-facing and upper south-facing slopes (Nelson, 1978). This distribution is in part a function of the geology: permafrost is more common in poorly-drained areas with finer sediments, such as silts and clays. Similarly, in the floodplain, it tends to occur in the swale and slough deposits, although it also exists in areas of sand and gravel. Comparison of permafrost in the two sediment types has revealed that silts and clays have a higher ice content than the coarser counterpart (Péwé et al., 1976). In relation to vegetation, shallow permafrost is often found where black spruce is most dominant (Viereck et al, 1986). Frozen soil does not usually form beneath large water bodies such as lakes and river channels due to their thermal influence. Near meandering rivers like the Chena, it is found around cut-banks and away from point-bars. Likewise, it is not found beneath major roads and buildings. The extent of permafrost in the floodplain appears to have decreased since Péwé first conducted surveys (1949-1952). This is likely due in part to the thermal effects of increased development (Yoshikawa, 2004).

Permafrost thickness varies widely within the floodplain: some borehole logs depict a thickness of only a few feet, while others show permafrost throughout the entire borehole (Cederstrom, 1963). Péwé et al. (1976) noted a range of 3-275 feet. Well logs often depict multiple layers. However, in reality there may be only a single layer that has undergone lateral thawing at different rates, thus creating a saw-tooth pattern in cross-section (Cederstrom, 1963). The US Army Corps of Engineers (1995) concluded such thawing was occurring based on the irregular and discontinuous zones encountered while drilling wells in the floodplain.

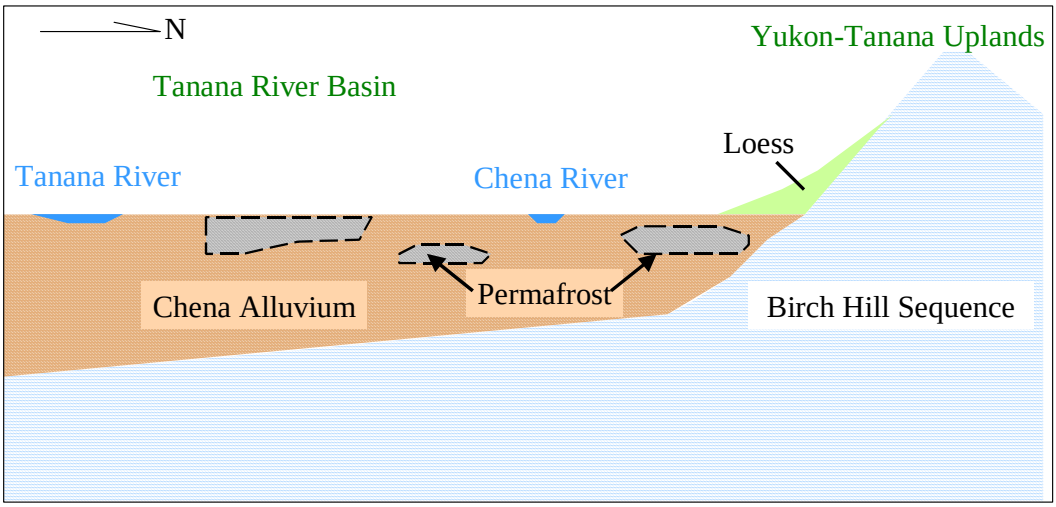

Figure 48: Simplified cross-section of geologic units on Fort Wainwright (modified from Péwé et al., 1976)

3.3 HYDROGEOLOGY

3.3.1 Ground-Water Flow Through Braided-Stream Deposits: Scale Issues

One of the major influences on the size, shape, and location of a capture zone is the aquifer's hydrogeologic framework. As noted in the previous section, the main surficial geologic formation of the Fairbanks floodplain (Chena Alluvium) consists of braided-stream deposits from the Tanana River. Braided rivers are known for their high sediment load, low channel stability, and relatively coarse sediment. Bristow and Best (1993) define braided streams as a series of channel segments that separate and reunite around bars in a regular pattern. This 'regular pattern' does not exist in the deposits, however. Due to the many processes and flow velocities involved with braiding, a mix of fine and coarse deposition occurs. The resulting deposits are very heterogeneous, in both their vertical and horizontal distribution. An enormous amount of data is required to quantify such heterogeneity, and so most field studies do not have enough sample points to determine fine-scale sediment distribution for the entire site. The high level of uncertainty in spatial distribution of soil properties makes modeling flow difficult, as high and low hydraulic conductivity zones cannot be incorporated into a field-scale model. Anderson et al. (1999) modeled ground-water flow through two braided-stream

deposits. Results showed that the determining factor of deposit transmissivity was the connectivity of high-conductivity units. Units with a high degree of connectivity acted as conduits and created preferential flow paths, especially when surrounded by low-conductivity units that acted as flow barriers. Reilly and Pollock (1993) also modeled a heterogeneous alluvial aquifer and found that different fine-scale hydraulic conductivity distributions can greatly alter areas contributing recharge to water-supply wells. They assert that a margin of error must always be added to capture-zone delineations because such spatial variation of hydrologic properties cannot be modeled with complete accuracy.

We are studying the Chena Alluvium on a sub-regional level. Due to the difficulty in determining small-scale heterogeneities in braided-stream deposits, we assign bulk properties to the entire volume of alluvium within the model domain. The magnitude and range of property values may therefore differ from those used at smaller scales.

3.3.2 Conceptual Model

As noted in section 2.1.1, a conceptual model is crucial first step in ground-water flow modeling. A conceptual model is a pictorial representation of the ground-water flow system. Its purpose is to simplify the field situation and organize field data so that the system can be analyzed with relative ease. Although the conceptual model should represent the true system as best as possible, the practical goal is parsimony (Anderson and Woessner, 1992). That is, the aim is to simplify as much as possible while retaining enough complexity to adequately simulate the system behavior. The accuracy of a mathematical model is highly dependent on the conceptual model design. An invalid representation can lead to major errors in the mathematical model's predictions.

Building a conceptual model involves defining hydrostratigraphic units, preparing a water budget, and defining the flow system (Anderson and Woessner, 1992). Within the floodplain and surrounding hills are four geologic units: the Birch Hill Sequence, the Fairbanks Loess, swale and slough deposits, and the Chena Alluvium (Figure 48). As stated in section 3.2.2.2, the swale and slough deposits occur as lenses throughout the

alluvium. Due to the nature of their distribution, they are not considered separately from the alluvium. We include permafrost as a hydrogeologic unit due to its distinctive properties and significant impact on flow in the floodplain. Thus, we have four hydrogeologic units altogether. Three of the four, the bedrock, silt and permafrost, are of relatively low hydraulic conductivity and do not yield significant quantities of water. Thus, the alluvium is the primary aquifer.

Figure 1 illustrates our conceptual model of the Fairbanks floodplain aquifer. The general flow is northwest between the Chena and Tanana Rivers. The Tanana acts as a ground-water source and the Chena a ground-water sink during most of the year. Natural ground-water divides occur in the bedrock uplands to the north and west, while the alluvial basin that feeds the Tanana to the south and east acts as a recharge boundary. The majority of the aquifer is unconfined. The water table generally follows the topography, having a 4 feet/mile gradient (Glass et al, 1996) and is typically 10 to 20 feet below ground surface.

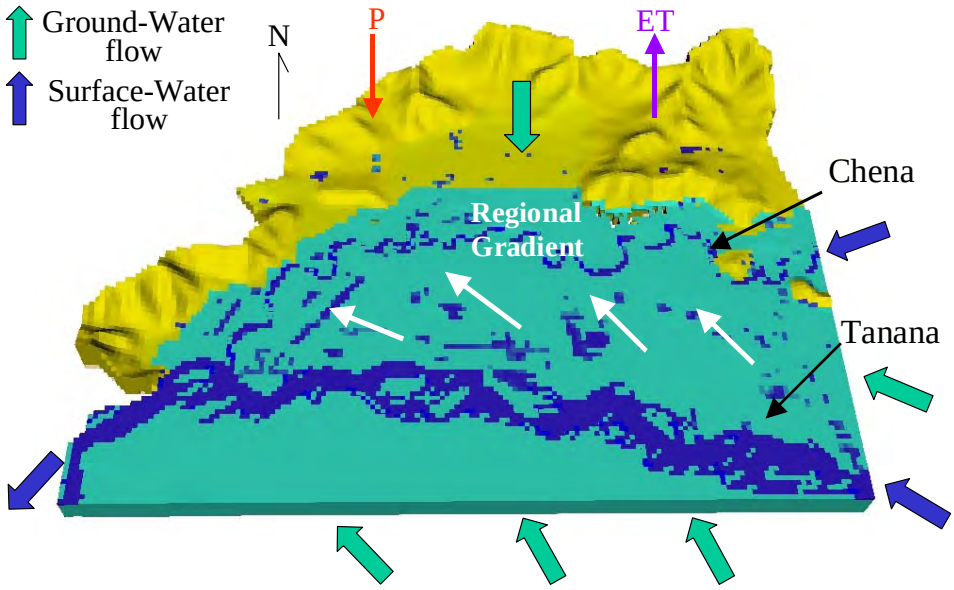

Figure 1. Conceptual model of the Fairbanks floodplain (turquoise) and bordering Uplands (yellow), plan view. Vertical exaggeration 5X

3.3.3 Aquifer Characteristics

One of the key elements in understanding a ground-water flow system is knowledge of its aquifer properties. When combined with water level data, they are used to determine the magnitude and direction of ground-water flow. This information can then be applied to capture-zone delineation.

We primarily use estimates from previous studies (Glass et al., 1996; Nakanishi and Lilly, 1998). Nakanishi and Lilly (1998) estimated aquifer properties on Fort Wainwright by simulating ground-water and surface-water interactions. MODFLOW was used to simulate the flow between the floodplain aquifer and the Chena River during periods of fluctuating river stage. They compared simulated water levels to those in observation wells. The property estimates were determined by selecting the simulated hydrographs that best fit observed hydrographs. The property values, namely riverbed conductance and vertical and horizontal hydraulic conductivity, are listed in Table 9. The authors note that the estimated parameters are non-unique and are valid only when used with all other values in the study.

Table 9: Estimates of aquifer properties. Adapted from Nakanishi and Lilly (1998).

HYDROGEOLOGIC UNIT	PARAMETER	SYMBOL	ESTIMATED VALUE
	riverbed conductance	R_c	350 ft^2/d
alluvium	horizontal hydraulic conductivity	K_h	400 ft/d
alluvium	vertical hydraulic conductivity	K_v	20 ft/d

Aquifer properties that were not estimated in the study were assumed. The values are averages of typical ranges for each aquifer material, as given in hydrogeologic texts such as Freeze and Cherry (1979). One assumed value that has undergone revision is porosity (n). During a four-year study (1999-2002), soil-moisture data were collected with probes installed at several sites on Fort Wainwright. Of these, four sites had probes within the saturated zone through at least part of the year. Water content of probes that were installed within the range of water-table fluctuation would rise and fall with the water level. Figure 50 shows the water content over time of probes at Fort Wainwright Monitoring Well (FWM) 7075. The probes whose plots plateau at their maximum water

content were assumed to have reached saturation. Probes that were always below the water table recorded a relatively constant measurement (i.e., a flat-line plot) and were assumed to be fully saturated. Appendix B shows plots and tables of probe data for all four sites. Since water content is equal to soil porosity under saturated conditions (McWhorter and Sunada, 1977), we assume these saturated values are a close approximation of porosity. Results show an average moisture content of 0.39, a value higher than previous estimates of 0.20 to 0.30 (ASCI/NANA, 2001; Dowl/Ogden, 1997; Braumiller, 2000).

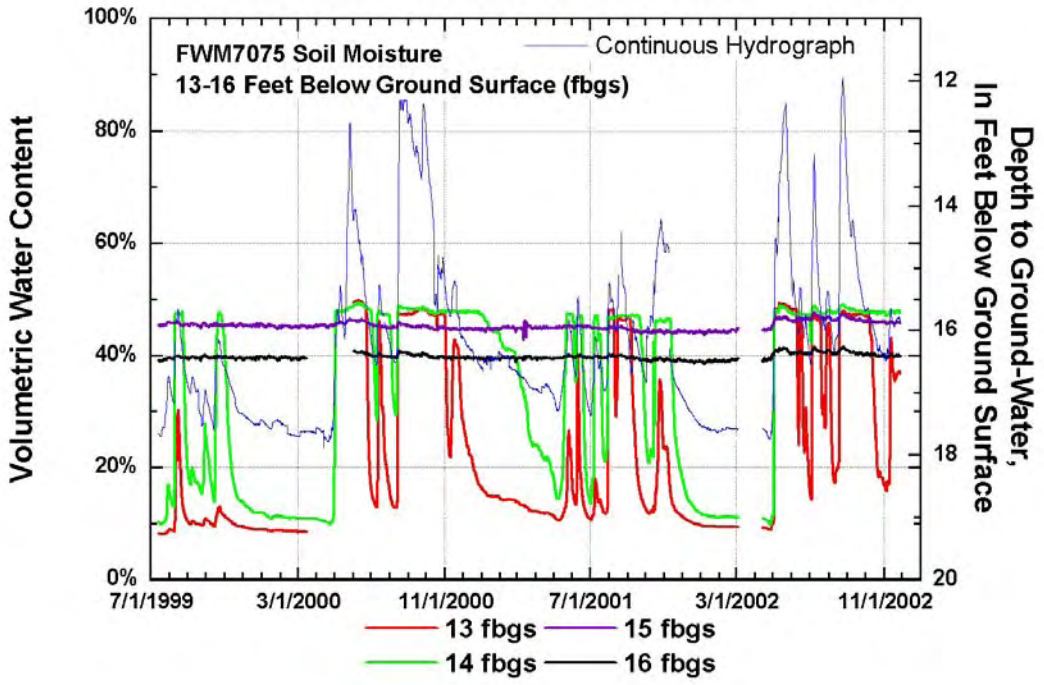

Figure 50. Soil moisture content of probes 13-16 fbgs at site FWM 7075.

The bedrock unit in our conceptual model is assigned a hydraulic conductivity that is approximately three orders of magnitude less than the alluvium. The difference in hydraulic conductivity between bedrock and alluvium indicate why the alluvium is considered to be the main aquifer formation. It is important to note that in fractured rock such as the Birch Hill Sequence, transmissivity can vary widely, perhaps only over a few

feet, depending on the degree of fracturing. Materials recovered from well drilling range from clay (most likely due to decomposed schist) with a hydraulic conductivity of 10E-4 ft/d, to heavily fractured quartzite with a hydraulic conductivity over 1,000 ft/d (Nelson, 1978). A high degree of weathering is unlikely in the floodplain, due to the lack of exposure that the sequence receives (Newberry et al., 1996).

Silts overlying the bedrock are also considered to be relatively low in hydraulic conductivity. Nelson (1978) noted that the vertical hydraulic conductivity of thawed silt is high enough to allow infiltration of rain and snowmelt, but that it is usually too low to yield a significant quantity of water.

3.3.3.1 Permafrost effects

Virtually impervious, the discontinuous permafrost of the Fairbanks floodplain locally acts as a confining layer (Nelson, 1978). Kane and Stein (1983) found that ice-rich frozen soil can have a hydraulic conductivity orders of magnitude less than unfrozen soils. Kane (1980) concluded that no significant recharge occurs to sub-permafrost aquifers in areas with shallow permafrost due to reduced hydraulic conductivity. This effect is more pronounced within the uplands, where silt deposits are more extensive. Within the floodplain, Cederstrom (1963) found that discontinuous permafrost inhibits flow only locally, with no effect on total recharge to the alluvial aquifer. On Fort Wainwright, local permafrost influence is seen at the interface of the floodplain and bedrock aquifers, around the base of Birch Hill. Lawson et al. (1998) investigated hydrogeologic conditions impacted by permafrost between Birch Hill and the Chena River. The conditions studied include the interaction between supra- and sub-permafrost aquifers, as well as flow rates and directions. The researchers concluded that the Birch Hill aquifer exercises a strong seasonal influence even though the overall flow pattern is controlled by the alluvial aquifer. Farris (1996) had similar findings after modeling ground-water flow and contaminant transport in the same vicinity. Model results indicated that permafrost creates steeper local gradients and channelizes flow and transport.

Concerning impacts on water supply, permafrost above or within the aquifer can make well installation more costly, as drillers must often penetrate through dozens of feet

in order to reach thawed alluvium. Furthermore, once a well is installed, maintenance may also be costly since the well may be prone to freezing (Nelson, 1978).

3.3.3.2 Ground-Water Discharge and Recharge

Most ground water leaving the Tanana Basin exits either as ground-water flow through the alluvium or as baseflow to streams and rivers. The Chena River is a chief point of discharge during most of the year. Major public water-supply wells in the greater Fairbanks area are also a source of discharge, although heavy pumping does not seem to have a large impact on water levels (Nelson, 1978). For example, a 24-hour pump test on Fort Wainwright produced only an inch of drawdown in an observation well 204 ft from the pumping well (Feulner, 1961). Results of other pump tests on Fort Wainwright and elsewhere in the floodplain are similar (Nelson, 1978). ET is another potential source of ground-water discharge. However, ET data within the floodplain are lacking. Though Dingman (1971) and Gieck (1986) investigated ET rates in the Fairbanks area, the study sites were in upland watersheds north of the floodplain.

The primary source of recharge to the Fairbanks sub-regional aquifer is ground-water flow from the south and east (Figure 49). At times of high stage, the Tanana and Chena Rivers also contribute recharge; these two rivers are discussed further in the following section. Adjacent bedrock is another source of recharge. In addition to horizontal flow from the uplands, evidence of upward vertical gradients in the alluvium (US Army/ACE/UAF, 2003) indicate that flow is also coming from underlying bedrock in the floodplain.

Lastly, snowmelt often contributes significant amounts of recharge. In a Fort Wainwright monitoring project that recorded ground-water levels through 4 years (1999-2002), levels on post rose by an average of 2 feet (US Army/ACE/UAF, 2003) during and immediately after spring snowmelt. Heavy rain has a similar impact following a storm event. However, normal precipitation events in cold regions such as interior Alaska do not contribute substantial amounts of recharge to aquifers. Due to typically light rainfall and moisture deficiencies in the shallow root zone, summer precipitation replenishes soil water lost to ET (Kane, 1980). The amount of precipitation reaching the

water table depends heavily on the surficial geology and landscape. That is, relatively permeable formations such as the alluvium receive higher volumes of recharge than the less-permeable silts. Likewise, flat terrain will allow more water to infiltrate than steep slopes, which allow for more runoff.

3.3.4 Surface Water Contributions

3.3.4.1 Tanana River

The Tanana's headwaters originate in the Wrangell Mountains. It is a braided river and flows primarily northwest for 550 miles before joining the Yukon River. It is the Yukon's chief southern tributary. As stated in section 3.3.3, the Tanana River is a transient source of recharge to the Fairbanks sub-regional aquifer. The river's average discharge between 1973 and 2002 was 20,186 cfs at the USGS Fairbanks gauging station (USGS, 2004). Approximately 85% of the Tanana's recharge is from snow and glacial melt in the Alaska Range, while the remaining 15% originates in the Yukon-Tanana Uplands (Anderson, 1970). Due to much of its recharge originating from glacial melt, the Tanana River discharge increases during hot, dry weather. Peak melting time in the Alaska Range is usually in July. However, at times of cool weather, low temperatures tend to coincide with higher precipitation rates. Therefore, the decrease in melting is sometimes offset by an increase in rain. The snow and glaciers of the Alaska Range act as reservoirs by storing water at times of relatively high precipitation and release it during warm, dry periods (Nelson, 1978).

3.3.4.2 Chena River

The Chena River is a tributary of the Tanana. The headwaters begin toward the north-central border of the Tanana Basin. The river meanders in a west-southwest direction. Unlike the Tanana, the Chena is more locally influenced, receiving most of its recharge from local snowmelt, summer precipitation, and baseflow. Peak flows tend to occur in May and August due to snowmelt and seasonal peak rainfall, respectively. The average discharge between 1949 and 2002 at the USGS gauging station at Fairbanks is 1360 cfs (USGS, 2004). The Chena River typically drains rather than feeds the floodplain aquifer. During periods of high discharge, however, a flow reversal occurs if the stage rises above

the adjacent ground-water level (Figure 51). Glass et al. (1996) found that ground-water levels within a ½ mile of the Chena respond rapidly to changes in river stage. For example, following a storm event in July of 2003, wells near the river showed a rise of over 5 feet (US Army/ACE/UAF, 2003). During bank recharge in the spring, Wegner (1997) found surface-water influx from the Chena River occurring between depths of 17.5 to 30.0 feet below ground surface and extending up to 100 feet laterally.

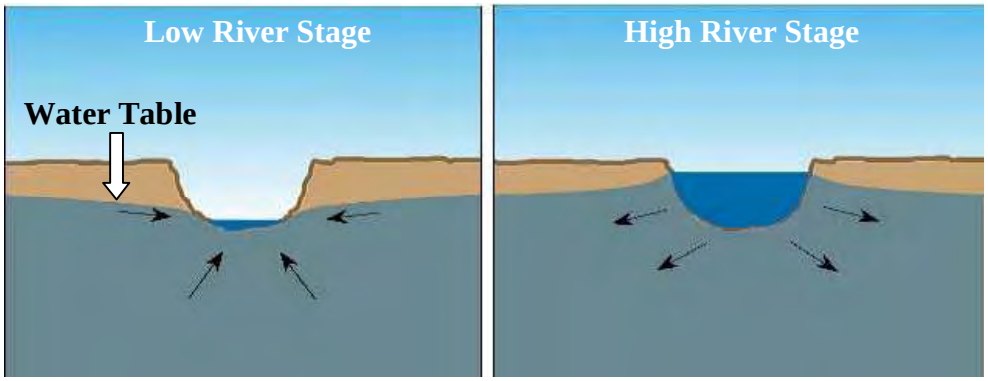

Figure 51: Ground-water flow reversal during high stage of Chena River (Wegner, 1997). Black arrows indicate flow direction.

3.3.4.3 *Fort Wainwright Cooling Pond*

The cooling pond on Fort Wainwright is used as a cooling system for the post's power plant. It is man-made and unlined. The pond is about 12 to 14 feet deep (Adams, 2005) and 500,000 square feet in area. Water circulates through the plant at rates ranging from 12,000 to 20,000 gpm (ASCI/NANA, 2001). In summer, the cooling pond is sometimes supplemented with a pumping well, located at the southeast corner of the plant, when the water temperature rises above a certain threshold (Malen, 2005). Frequency and rates of pumping are unknown, as pumping records are not available. Due to ice-fog induced by the pond, its use will be discontinued in the next few years and replaced with an air circulation system. However, there are currently no plans to alter the pond.

The pond lies about a quarter-mile up-gradient of WS 3559. Studies have shown that the cooling pond exerts a significant thermal effect on the ambient ground water. Shallow ground-water samples near the pond have been over 20°F warmer than the elsewhere on

Fort Wainwright (Pollen, 1999). WS 3559 appears to be within this thermal plume, as ground-water temperatures from the well historically match those of the pond. Fluoride levels between the two also correspond (Pollen, 1999). Hydrologic effects of the pond's heated water may include increased infiltration, which could possibly induce local mounding of the water table (ASCI/NANA, 2001), although no evidence has been presented. Section 3.4.2 describes further research on the pond's influence.

3.4 PREVIOUS CAPTURE-ZONE DELINEATIONS ON FORT WAINWRIGHT

Prior to WHP and SWA plans, state regulations concerning Fairbanks-area ground water were primarily issue- and site-specific. Law-makers focused on issues such as wastewater disposal (Nelson, 1978) and on sites that with existing contamination. Only within the past 10-15 years have comprehensive efforts been made to protect Fort Wainwright's ground-water supply.

3.4.1 Wellhead Protection and Source Water Assessment Programs

In 1997, the DOWL and Ogden Joint Venture completed a Wellhead Protection report on Fort Wainwright for the Army Corps of Engineers in accordance with EPA national guidelines (DOWL/Ogden, 1997). As a first step in the program, they selected the CFR method to delineate WHPAs. More sophisticated methods such as hydrogeologic mapping, analytical solutions and numerical models were also considered but not chosen due to a reported lack of data. For example, theses methods require knowledge of the hydraulic gradient. The authors felt that an accurate hydraulic gradient (i.e., one that accounts for pumping effects) could not be calculated due to incomplete pumping records and discontinuous pumping intervals (DOWL/Ogden, 1997). As discussed earlier, CFR has many limitations, such as the inability to account for well interference; Figure 52 shows the overlapping delineations. However, the authors deemed the method acceptable because most of the delineated wells operate at different time intervals.

Figure 52: Example of Fort Wainwright WHPAs delineated using CFR (Dowl/Ogden, 1997). WS 3559 and its delineation are marked in red.

The Army also produced a Source Water Assessment report a few years later (US Army Corps of Engineers, 2000). It is essentially an update of the WHP report; the only significant differences are the inclusion of newly-operating wells and omission of inactive wells. The report assesses the main drinking water supply wells on post, as well as eleven wells used for backup, fire protection, and areas outside of the main distribution system (US Army Corps of Engineers, 2000).

ADEC also produced SWA reports for Fort Wainwright water-supply wells (ADEC, 2004). All Class A wells (i.e., wells serving communities or non-transient non-

community populations) on post were delineated, for a total of eight wells (Figure 53). The ADEC SWA Program was referred to earlier in section 1.2 because we apply the analytical portion of their capture-zone delineation method in our study. ADEC used a range of parameter values based on USGS reports, well logs, and textbook estimates. The capture zones were drawn to follow three water-table configurations that occurred during varying stages of the Chena and Tanana Rivers between 1986-1988 (Glass et al., 1996). ADEC's methodology also includes safety factors to account for method error and hydrogeologic uncertainty. We briefly compare the WS 3559 delineation with our results in section 5.

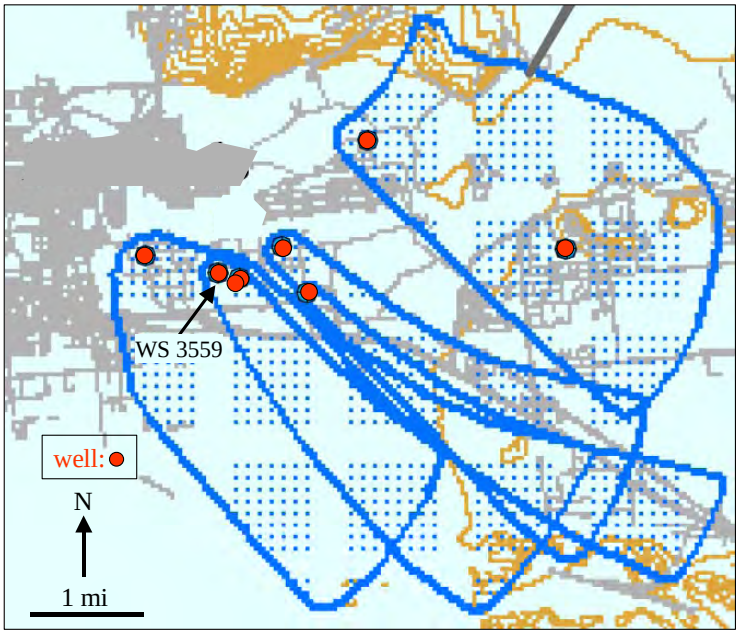

Figure 53. ADEC capture-zone delineation of Fort Wainwright water-supply wells (Modified from ADEC, 2004).

3.4.2 Ground-Water Contamination Studies

There have been many ground-water contamination studies on Fort Wainwright over the past decade. Most contamination is due to fuel, lubricant, and solvent spills and leaks. Covering all of these studies is beyond the scope of this paper. Here we cover a few that involved the primary water-supply wells.

In 1994, Harding Lawson and Associates investigated the extent of contamination from several sources around Building 3564 (Figure 45). The building is southeast of the current and past primary water-supply wells on post (WS 3559, WS 3563, and WS 3565). In terms of the regional ground-water flow, the site is up-gradient of the wells. Data were gathered from soil borings, shallow and deep ground-water probes, and monitoring wells. Investigators sampled for gasoline range organics (GROs), diesel range organics (DROs), volatile organic compounds (VOCs), and benzene, toluene, ethylbenzene, and xylene (BTEX). DRO contamination was found at and below the water table at the site and also in an area about 800 feet down-gradient of the site. Since there was no apparent source at the down-gradient location, it was hypothesized that a plume had formed and moved from the site to that sampling area. However, in 1995 CH2MHILL continued the investigation and revised the results of 1994 so that the down-gradient DRO levels were considered to be at 'non-detectable' levels (CH2MHILL, 1996a). Thus, the levels were no longer linked to contamination around the source area and the original hypothesis was rejected. Nonetheless, the areas determined to have significant ground-water contamination fell within the Army's WHPA.

As a follow-up to that investigation, a numerical model was designed to simulate ground-water flow at the site, with the objective of evaluating the hydraulic influence of the water-supply wells mentioned above (CH2MHILL, 1996b). They examined whether the pumping wells caused contaminants, namely diesel fuel, to be pulled downward through advection. A finite-element model and particle tracking were used to delineate the wells' capture zones (Figure 54). It was concluded that the primary water supply well, WS 3559, does have a significant impact on contaminant movement, and that contaminants will reach the well's screened interval unless otherwise diluted, retarded, or biodegraded enough to reduce concentrations to non-harmful levels. Modelers noted that result credibility was limited by uncertainty of parameter values, especially the vertical hydraulic conductivity; hence, conclusions could change considerably if local aquifer tests revealed values that were far different from those applied in the model

(CH2MHILL, 1996b). In addition, the influence of surface-water bodies, such as nearby ponds, were not taken into account because they were not simulated in the model.

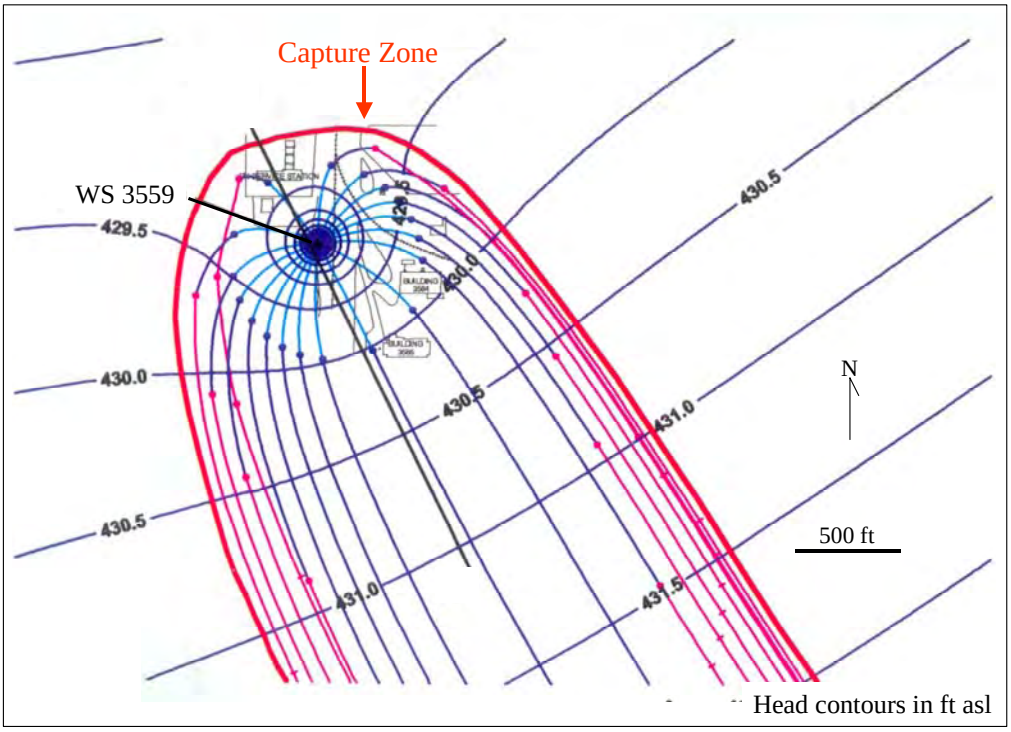

Figure 54. WS 3559 capture zone as delineated by CH2MHILL (modified from CH2MHILL, 1996b).

To look at the degree and effects of pond recharge to the primary water supply wells, Northern Testing Laboratories (NTL) conducted a study in 1999 (Pollen, 1999). The study was prompted by evidence that WS 3559 was receiving recharge from one or both of the two nearby ponds. One pond is the power plant cooling pond, while the other is the smaller discharge pond for the post's water treatment facility (section 3.1.1). Signs of pond influence included the following:

- a biofilm appearing on the surface of manganese greensand filters;
- algal growth on the walls of a water treatment facility sink, in which well water was discharged;

- high algae and diatom levels in a microbial particulate analysis (MPA) in 1995; and
- unusually high temperatures (57F-64F) of WS 3559 water, which were historically similar or equivalent to those of the cooling pond

NTL performed a chemical analysis, MPA, and tracer study of the two ponds and nearby pumping wells (including WS 3559). They found strong similarities between the cooling pond and WS 3559 in regards to temperature and fluoride concentration. The MPA showed only a weak correlation, however, and the species of algae found in the water treatment facility's sink did not match any species within either pond. Researchers concluded that the cooling pond directly influences shallow water-supply wells such as WS 3559, although the travel time for pond water to reach the wells is unknown. The wells are believed to be in the path of the cooling pond's thermal plume, and seasonally warm water from the settling pond may also contribute recharge. However, microbial data did not show direct influence from either pond according to ADEC's regulatory criteria. The report states that even though there had been an indication of limited influence over the four years preceding the study, data suggest that natural attenuation is effectively removing or inactivating the indicators. For instance, coliform bacteria levels in the ponds ranged from 146 to 470 cfu/ml, while the well samples were all less than one cfu/ml (Pollen, 1999).

Another potential source of contamination near the primary water supply wells is the coal storage yard, an area directly south of the post's power plant (Figure 45). The coal storage yard has existed since 1960 and was used as a fuel staging area for the plant. It is unlined and was routinely sprayed with petroleum, oils, and lubricants to enhance the fuel's energy content between 1960 and 1993. The spraying resulted in soil and ground-water contamination that exceeded ADEC Cleanup Standards and EPA Region 3 Risk-Based Concentrations (ASCI/NANA, 2001). Sampling of soil and monitoring wells began in 1997, along with a combined soil vapor extraction and air sparging system east of the coal pile, and continued through 2000. One study (ASCI/NANA, 2001) delineated the ZOC around WS 3559, which lies down-gradient (i.e., northwest) of the coal storage

yard (Figure 55). The authors delineated the ZOC to determine whether monitoring well locations were adequate to detect contamination. An analytical solution was applied and consisted of three parts: Neuman's solution, the UFE, and a TOT equation. Neuman's solution calculates drawdown in unconfined aquifer using the well function ($W(u_A u_B,L)$). The UFE defines the ZOC as described in section 1.1.2.3, with the addition of a third dimension: the maximum depth up-gradient of the ZOC (z_{max}). This maximum depth is computed as ($2\, y_{max}/a$), where a is the ratio of horizontal to vertical hydraulic conductivity. The TOT equation calculated the distance up-gradient from which contaminants traveled over a given time:

$$t = \frac{S}{v\left(d_n - r_w\right)} + x_{sp} \ln\left[\frac{x_{sp} + r_w}{x_{sp} + d_n}\right] \tag{27}$$

where S is storativity and d_n is the up-gradient distance traveled parallel to the flow direction in n years (ASCI/NANA, 2001). Since the equation solves for time, the distance d_n must be substituted into the equation iteratively until t equals the desired TOT.

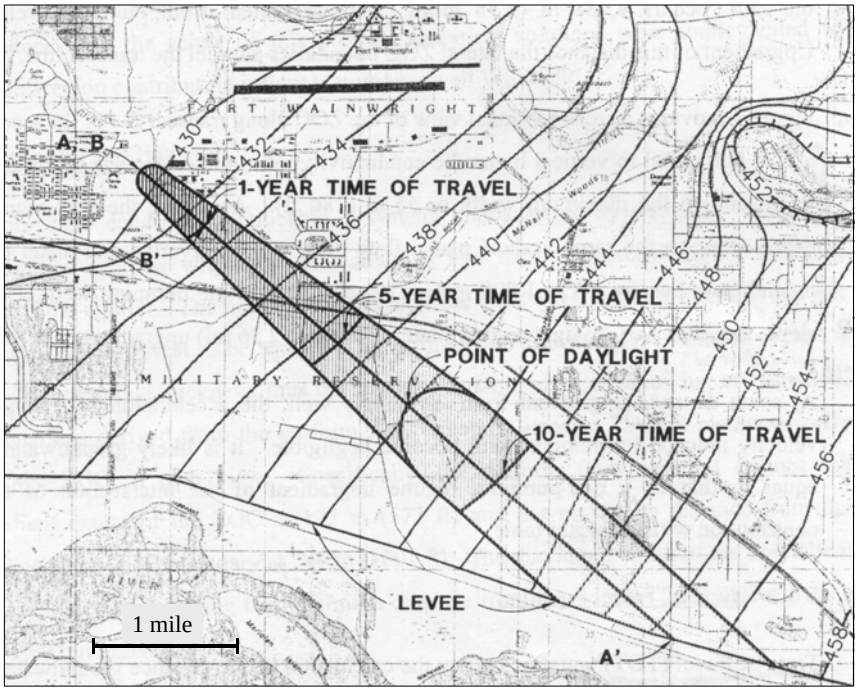

Figure 55. WS 3559 ZOC, as delineated by ASCI/NANA Joint Venture (2001).

The contamination source-area did not lie within the resulting ZOC. However, two samples from one of the study's sampling events contained contamination level excedences and were within the ZOC. In evaluating the monitoring well coverage, 18 of the 20 fell within the ZOC, although only 5 were screened through it. Due to the upward vertical gradient found in the ground water at the site, researchers concluded that light non-aqueous phase liquid (LNAPL) contaminants would not migrate downward, but that dense non-aqueous phase liquids (DNAPL's) did pose such a risk. The report recommends shallow monitoring wells be installed to detect such migration. Furthermore, the report notes the limitations of the delineation method due to its many assumptions. For example, contaminants are assumed to move advectively with the ground water because the UFE does not account for contaminant transport processes such as dispersion, sorption, and attenuation.

4 FIELD CASE APPROACH

In our field case, we apply the four delineation methods used in the synthetic case studies (section 1.2). Input parameters of the first three methods (CFR, UFE-Thiem, and WHPA) are similar to those of Case 1. However, due to the numerical method's ability to incorporate large amounts of field data, its design is far more extensive than in previous cases. The following sections are devoted to its development.

It is important to note that the numerical model was not created specifically for this study. It was designed to simulate ground-water flow over the entire Fairbanks floodplain. The domain encompasses a much larger area than our site. It is a sub-regional model that was developed by the USGS in the 1990's. MODFLOW-88 was the original version used. We have recreated the model in MODFLOW-2000 using the original input files, with a few updates based on the analysis of new data (section 3.3.3).

4.1 ASSUMPTIONS

Although numerical modeling is more sophisticated than our other methods, assumptions must still be made due to limits on data and model capability. Our assumptions in the design and application of the sub-regional model are as follows:

1. Steady-state hydrologic conditions prevail. That is, there is no change in head or storage with time. Though transient conditions can significantly affect the flow regime, it is standard modeling procedure to first simulate steady-state conditions in order to understand the fundamentals of ground-water flow, and then move on to transient conditions. Furthermore, Reilly and Pollock (1995) found that cyclic stresses do not appear to impact capture areas if the ratio of travel-to-stress time is much greater than one (section 1.1.3). This indicates that seasonal processes might not impact the capture area significantly when using our ten-year TOT. Thus, although transient simulations will help to further understand the system, steady-state conditions meet our present objective of studying flow to WS 3559.
2. Due to their relatively stability, late-winter water levels best approximate steady-state conditions and are therefore used in model verification.

3. Effects of small-scale heterogeneities of the Chena Alluvium have a negligible impact on flow at a sub-regional scale. Hence, the alluvium is assigned an average (or bulk) hydraulic conductivity value (section 3.3.1).
4. The alluvial portion of the southern and eastern limits of the model domain can be represented as specified-head (constant-head) boundaries (section 4.2.2).
5. The aquifer receives recharge aerially. The top surface of the model is therefore a specified-flow boundary.
6. All other model boundaries (North, West, and bottom) are considered no-flow (section 4.2.2).
7. Ground-water enters the aquifer system through areal recharge and the constant-head boundaries.
8. Ground-water exits the system primarily through the Chena and Tanana Rivers, and also through discharge wells and the constant-head boundaries.
9. Evapotranspiration is incorporated into the net recharge term
10. The simulated discharge wells pump continuously at constant rates. Available pumping records show only small variations among average daily rates.
11. Intermittent pumping of back-up and emergency water-supply wells on Fort Wainwright has a negligible impact on long-term (i.e., pseudo-steady state) conditions.
12. Surface-water features not simulated in the model, such as Noyes Slough, do not impact our results. Based on evidence of the Chena River's effects on ground-water flow (Wegner, 1997; Glass et al., 1996), localized influence of these features is unlikely to reach our study area.
13. Permafrost effects are considered negligible at our study site. Although the presence and influence of permafrost on Fort Wainwright has been heavily studied north of the Chena River (Farris, 1996; Lawson et al., 1998), little information exists on permafrost south of the Chena River. Significantly less permafrost is believed to exist on the south side (Péwé et al., 1975)

4.2 GENERAL FEATURES

The sub-regional model was re-created in MODFLOW-2000 using a USGS pre-processor known as MFI (Harbaugh, 2002). A number of input parameters are entered into MFI to construct the model grid. MODFLOW groups the parameters into modules, or 'packages.' They are listed in Table 10. The sub-regional model's general features are described in the following sections. Appendix C contains the package files used in our simulation.

Table 10: Input parameters used in our MODFLOW model.

MODFLOW Package	Name	Input Data	Data Format
Discretization	**DIS**	**horizontal grid spacing**	**2-D array/layer**
		(no. row and column, dimensions)	
		vertical spacing	**2-D array/layer**
		(bottom elevation per layer)	
		Layer type (e.g., confined)	**single values**
Basic	**BAS**	**hydraulic boundary conditions**	**2-D array/layer**
		(specified-head, no-flow, variable-head)	
		initial head conditions	**2-D array/layer**
Block-Centered Flow	**BCF**	**hydraulic conductivity**	**2-D array/layer**
		(horizontal and vertical per layer)	
Solver: Pre-Conjugate	**PCG**	**solver specifications**	**single values**
Output Control	**OC**	**result fomatting**	**single values**
		times for saving heads and flows	**single values**
Recharge	**RCH**	**recharge rates**	**2-D array/layer**
Wells	**WEL**	**pumping rate per well**	**list: 1 line/cell**
Rivers	**RIV**	**river specifications**	**list: 1 line/cell**
		(conductance, stage, bottom elevation)	**list: 1 line/cell**
Observation Process	**OBS**	**head observations**	**list: 1 line/cell**
MODPATH	**MPATH**	**particle-tracking specifications**	**2-D array/layer**

4.2.1 Model Extent and Discretization

The model domain is designed to best simulate our conceptual model (section 3.3.2). The grid is 15 miles from West to East, and 11.2 miles North to South. However, due to the rectangular nature of the grid, the model contains many inactive cells around its borders, and so the actual domain extent is less in some areas. The horizontal grid divides the domain into 118 rows and 158 colums, with square cells 500 feet on a side (Figure 56). Vertically, the model varies in thickness. The average thickness of the model in the floodplain region is approximately 1200 feet. It consists of four layers. A DEM was created to represent the land surface; elevations were extrapolated from USGS 1:24000

topographic maps of the area. The DEM was then used to create the top and bottom elevations of layer 1. Layer 2 is a constant thickness of 100 feet. Layers 1, 3, and 4 are of variable thickness, although layers 1 and 3 are constant throughout much of the model: within the floodplain, layer 1 remains at 55 feet, and layer 3 remains at 150 in the northern half of the domain. South of the Chena River, layer 3 begins increasing in thickness (Figure 57). This is due to the fact that the layer 3-4 interface is modeled after the bottom of the alluvial aquifer. In other words, the top surface of the underlying bedrock is the top of layer 4. The aquifer thickness increases to the south as the bedrock elevation deepens. The bottom of the model remains constant at 600 feet below sea level.

It is important to note that the model's depth to bedrock was interpolated. The modelers based their interpretations on available borehole and well depths throughout the floodplain, and on the geologic history of the region.

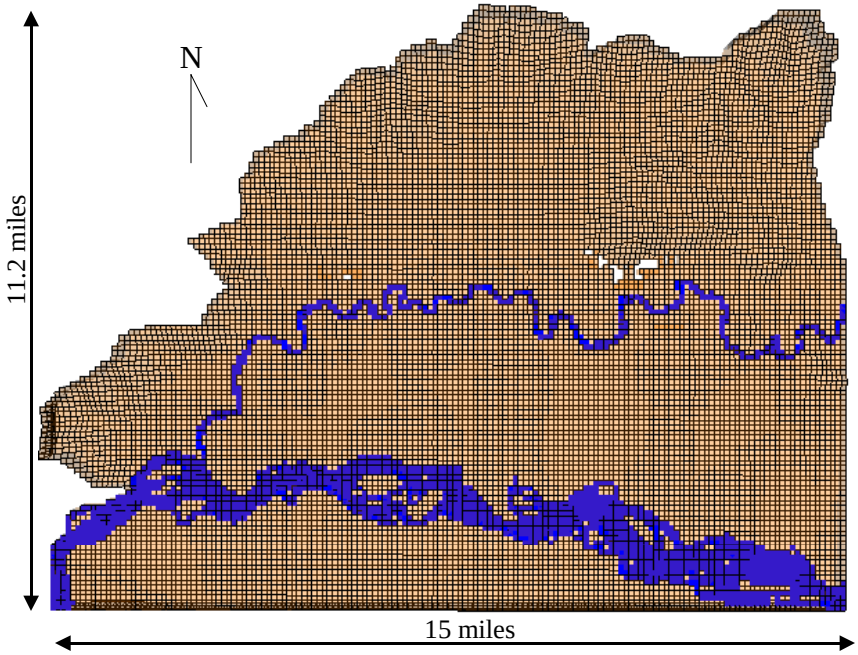

Figure 56. Plan view of the 3-D finite difference model grid. Grid is horizontally discretized into 500x500 foot cells.

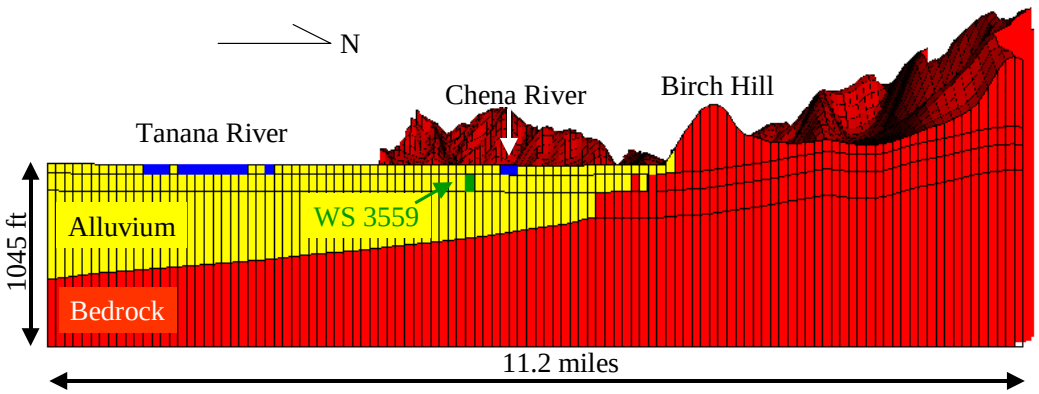

Figure 57. North-South cropped section through column 110 of the model. Vertical exaggeration 5X.

4.2.2 Boundary Conditions

Boundary conditions are specified in the Basic package of MODFLOW. Each layer requires a 2-D array of cell codes known as IBOUND arrays. The codes are as follows:

Specified-Head: IBOUND < 0

No-Flow: IBOUND = 0

Variable-Head: IBOUND > 0

As stated in section 4.1, there are constant-head boundaries on the south and east sides of the model grid. These cells receive a negative IBOUND value. Along the southern border, the constant head boundary covers the full extent of the top three layers, while the extent over the eastern border is more limited (Figure 58). These cells represent all of the alluvium at the limits of the model domain. They are constant-head due to the ground-water flow entering and leaving the sub-regional aquifer to the south and east (Figure 49).

Other than the entry and exit points of the Chena and Tanana Rivers, the rest of the model's boundaries consist of bedrock. These bedrock cells are set as no-flow boundaries. A no-flow boundary condition is assigned because the amount of ground-water flow entering and exiting the alluvial aquifer through bedrock is considered negligible.

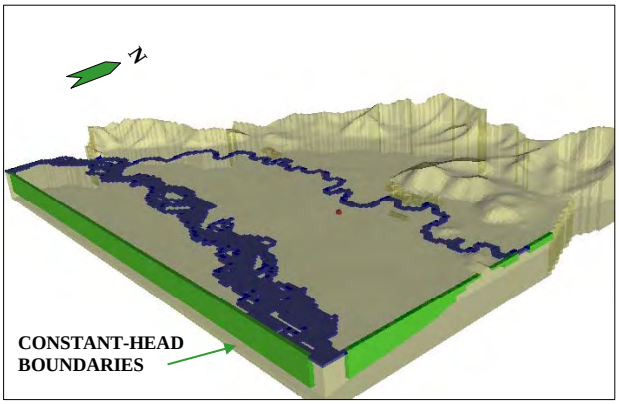

Figure 58. Illustration of constant-head boundaries (green) at southern and eastern edges of model domain. Vertical exaggeration 5X.

4.3 SYSTEM PARAMETERS

Horizontal and vertical hydraulic conductivity are required input to an MODFLOW model. In addition to these, the sub-regional model includes parameters to simulate aerial recharge, wells, and rivers.

4.3.1 Hydraulic Conductivity

Horizontal hydraulic conductivity values in the model are part of MODFLOW's Block-Centered Flow (BCF) Package. They are divided into zones based on the hydrogeologic units (3.3.2) in each layer. There are seven zones altogether (Table 11). They were represented in the IBOUND codes of the Basic package. Figure 59 displays the zones.

To simulate vertical anisotropy, the hydraulic conductivity between layers is equal to 1/20 the horizontal component in alluvial cells. In bedrock and silt cells, the vertical and horizontal hydraulic conductivities are equal. Vertical hydraulic conductivity is not specified as an independent term in the BCF Package. Rather, it is input as a vertical conductance, which is a function of thickness as well as hydraulic conductivity. The vertical hydraulic conductivity of a given cell applies to the downward movement toward the underlying cell. To calculate vertical conductance, the vertical conductivity is divided by the distance between the cell's node and the node of the cell directly beneath it. As such, vertical conductance is not specified for cells in the bottom layer of the model.

Table 11. Horizontal hydraulic conductivity zones in sub-regional model.

Color	Zone	Formation	value (ft/d)
	K_1	alluvium	400
	K_2	silt	1.0
	K_3	silt/bedrock	0.75
	K_4	bedrock	0.75
	K_5	ponds	2500-25000
	K_6	permafrost	0 (inactive)
	--	rivers	--

Layer 1

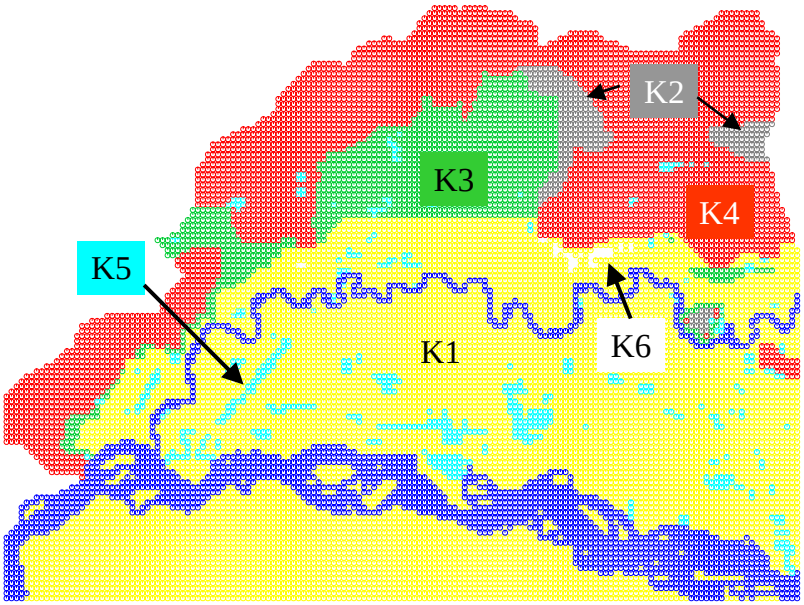

Layer 2

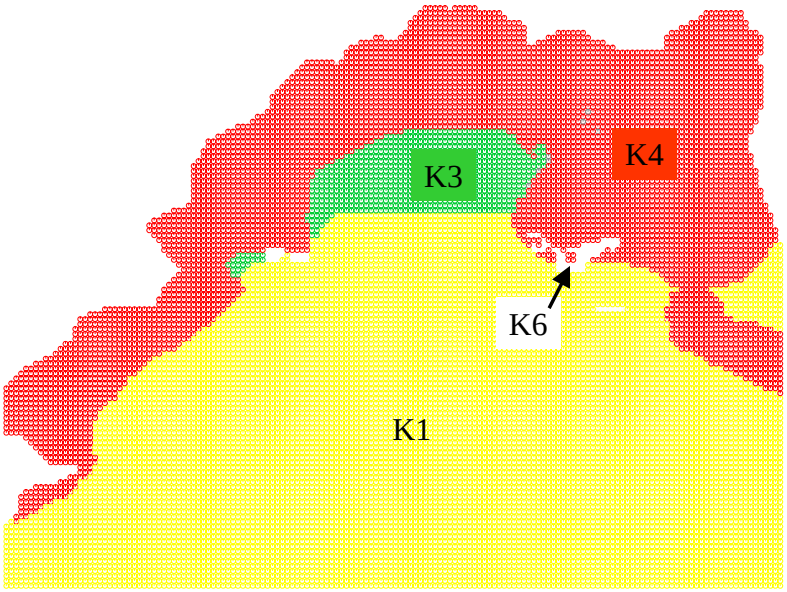

Figure 59. Hydraulic conductivity zones in the Fairbanks sub-regional ground-water flow model for layers 1 through 4, with layer 4 being the deepest.

Layer 3

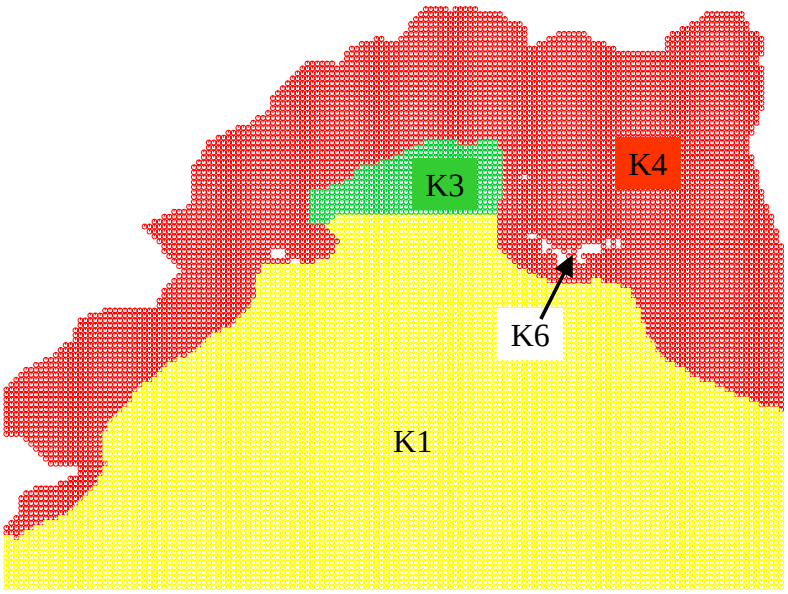

Layer 4

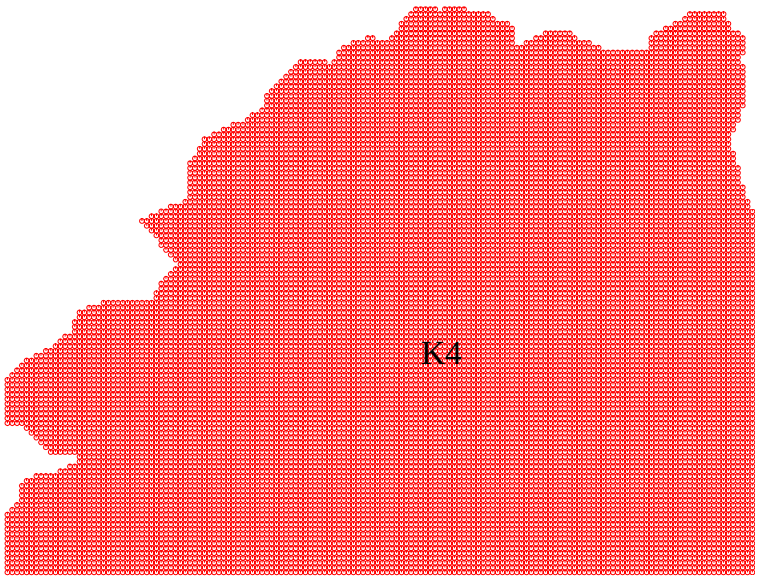

Figure 59 (continued).

As the table indicates, inactive (white) areas represent permafrost. They are located at the base of Birch Hill and at UAF. These cells are a partial representation of permafrost extent in the floodplain. Refinement of permafrost distribution should be a major objective of future modeling (section 4.5). Because the permafrost cells that currently exist are not near or up-gradient of WS 3559, they do not impact our simulation results.

Note that ponds are simulated as high-K cells. Their K-value is 25,000 feet/day, although the actual cell values were assigned a range of 2500-25,000 feet/day based on the percent of the cell that is occupied by the pond. Assigning high-K values to cells is one method of simulating surface-water bodies in MODFLOW. The method may be used in settings where no significant stress (e.g., a nearby pumping well) is applied to the surface-water body. As such, the cells representing the Fort Wainwright cooling pond are not simulated using high-K values. Due to its potential impact on flow to WS 3559, the cooling pond is simulated using MODFLOW's River Package (section 4.3.4). We selected the River Package (section 4.3.4) because it provides a more realistic representation of surface-water interaction with the aquifer.

4.3.2 Recharge Package

Recharge is applied to the top layer of our model as a depth per unit time. The domain area is divided into five recharge zones (Figure 60). Each is an estimated fraction of the average annual precipitation (11 inches/year) that reaches water table. They are based on surficial geology and landscape. For instance, flatter areas with a lot of standing water (e.g., floodplain) tend to receive more recharge than steep slopes. Likewise, highly permeable formations receive more recharge than less permeable formations. Table 12 provides a summary.

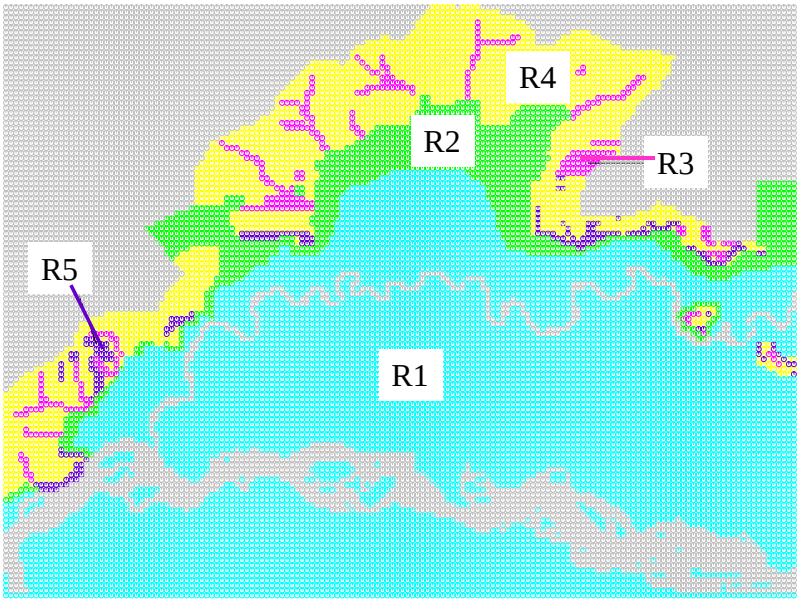

Figure 60. Recharge zones applied to layer 1 in sub-regional model. Gray indicates areas of no recharge.

Table 12: Explanation of recharge terms in Figure 60.

RECHARGE ZONE	VALUE (IN/YR)	% OF PRECIP	REGION
R1	8.8	80	floodplain
R2	6.6	60	silty areas
R3	4.4	40	flat areas of uplands
R4	2.2	20	bedrock
R5	1.1	10	steep slopes

4.3.3 Well Package

The sub-regional model thus far includes the four major public water-supply wells in the Fairbanks area. Figure 61 shows well placement, and Table 13 lists pumping information.

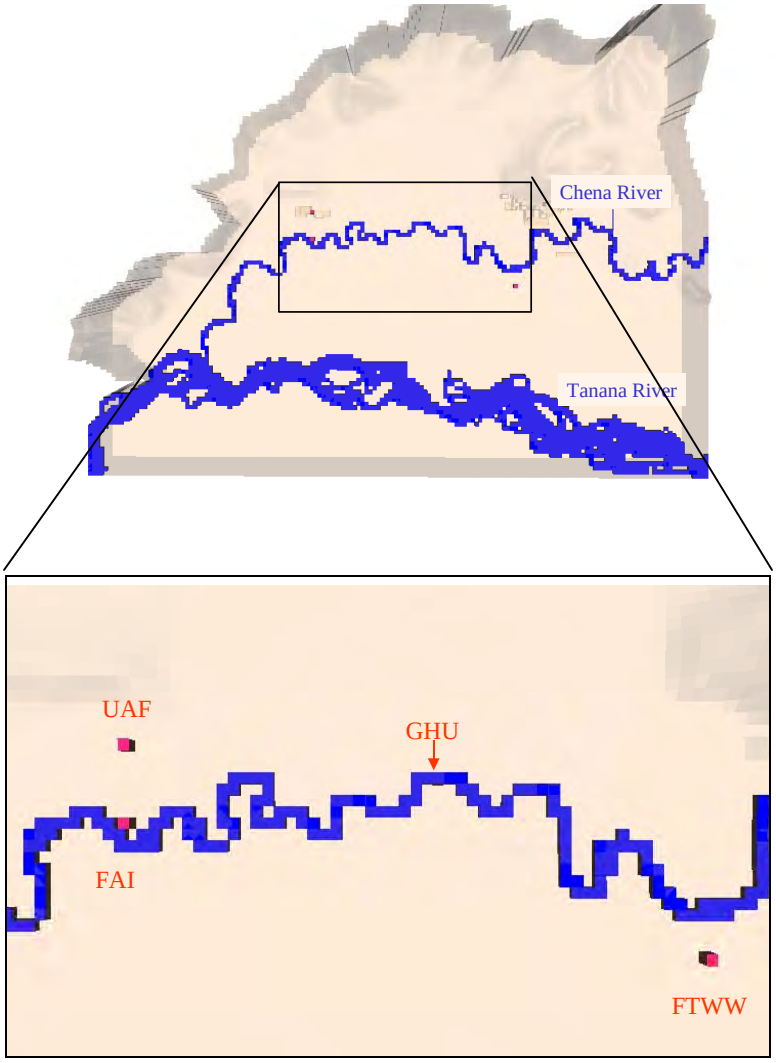

Figure 61. Close-up of water-supply wells in sub-regional model. Note that GHU well lies adjacent to the Chena River.

Table 13. Public water-supply wells in sub-regional model.

Well	Abbreviation	Average Pumping Rate (gpm)	Screened Layer
Fort Wainwright	FTWW	1100	2
Golden Heart Utilities (Municipal)	GHU	2100	2
Fairbanks International Airport	FAI	1000	2
University of Alaska Fairbanks	UAF	250	2

4.3.4 River Package

MODFLOW's River Package simulates ground-water interaction with surface-water through a head-dependent boundary condition. Each cell that is part of a river reach is treated as a separate entity, and so surface-water flow is not actually represented. The side-walls of the cells are set as impermeable, and so the bottom of the cell is the only cell-face interacting with the aquifer. The user specifies three constants: the river stage (H_{RIV}), river bottom elevation (R_{BOT}), and riverbed conductance (C_{RIV}). Conductance is calculated as:

$$C_{RIV} = \frac{K_v LW}{M} \tag{28}$$

where K_v is the riverbed's vertical hydraulic conductivity; L is the reach length; W is the reach width; and M is the riverbed thickness. The three input terms are used to calculate flow into the aquifer (Q_{RIV}):

$$Q_{RIV} = C_{RIV}(H_{RIV} - R_{BOT}) \qquad \text{if } h < R_{BOT} \tag{29}$$

$$Q_{RIV} = C_{RIV}(H_{RIV} - h) \qquad \text{if } h > R_{BOT} \tag{30}$$

According to this relationship, Q_{RIV} is negative if $h > H_{RIV}$, and flow reverses into the river.

We use the River Package to simulate the Chena and Tanana Rivers in layer one of the model. Data from USGS gauging stations were used to calculate average values of

river stage (H_{RIV}) and bottom elevation (R_{BOT}). Averaged data from three gauging stations were used for the Tanana River values, while 13 stations were used for the Chena River. The averaging assumes a constant linear slope in the stage and bottom of both rivers. Values for river conductance (C_{RIV}) were calculated using a riverbed hydraulic conductivity (K) of 5 feet/day and a riverbed thickness (M) of 1 foot. This allows for a maximum conductance of 1.25×10^6 feet^2/day, since cell dimensions (LxW) are 500x500 feet. In instances where river dimensions do not fill the cell, values are lower; the minimum value per cell is 9.39×10^4 feet^2/day. Thus, cell conductance values depend on what portion of its area is occupied by the river.

The Fort Wainwright cooling-pond cells are also simulated with the River Package, as noted in section 4.3.1. Measurements of pond-surface elevation were used to estimate H_{RIV} (431 ft asl). In the conductance calculation, we assume the K_v of the unlined pond bottom is equal to that of the aquifer (20 feet/day), and the bottom thickness is set to one foot. These values produce a maximum conductance of 5.0×10^6 feet^2/day, but like the Chena and Tanana River simulations, the value is less where the cooling pond does not cover the full area of the cell.

4.4 MODEL VERIFICATION

During the model's original development, calibration efforts were performed. Modelers compared simulated heads with available water table maps (Glass et al., 1996) and other ground-water level observations in the floodplain. Boundary conditions and input parameters were adjusted until comparable simulated heads were achieved. We verify some of these simulated head values in our study. Our objective is to model ground-water flow to Fort Wainwright's primary water-supply well. The model is used as a tool for delineating the well's capture zone. Thus, rather than verify results of the entire model domain, we focus on model output within our study area. In this section, we briefly examine the model's water budget and verify simulated heads with water-level observations on Fort Wainwright. Further modeling results (e.g., budget and head output for all cells in the grid) are provided in Appendix C.

4.4.1 Water Balance

Table 14 shows the water budget analysis of our sub-regional model simulation. Because this is a steady-state simulation, no change in storage occurs. We see that inflow comes from recharge at the upper model surface and from constant-head cells at the southern and eastern boundaries (Figure 58). Note that these two sources make approximately equal contributions (46% from recharge, 53% from constant head). Also note a small portion (1.1%) of inflow coming from river leakage; this inflow is provided by the cells that represent the cooling pond (section 4.3).

Table 14. Water Balance of sub-regional model simulation.

Water Balance of Cumulative Volumes (ft^3)	
IN	
Constant Head	4.84E+06
Recharge	5.64E+06
River Leakage	1.21E+05
TOTAL	1.06E+07
OUT	
Constant Head	9.65E+05
Wells	8.57E+05
River Leakage	8.78E+06
TOTAL	1.06E+07
IN - OUT	2038
Percent Discrepancy	0.02

Constant-head cells also serve a source of outflow, though to a lesser degree than their inflow component (8.6% versus 53%). Figure 62 displays flow vectors in the southwestern corner of model layer 1. The vectors show flow moving in a southwesterly direction. Ground water is exiting through constant head cells in this region. This shift in ground-water flow follows the southwesterly shift in the Tanana River.

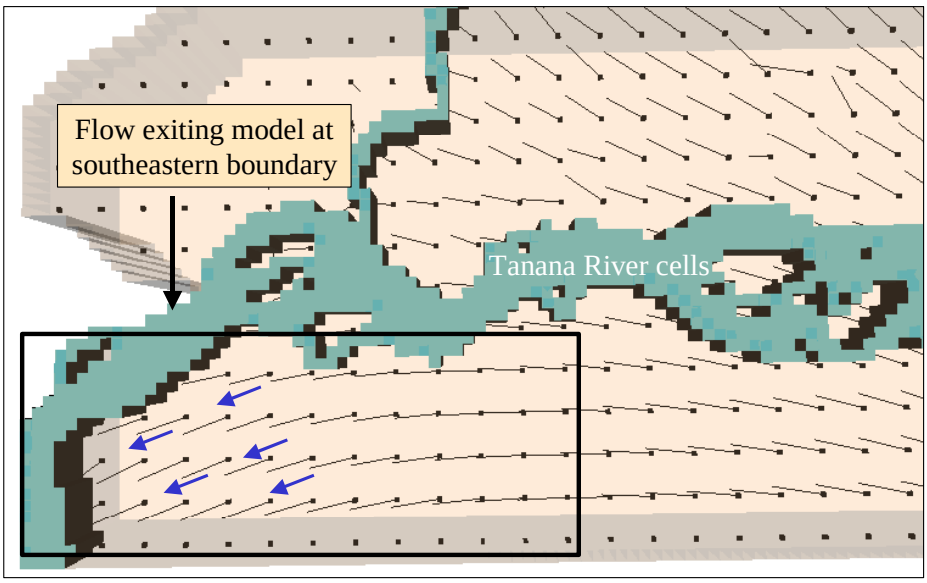

Figure 62. Flow-vector analysis of southeastern portion of sub-regional model. Note the shift in flow direction follows the Tanana River. Nodes depict vector starting points.

Other than constant-head cells, discharge wells act as another source of outflow. A similar amount of flow leaves through these wells as compared to the constant heads (8.1%). The majority of outflow (83%) is through the river cells, with most flow entering the Chena River.

4.4.2 Water-Level Observations

MODFLOW-2000 offers a utility for verifying head results; it is known as the Observation Process. The Observation Process is used for three purposes: 1) to calculate simulated equivalents (i.e., simulated heads and flows) of user-specified observations by interpolating values generated at cell nodes in the grid, 2) to compare observations to these simulated equivalents, and 3) to determine observation sensitivities. We apply the first two steps of this process.

Average March water levels were used as head observations because late-winter conditions most closely resemble those of steady-state. The levels were collected during a 1998-2003 study on Fort Wainwright (US Army/ACE/UAF, 2003), with most site-records spanning a slightly shorter interval (1999-2002). A total of 24 observations are

used. Nearly all values were averaged from continuously-recorded (i.e., hourly) data, while one (FWM 5956) is an average of manual readings taken once each year in March. Most sites lie south of the Chena River, either near or up-gradient of WS 3559; a few also are located along the north side of the Chena River. Figure 63 shows site locations. Appendix C provides a table of site coordinates and annual averages used to calculate the overall average water levels in March.

Figure 64 plots the observations versus simulated equivalents. A line with a slope of 1.0 is inserted to show the head discrepancy in the data. Data that show no errors (i.e., observation = simulated equivalent) would fall along this line.

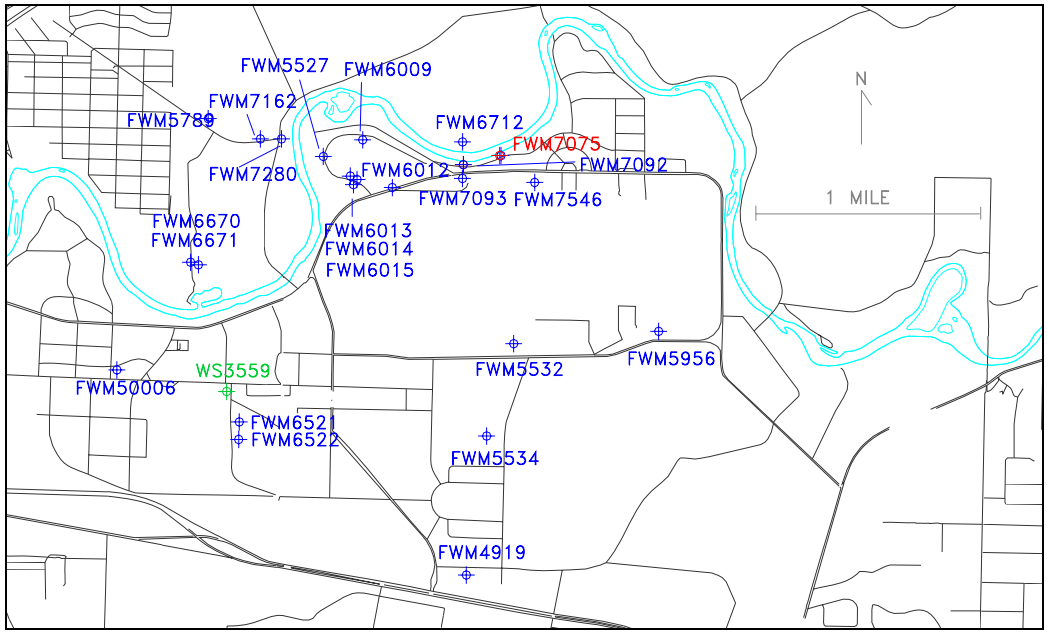

Figure 63. Observation wells (blue) used in model verification. Red denotes a large error in simulated equivalent.

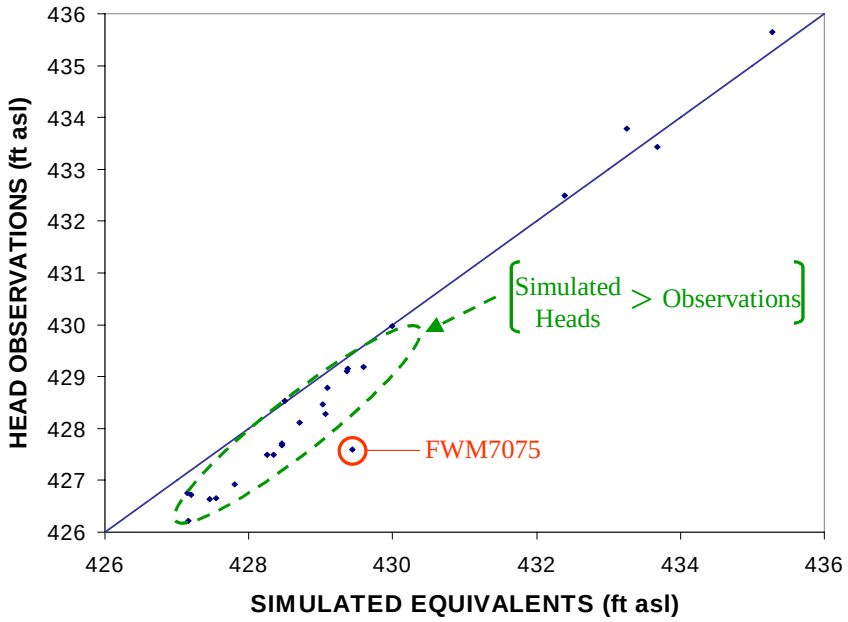

Figure 64. Unweighted observations versus simulated equivalents

Most of the head observations show a discrepancy less than 1 foot, which is deemed acceptable for our current modeling purposes. Only one observation has a residual greater than one (FWM7075, -1.85 ft). The cause for this discrepancy is unclear. As Figure 63 shows, it is very close to the Chena River. Thus, once source of error could be inaccurate modeling of water levels immediately adjacent to the river. On the other hand, measurement error may be a factor; for instance, poor surveying of the well's measuring-point elevation would have led to inaccurate water-level readings.

After computing the observation residuals, the Observation Process calculates statistics that aid in interpreting the results. These are listed in Table 15. The average residual (-0.496) as well as the number of positive and negative residuals (4 and 20, respectively) indicate a predominance of negative values (Figure 64). Since residuals are calculated by subtracting simulated equivalents from observations, negative values signify that simulated heads are higher than the field data. A predominance of negative residuals may mean that the residuals are not normally distributed (i.e., non-random).

Another statistic that provides insight into data distribution is the 'correlation of ordered weighted residuals to normal ordered statistics for observations'. It is used to test

the hypothesis that the weighted residuals are independent and normally distributed (Hill, 1998). If the correlation is greater than some critical value, we accept the hypothesis. The critical value at the 5% significance level is 0.944; that is, a correlation greater than 0.944 indicates the probability of the hypothesis of being wrong is less than 5%. Our correlation statistic is 0.940, and so we reject the hypothesis.

However, this does not necessarily mean that the residuals are not independent or normally distributed. By applying the critical value, we assume that we are using an ample number of data points. Our data set is limited, and so additional observations should be included in the analysis. This can be accomplished by obtaining data collected in other environmental investigations on post. Furthermore, we are assuming that the residuals do not need weighting. Once measurement errors are estimated for the observations and weighted residuals are calculated, the hypothesis should be retested.

If a predominance of negative residuals and low correlation value still result after further analysis, the statistics likely indicate a problem with model design. In this case, the next logical step is to perform a sensitivity analysis to determine which model parameters are most influential. In addition, using the automated parameter estimation process in MODFLOW-2000 would serve to better define parameter values.

Table 15. Statistics for head residuals

STATISTIC	VALUE
Maximum residual	0.529
Minimum residual	-1.850
Average residual	-0.496
Residuals > 0	4
Residuals < 0	20
Sum of squared residuals	11.617
Number of runs statistic	-0.910
Correlation between ordered weighted residuals and normal order statistics for observations	0.940

4.5 MODEL LIMITATIONS

The sub-regional model has several limitations due to its assumptions (section 4.1). For example, because we assume steady-state conditions, we must ignore transient hydrologic processes. These include variably and intermittent pumping-well rates, as well as seasonal and annual fluctuations in river stage, precipitation, and evapotranspiration.

Another limitation is the uncertainty in hydrogeologic unit locations. For instance, permafrost distribution could have a significant impact on flow around the water-supply well. In addition, the actual aquifer thickness likely varies from the modeled thickness due to the uncertainty of bedrock depth.

Uncertainty of parameter estimates and boundary conditions may be the most significant limitation. Slight alterations in parameters such as hydraulic conductivity and recharge can lead to dramatic differences in model output. Similarly, boundary conditions strongly control the flow regime, and so a poor representation can result in an inaccurate model.

To reduce these limitations as much as possible, we make the following recommendations for future modeling:

1. Improve mapping of permafrost distribution as data becomes available. This requires both defining the location of permafrost and assigning accurate parameter values (e.g., K_h, K_v).
2. Perform transient-model runs. Transient simulations will help us to understand effects of several influential factors, including pumping rate and seasonal river fluctuations.
3. Perform sensitivity analyses and parameter estimation with MODFLOW's Observation and Sensitivity Package. A sensitivity analysis will provide a great deal of insight into which parameters are most influential. While previous calibration (Nakanishi and Lilly, 1998) has generated useful parameter estimates, MODFLOW's automated process will further benefit future modeling efforts because it is a relatively objective, efficient, and systematic approach.

4.6 FORT WAINWRIGHT DELINEATION

4.6.1 Input Parameters

In our Fort Wainwright capture-area delineation, the four methods are applied as in the case studies. Table 16 lists the input parameters for CFR, UFE-Thiem, and WHPA. In the UFE-Thiem solution, note that real observational data near the pumping well is now used rather than the head output from MODFLOW; that is, h_1 and r_1 replace h_w and r_w in the Thiem equation.

Table 16. Input parameters for CFR, UFE-Thiem, and WHPA methods in Fort Wainwright delineation.

Input Parameters	symbol	unit	value
well discharge	Q	gpm	1100
horizontal hydraulic conductivity	K_h	ft/d	400
regional hydraulic gradient	I	ft/mi	4
aquifer thickness	b	ft	400
time of travel	TOT	yr	10
flow direction[1]	α	degrees	235
vertical hydraulic conductivity	K_v	ft/d	20
porosity	n	--	0.39
well-screen thickness	l	ft	20
head near well[2]	h_1	ft	429
distance between well and h_1	r_1	ft	300

[1]flow direction specified in WHPA; due West is set to zero degrees
[2]h_1 is the average March water level in an observation well (FWM6521)

4.6.2 Results and Comparisons

Figure 65 shows the four capture-zone delineations in plan view. There are two notable features in the MODPATH delineation. First, note the slight curve in its southwestern area. Secondly, note the bend in the delineation at the northwestern corner

of the cooling-pond cells. This complex shape of the capture area is due to surface-water interaction. The ground water is interacting with both the Chena River and the Fort Wainwright cooling pond.

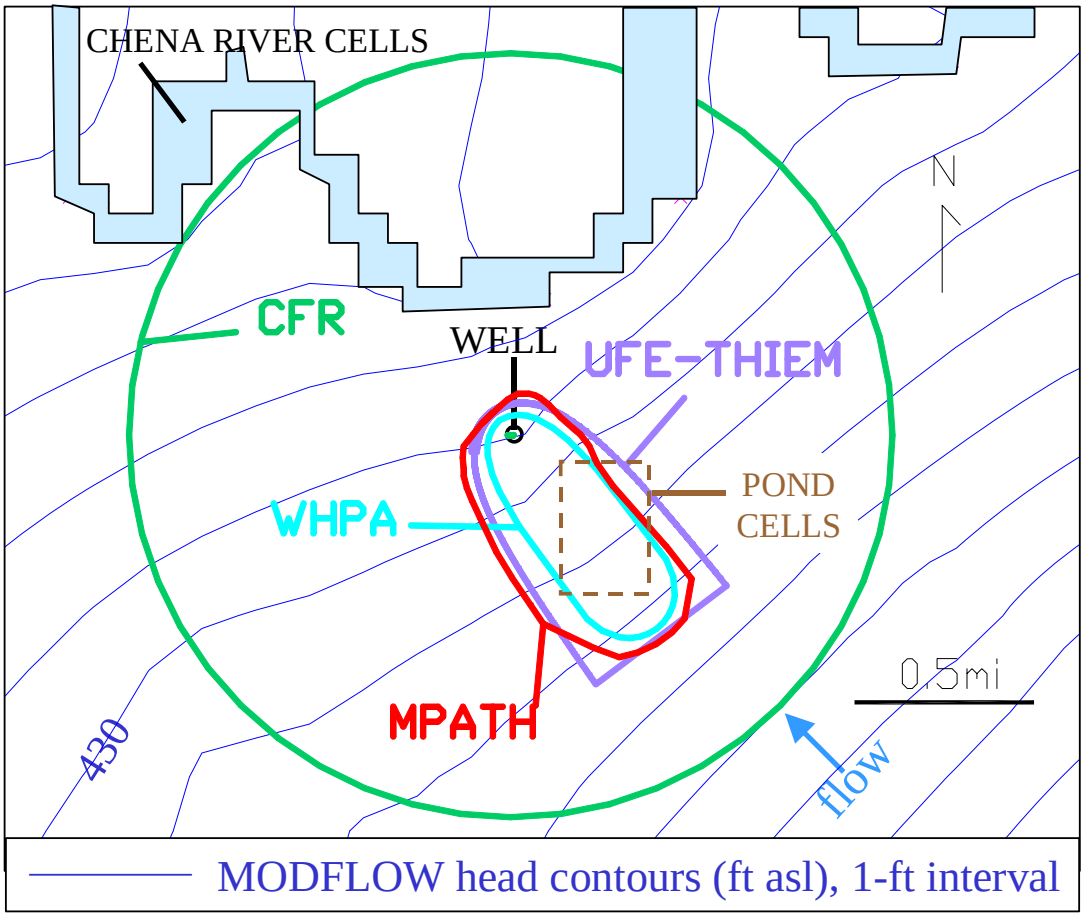

Figure 65. Capture zone delineations of Fort Wainwright field case. The sub-regional model's Chena River and cooling pond cells are also shown.

If a line parallel to the regional flow gradient (i.e., a northwest-southeast trending line) was drawn through the well, we would see that the UFE-Thiem and WHPA delineations display biaxial symmetry. In contrast, the MODPATH delineation is asymmetric. Its southwestern half is larger than its northeastern half. The asymmetry occurs because flow paths are bending from a northwest to north-northwest direction as they move toward the well. The shift is partly due to the Chena River. That is, in addition

to being affected by pumping, flow is affected by the Chena River. Recall from section 3.3.4.2 that the Chena River stage is usually below adjacent ground-water levels, and so the aquifer recharges the river. This flow adds a more northerly component to the sub-regional gradient in this area. Figure 66 shows a plan view of flow vectors in layers 1 and 2 near the well and river. Note that the vectors are directed toward the well and river cells.

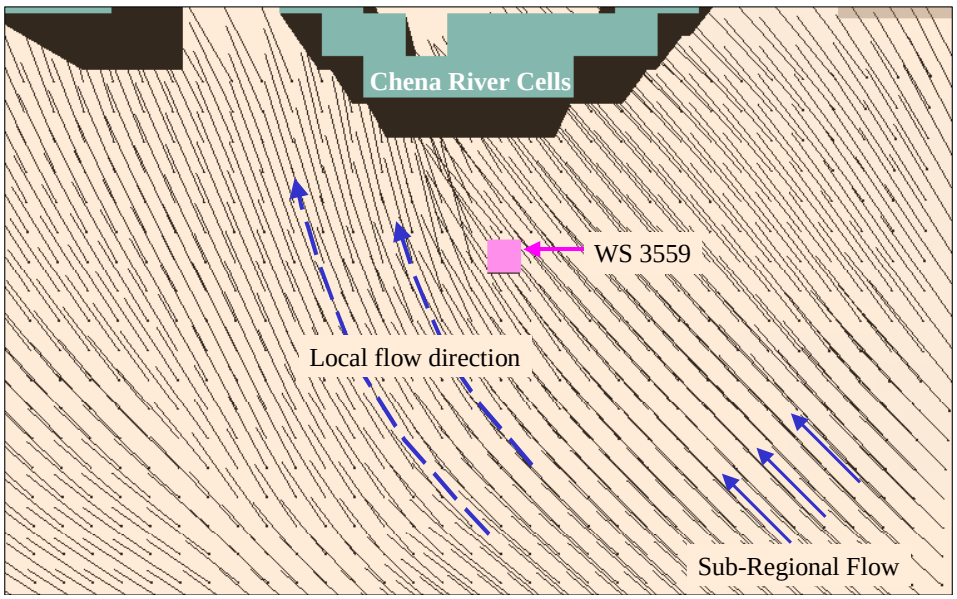

Figure 66. Plan view of flow vectors near WS 3559 and the Chena River in layers 1 and 2 of sub-regional model.

Unlike the Chena River, the cooling pond acts as a source to the aquifer because its stage is higher than ambient ground-water levels. Due to its close proximity up-gradient of WS 3559, the cooling pond acts as a source of recharge to the well. Its water surface in MODFLOW is about 1.4 feet higher than the head in the pumping well's cell. A MODPATH pathline analysis reveals that the pond is contributing a significant amount of recharge: nearly one-third of the well's particles originate in the pond cells. Figures 67 and 68 show the well's pathlines in plan view and in cross-section, respectively. Note the pathlines originating in the pond cells represent recharge provided by the pond.

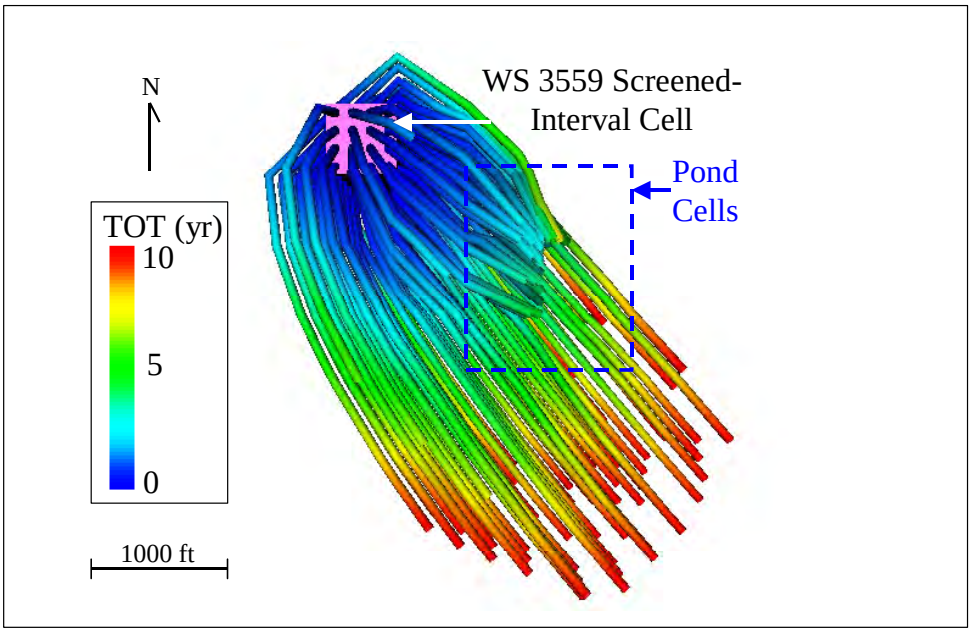

Figure 67. Plan view of MODPATH pathlines entering pumping-well cell in 10-yr TOT.

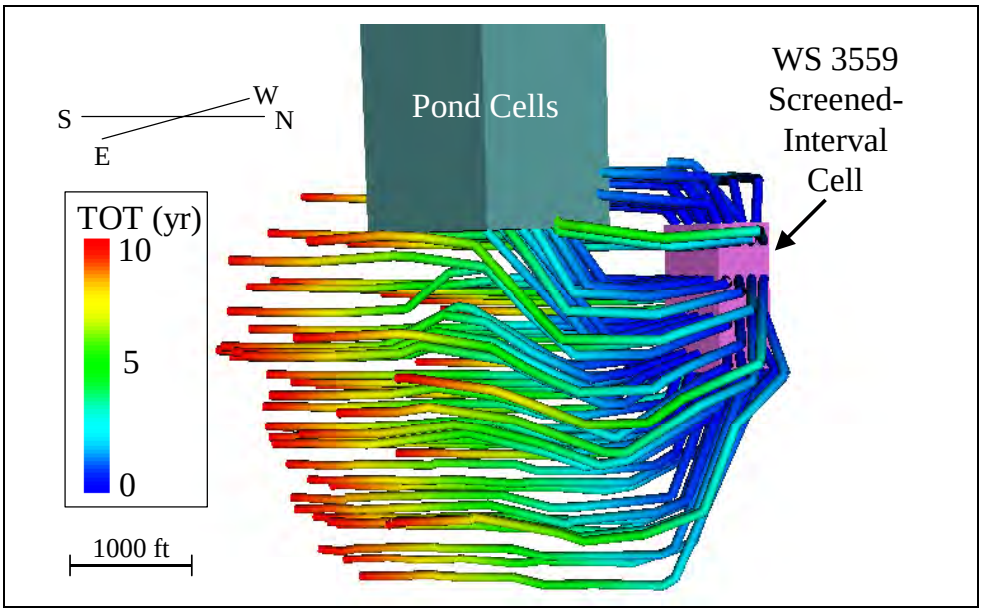

Figure 68. Cross-section of MODPATH pathlines for the 10-yr TOT.

If we remove the cooling-pond cells from our sub-regional model and re-run MODFLOW and MODPATH, the new delineation does not differ significantly; Figure

69 shows that the new delineation extends only slightly farther up-gradient. Thus, it may appear that simulating the pond does not greatly influence the capture area's size and shape. However, MODPATH results are very sensitive to the pond stage. For example, if the pond level is raised 2 feet, the well derives recharge from only the pond cells, which decreases the capture area substantially.

There is room for future improvement in the pond simulation. Pond-level data was limited, and so there is uncertainty in our simulated value. In addition, the pond may be more accurately represented with a variable-head rather than constant-head boundary, such as in MODFLOW's Lake Package. Further study of the pond level relative to ambient ground water will help to better conceptualize the problem.

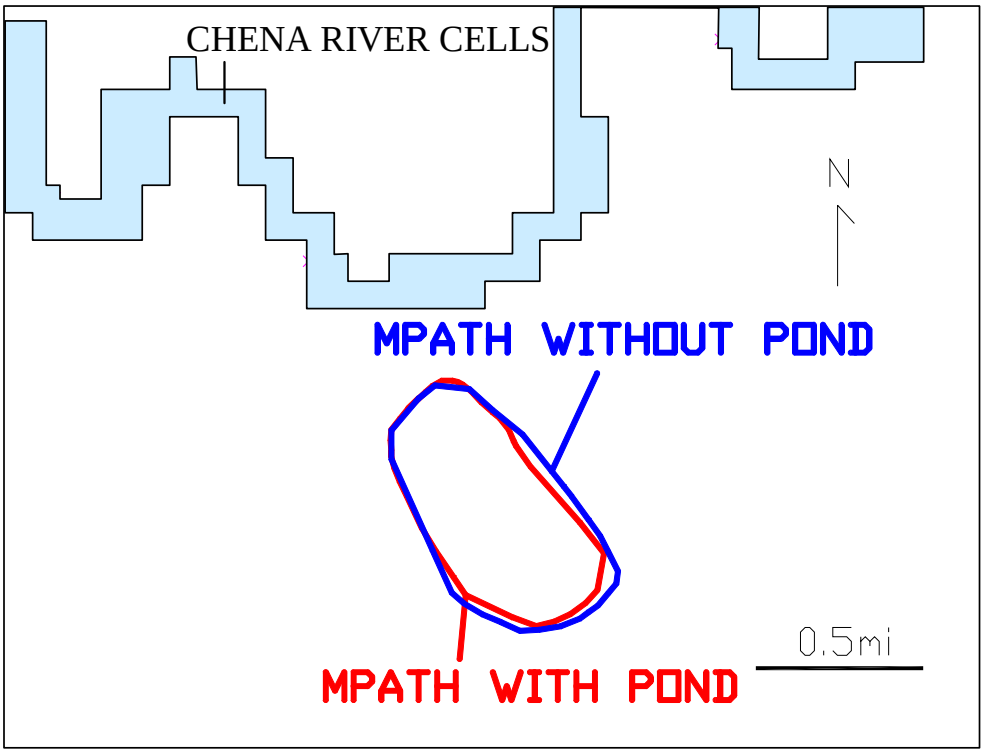

Figure 69. Comparison of WS 3559 MODPATH capture areas with and without cooling-pond simulation.

Figure 70 shows the total net capture area of each method, and Figure 71 compares the simpler methods' net areas to MODPATH results. We see that CFR overestimates the MODPATH capture area yet again; its net area is over an order of magnitude larger. It shares 7.6% of its area with MODPATH, leaving 92% extra.

Similar to our case-study results, the UFE-Thiem capture area is the closest in size, shape, and location to MODPATH out of the three simpler methods. Its up-gradient extent matches MODPATH, which is a sign of its slightly conservative nature. Recall that anisotropy is one of the complexities in our system (K_h:K_v = 20) and that the up-gradient Thiem radius does not lengthen to account for anisotropy (section 2.2.3). The UFE does account for anisotropy, and so we see the capture area is wide enough to cover almost all of MODPATH's area laterally.

However, UFE-Thiem cannot account for surface-water interaction. It consequently misses a small area (8.5%, Figure 71) where the MODPATH delineation bends due to the Chena River's influence on the local flow direction. UFE-Thiem overestimates on the opposite (northeast) side of the capture area, with 16% extra area, due to the pond's influence. Thus, UFE-Thiem's underestimation and overestimation of the MODPATH delineation are both the result of surface-water interaction.

The WHPA delineation is also in line with case-study results. Recall that the difference between WHPA and MODPATH areas increased with complexity. Similar to Case 3, there are two major complexities in this case (anisotropy and surface-water interaction). Our results show that the WHPA capture area is significantly smaller than MODPATH's delineation and misses 36% of its area. This percent-missed value is less than that of Case 3 (60%) due to several factors. First, different complexities have different effects on the MODPATH area. For example, the pond-interaction (field case) shrinks the MODPATH capture area, while multiple wells (Case 3) enlarge it. Secondly, lower parameter values, such as a lower pumping rate and anisotropy ratio, cause less expansion of the MODPATH area than in Case 3.

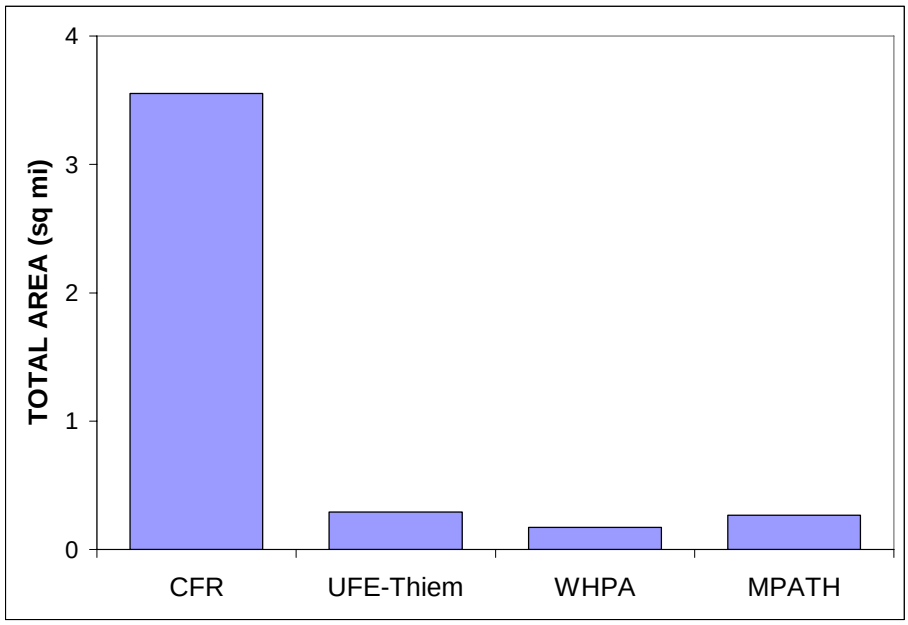

Figure 70. Total area per method for Fort Wainwright field case.

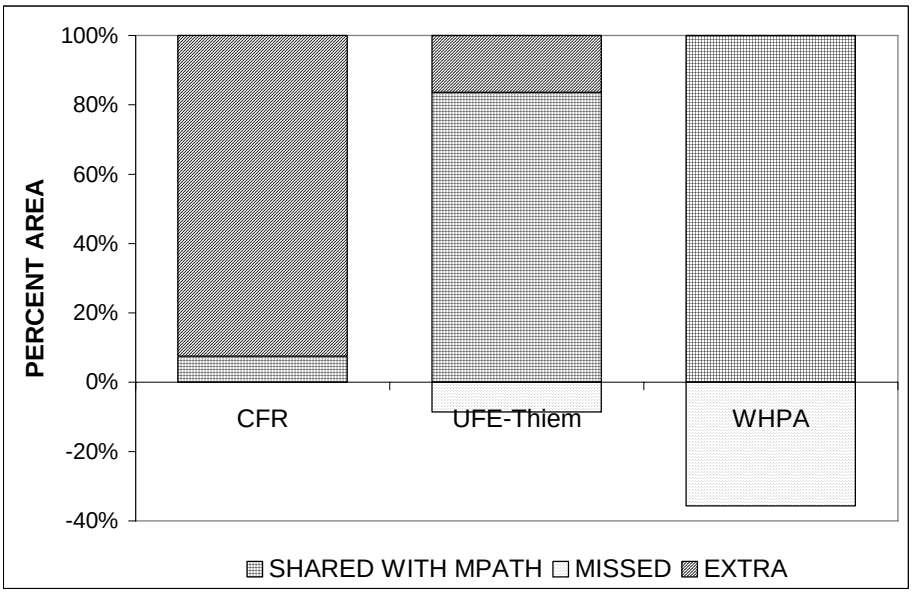

Figure 71. Comparison of CFR, UFE-Thiem, and WHPA delineations to MODPATH results in Fort Wainwright case.

5 CONCLUSIONS AND RECOMMENDATIONS

Recall that our hypothesis was designed to test whether the capture areas of the simpler methods 1) significantly differ from MODPATH results, and 2) whether the differences increase with complexity and the number of assumptions made by each method. The following sections evaluate the results of each method. Table 17 summarizes the percent differences in area for all cases.

Table 17. Summary of percent-area differences for all cases.

		CFR	UFE-Thiem	WHPA
CASE 1	EXTRA	96.0%	62.0%	2.6%
	MISSED	0.0%	0.0%	0.0%
CASE 2	EXTRA	91.0%	29.0%	6.0%
	MISSED	0.0%	4.5%	22.0%
CASE 3	EXTRA	81.0%	15.0%	0.0%
	MISSED	0.0%	15.0%	60.0%
CASE 4	EXTRA	78.0%	31.0%	0.0%
	MISSED	0.0%	40.0%	75.0%
FIELD CASE	EXTRA	92.0%	16.0%	0.0%
	MISSED	0.0%	8.5%	36.0%

5.1 CFR

Table 17 shows that CFR results consistently differed the most from those of MODPATH. That is, CFR had the highest percent-area difference (78%-96% extra) in each case due to its overestimation of the capture area. This is not surprising, as CFR makes the most assumptions of the three simpler methods. Even in very simple settings such as Case 1, CFR's symmetrical shape does not resemble the true capture zone because it is not accounting for the natural hydraulic gradient. Provided that the radial distance is adequate, the area largely overestimates the capture zone. Thus, CFR is not an accurate method of capture zone delineation. We therefore accept the first part of our hypothesis, as all of our CFR delineations differed significantly from those of MODPATH.

However, note that the percent-extra area slightly decreased with the added complexity of each case. The growing size of MODPATH covered a larger portion of CFR's area. Thus, we reject the hypothesis that the difference increases with complexity. With this in mind, it may be useful to use CFR as a first estimate of a capture zone in

complex settings with a high degree of hydrogeologic uncertainty. That is, if numerical modeling is not an option due to limited data, time, resources, or user-experience, CFR may serve as an initial estimate until numerical modeling is feasible. CFR is easiest and quickest to apply, and since analytical methods may underestimate the true area, its conservative nature provides the most confidence that the true area is covered.

Note that we do not recommend CFR as a final delineation method. With such a huge overestimate of the real capture area, significant consequences may result from applying this method for ground-water protection purposes. The consequences depend on whether the overestimate is taken seriously by state and local agencies. If a CFR delineation is taken seriously, it could pose costly land-use restrictions and monitoring of low-priority sites within the capture area. On the other hand, if its overestimation is acknowledged and it is not taken seriously, the delineation might fail to play an important role in prioritizing ground-water protection and contaminated-site remediation.

5.2 UFE-THIEM

As with CFR, we accept the first part of our hypothesis that the UFE-Thiem delineations significantly differ from MODPATH delineations. Out of the five cases, we saw the minimum difference in the Fort Wainwright case (Table 17), where the percent-extra area is 16% and the percent-missed area is 8.5%. The sum of these areas is 24.5%, which we consider as significant.

Of the three simpler methods, UFE-Thiem produced capture areas that most closely matched those of MODPATH. The similarity in MODPATH and UFE-Thiem results is partly due to UFE-Thiem's conservative nature relative to our other analytical solution (WHPA). For example, as shown in Case 1, UFE-Thiem overestimated the capture area in a setting where nearly all simplifying assumptions were valid, whereas WHPA matched the MODPATH delineation almost exactly. However, as we moved to Case 2 and well interference was assumed negligible, the WHPA area missed a substantial amount of MODPATH's area and the UFE-Thiem area was more similar. This increase in similarity from Case 1 to Case 2 shows that we must reject the second part of our hypothesis, as differences do not necessarily increase with the number of invalid

assumptions. The further increase in UFE-Thiem and MODPATH similarity from Case 2 to Case 3 showed that the difference does not necessarily increase with aquifer complexity either. This is due to UFE-Thiem's ability to account for certain complexities, such as anisotropy.

Because UFE-Thiem was the most comparable method in our cases, it may be the best alternative (relative to the other two methods) until numerical modeling is possible. However, unlike CFR, the risk of underestimating the capture area exists. One way of reducing this risk is to add a margin of error that will enlarge the capture area to a certain degree. As mentioned in sections 1.2.2.1 and 3.4.2, ADEC incorporates multiple safety measures into their methodology, which enlarge the UFE-Thiem delineation to account for method inaccuracy and uncertainty of input parameters. However, their chosen safety measures have produced delineations that extend well beyond realistic limits. For example, Figure 72 shows our results overlain onto ADEC's delineation of the Fort Wainwright primary water-supply wells (note that the delineation includes back-up wells WS 3565 and WS 3563). Our UFE-Thiem delineation is more than an order of magnitude smaller. This difference in area is comparable to the difference between CFR and MODPATH. Thus, applying an overly conservative margin of error can lead to the same degree of overestimation as CFR, and therefore the same potential consequences.

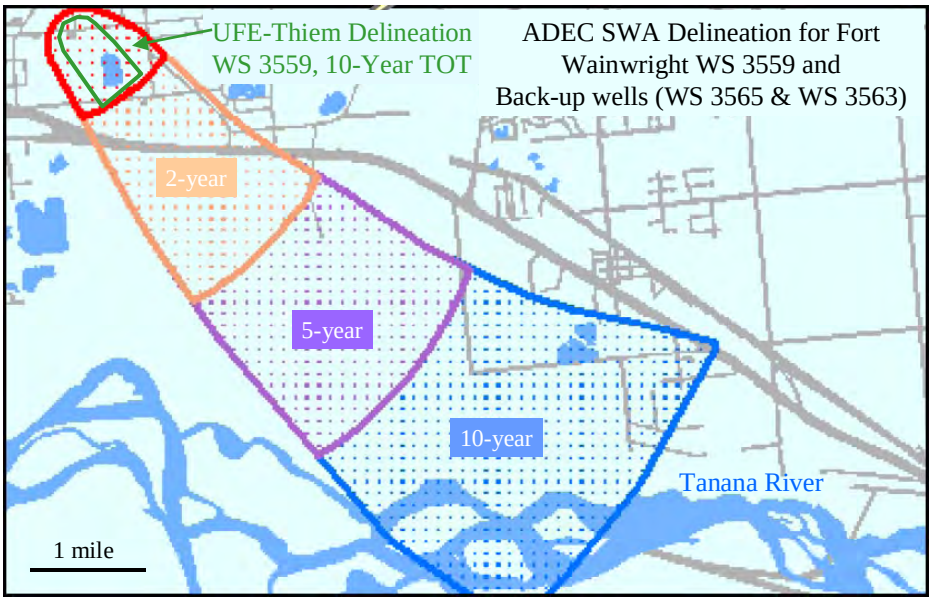

Figure 72. ADEC capture-zone delineation of primary water-supply wells on Fort Wainwright (Modified from ADEC, 2004). Our UFE-Thiem delineation is overlain for comparison.

Applying an appropriate margin of error is critical to an effective delineation. The margin should be based on the levels of parameter uncertainty and system complexity. A systematic approach is recommended, in which the user defines a reasonable range of parameter values. This range can be determined from existing data and relevant literature. The values are input into the solution with the aim of accurately representing potential variation in results. Finally, the values that render the most conservative capture area are selected. While ADEC does use this approach, it is one of many conservative measures in their methodology; the combined effect of all measures is what renders the large overestimation.

In addition to studying effects of input parameters common to UFE-Thiem and MODPATH (e.g., K_h, n), the user must determine the effects of complex parameters that are not represented in the UFE-Thiem solution. This can be accomplished through further quantitative comparison of UFE-Thiem and MODPATH capture areas in hypothetical systems. The variation in percent-area difference should be examined as a particular

parameter is varied. For instance, because UFE-Thiem cannot fully account for anisotropy, we see that its delineation may miss part of MODPATH's area (Case 3). To estimate a percent-missed area that can be applied to real systems, we must study the variation in percent-missed area over a realistic range of anisotropy ratios. Based on this variation, we can obtain a conservative percent-missed estimate to factor into a delineation's margin of error.

5.3 WHPA

We reject the first part of our hypothesis as it applies to WHPA. That is, WHPA delineations do not necessarily differ significantly from those of MODPATH. We fail to accept this part of the hypothesis due to our Case 1 results, which showed that the WHPA capture area was comparable to the MODPATH area in a very simplified setting. With added complexity, however, WHPA significantly underestimated the capture area. The differences between MODPATH and WHPA results increased with aquifer complexity and the number of assumptions made by WHPA. Therefore, we accept the second part of our hypothesis. The degree of underestimation was substantial in all cases but the first, and so we do not recommend WHPA for capture-zone delineation.

5.4 MODPATH

The case studies have provided insight into the numerical method. We were able to quantitatively examine how flow in the model was affected by specific complexities, including multiple wells, anisotropy, heterogeneity, and surface-water interaction. The case studies showed that the size and shape of MODPATH capture areas were significantly altered with single changes to the aquifer system. The MODPATH results were clearly distinguished from the others in all but the simplest case (where WHPA and MODPATH were very similar) due to the numerical model's superior ability to simulate complex conditions. We conclude that numerical modeling can potentially delineate capture zones with a much higher degree of accuracy than the other three methods.

However, it is important to note that a numerical model is only as good as the quality of the input data. If uncertainty exists in the data, model results may not be representative of the true flow system. This is not a concern in our synthetic case studies, but it is

relevant to our field case; for instance, we assumed the alluvial aquifer is homogeneous and the water level of the cooling pond is constant. In addition, MODPATH results can be affected by particle-tracking methodology. For example, the velocity distribution is partly a function of grid discretization, and so flow paths may be influenced by cell dimensions. Therefore, we recommend a margin of error be added to MODPATH results to account for the effect of invalid assumptions and particle-tracking methodology. As with the UFE-Thiem method, the error margin should be a reasonable estimate that is based on the specific complexities and assumptions that apply to the particular system.

Most importantly, the user must exercise sound hydrogeologic judgment when employing a sophisticated method such as numerical modeling. Sound judgement should be applied in all methods, but it is especially needed in designing numerical models due to their increased capabilities. The more complex the model, the more factors there are to be considered, such as boundary conditions, aquifer properties, and system stresses.

Regardless of the chosen method, an awareness of the assumptions being made is crucial to evaluating result accuracy. This point cannot be overemphasized. The user must not only identify the assumptions, but also understand how they are quantitatively impacting the results. Such an understanding is needed to delineate capture zones that are both safe and credible.

LITERATURE CITED

Adams, Brian, Fort Wainwright Department of Public Works. Personal Communication, February 2005.

ADEC, 2004. Source Water Assessment: A Hydrogeologic Susceptibility and Vulnerability Assessment for Fort Wainwright Water Treatment Plant Wells 3563, 3565, 3559A, and 3559B, Fort Wainwright, Alaska, PWSID 310918. Drinking Water Protection Program Report 1285, 55p.

Anderson, G.S. 1970. Hydrologic Reconnaissance of the Tanana Basin, Central Alaska. US Geological Survey Hydrologic Investigaions Report HA-319.

Anderson, M.P., Aiken, J.S., Webb, E.K., and D.M. Mickelson, 1999. Sedimentology and hydrogeology of two braided stream deposits. Sedimentary Geology, v.129, pp.187-199.

Anderson, M.P. and W.W. Woessner, 1992. Applied Groundwater Modeling. San Diego: Academic Press, 181p.

ASCI/NANA Joint Venture, 2001. Draft: Groundwater Protection Report: Coal Storage Yard, Fort Wainwright, Alaska, 27p.

Barlow, P.M., 1997. Particle-tracking analysis of contributing areas of public-supply wells in simple and complex flow systems, Cape Cod, Massachusetts: U.S Geological Survey Water-Supply Paper 2434, 66 p.

Bear, J., and M. Jacobs. 1965. On the movement of water bodies injected into aquifers. Journal of Hydrology. 3 (1): 37-57.

Blandford, T.N. and P.S. Huyakorn. 1991. WHPA: A Modular Semi-Analytical Model for the Delineation of Wellhead Protection Areas, Version 2.0. US EPA Office of Ground-Water Protection, Washington, DC, 246p. EPA 68-08-0003.

Braumiller, S., 2000. Solution spreadsheet used in ADEC capture-zone delineations. Obtained from ADEC Drinking Water Protection Program, 2003.

Braumiller, S. Personal communication, October 2004.

Bristow, C.S. and Best, J.L., 1993. Braided rivers: perspectives and problems, *in* Best, J.L. and Bristow, C.S. (eds), *Braided Rivers*, Geological Society Special Publication No.75, pp.1-11.

Cederstrom, D.J., 1963. Ground-water resources of the Fairbanks area, Alaska: U.S. Geological Survey Water-Supply Paper 1590, 84p.

CH2MHILL, 1996a. Release Investigation Report (Phase 2) Building 3564, Delivery Order 5, Fort Wainwright, AK. Prepared for the US Army Engineer District, Alaska, July 1996.

CH2MHILL, 1996b. Groundwater Modeling at Building 3564, Delivery Order 5, Fort Wainwright, Alaska. Prepared for the US Army Engineer District, Alaska, December 1996.

Dingman, S.L., 1971. Hydrology of the Glenn Creek Watershed, Tanana River Basin, central Alaska: US Army Cold Regions Research and Engineering Laboratory Research Report 297, 110p.

Dingman, S.L., 1973. The water balance in arctic and subarctic regions – Annotated bibliography and preliminary assessment: US Army Cold Regions Research and Engineering Laboratory Special Report 187, 131p.

Dowl/Ogden Joint Venture, 1997. Wellhead Protection Plan, Fort Wainwright, Alaska. Work Order D55710.

Farris, A.M. 1996. Numerical Modeling of Contaminant Transport in Discontinuous Permafrost: Ft. Wainwright, Alaska. M.S. Thesis. University of Alaska. 109 pp.

Fetter, C.W., 1994. Applied Hydrogeology, third edition. New York: Macmillan College, 706p.

Feulner, A.J., 1961. Geology and water conditions at Ladd Air Force Base, Alaska: U.S. Geological Survey Hydrologic Data Report 13, 17p.

Franke, O.L., T.E. Reilly, D.W. Pollock, and J.W. LaBaugh, 1998. Estimating Areas Contributing Recharge to Wells: Lessons from Previous Studies. US Geological Survey Circular 1174, 14p.

Freeze, R.A. and Cherry, J.A., 1979. *Groundwater*. Englewood Cliffs: Prentice-Hall, 604 p.

Gallagher, Jan. 1990. Citizen's Guide to Ground-Water Protection. US EPA Office of Ground-Water Protection. EPA 440/6-90-004, 34p.

Glass, R.L., M.R. Lilly, and D.F. Meyer. 1996. Ground-water levels in an alluvial plain between the Tanana and Chena Rivers near Fairbanks, Alaska, 1986-1993. US Geological Survey Water-Resources Investigations Report 96-4060.

Gieck, R., 1986. A Water Resource Evaluation of Two Subarctic Watersheds. MS Thesis. University of Alaska Fairbanks, Fairbanks, 90 p.

Gorelick, S.M., Freeze, A.R., Donohue, D., and J.F. Keely. 1993. *Groundwater Contamination: Optimal Capture and Containment*. New York: Lewis Pub, 385p.

Haitjema, H.M. 1995. Analytic Element Modeling of Groundwater Flow. Academic Press, Inc.

Hansen, C.V., 1991. Description and evaluation of selected methods used to delineate Wellhead protection areas around public supply wells near Mt. Hope, Kansas. USGS Water-Resources Investigation Report 90-4102.

Hantush, M.S.,1961. Drawdown in a partially penetrating well. Journal of Hydraulic Division, Proceedings of the American Society of Civil Engineers, 87 (4): 83-98.

Harbaugh, A.W., 2002. A data input program (MFI2K) for the U.S. Geological Survey modular ground-water model (MODFLOW-2000): U.S. Geological Survey Open-File Report 02-41.

Hill, M.C. 1998. Methods and Guidelines for Effective Model Calibration: USGS Water-Resources Investigations Report 98-4005, 91p.

Javandel, I., Doughty, C., and F. Tsang. 1984. *Groundwater Transport: Handbook of Mathematical Models*. American Geophysical Union, Water Resources Monograph 10, 228p.

Javandel, I., and C.F. Tsang, 1986. Capture-Zone Type Curves: A Tool for Aquifer Clean Up. Ground Water. 24:(5), 61-65.

Kane, D. L., 1980. Snowmelt Infiltration into Seasonally Frozen Soils. *Cold Regions Science and Technology*, 3, pp. 153-161.

Kane, D.L. and Stein, J., 1983. Field evidence of groundwater recharge in interior Alaska *in* Proceedings of Permafrost: 4th International Conference. National Academy Press, Washington, D.C., pp. 572-577.

Knochenmus, L.A., and Robinson, J.L., 1996, Descriptions of Anisotropy and Heterogeneity and Their Effect on Ground-Water Flow and Areas of Contribution to Public Supply Wells in a Karst Carbonate Aquifer System: Water Supply Paper 2475, 47p.

Krohelski, J. 2003. *Why Are There Groundwater Quantity Issues in Wisconsin?* USGS Presentation given at 2003 Wisconsin Lakes Convention. Retreived from http://www.dnr.state.wi.us/org/water/dwg/gcc/WGWA2_jk.pdf

Lawson, D.E., Arcone, S.A., Delaney, A.J., Strasser, J.D., Strasser, J.C., Williams, C.R., and T.J. Hall. 1998. Geological and Geophysical Investigations of the Hydrogeology on

Fort Wainwright, Alaska: North-Central Cantonment Area. US Army Cold Regions Research and Engineering Laboratory. CRREL Report 98-6, 73p.

Malen, Joe, Personal communication, March 2005.

McDonald, M.G., and A.W. Harbaugh, 1988. A Modular Three-Dimensional Finite Difference Ground-Water Flow Model. Techniques of Water-Resources Investigations of the USGS. Book 6, Chapter A1.

McWhorter, D.B. and D.K. Sunada. 1977. Ground-Water Hydrology and Hydraulics. Highlands Ranch: Water Resources Publications, 290p.

Muldoon, M. and J. Payton, 1993. Determining Wellhead Protection Boundaries: an Introduction. Wisconsin Department of Natural Resources Publ WR 313-92.

Nakanishi, A.S., and M. R. Lilly, 1998. Estimate of aquifer properties by numerically simulating ground-water/surface-water interactions in cross section at Fort Wainwright, Alaska. US Geological Survey Water-Resources Investigations Report 98-4088, 35 p.

National Weather Service, 2005. Climate statistics for Fairbanks International Airport, 1904-2004, Fairbanks, Alaska, courtesy of Ed Plumb.

Nelson, G.L. 1978. Hydrologic information for land-use planning, Fairbanks vicinity, Alaska: U.S. Geological Survey Open-File Report 78-959, 47p.

Newberry, R.J., Bundtzen, T.K., Clautice, K.H., Combellick, R.A., Douglas, T., Laird, G.M., Liss, S.A., Pinney, D.S., Reifenstuhl, R.R., and Solie, D.N., 1996. Preliminary geologic map of the Fairbanks Mining District, Alaska. Alaska Division of Geological and Geophysical Surveys, Public Data File 96-16, 17 p.

Péwé, T.L., Bell, J.W., Forbes, R.B., and Weber, F.R., 1976. Geological map of the Fairbanks D-2 SE quadrangle, Alaska: US Geological Survey Miscellaneous Investigations Series Map I –942, scale 1:24,000.

Péwé, T.L., and J.W. Bell, 1975. Map showing distribution of permafrost in the Fairbanks D-2 SE quadrangle, Alaska. U.S. Geological Survey Miscellaneous Field Studies Map MF-669-A (1976).

Plumb, E.W. and M.R. Lilly. 1996. Snow-depth and water-equivalent data for the Fairbanks area, Alaska, spring 1995: U.S. Geological Survey Open-File Report 96-414, 16p.

Pollen, M.R., 1999. Fort Wainwright Potable Water Well Infiltration Study: Final Report. Northern Testing Laboratories, Inc., 12p.

Pollock, D.W. 1994. User's Guide for MODPATH/MODPATH-PLOT, Version 3: A particle tracking post-processing package for MODFLOW, the US Geological Survey finite-difference ground-water flow model. US Geological Survey Open-File Report 94-464, 249p.

Reilly, T.E. and D.W. Pollock, 1995. Effect of Seasonal and Long-Term Changes in Stress on Sources of Water to Wells: US Geological Survey Water-Supply Paper 2445, 25p.

Reilly, T.E. and D.W. Pollock, 1993. Factors affecting areas contributing recharge to wells in shallow aquifers: US Geological Survey Water-Supply Paper 2412, 21p.

Rozell, N. 2003. Fixing the Fatal Flaw of Fairbanks. Alaska Science Forum, Article 1663, 11 September 2003.

Rygh, S., Personal communications, 2003-2004.

Strack, O.L. and H.M. Haitjema. 1981. Modeling double aquifer flow using a comprehensive potential and distributive singularities 1. Solution for homogeneous permeabilities. Water Resources Research, 17 (5): 1535-1549.

US Army Alaska, US Army Corps of Engineers Alaska District, and University of Alaska Fairbanks. 2003. Geohydrologic Investigations, Fort Wainwright, Alaska (http://www.uaf.edu/water/projects/ftww/ftww.html)

US Army Corps of Engineers, July 1995. The development and Application of Initial Hydrogeologic Flow Model for the Chena River Lakes Flood Control Project. Davis, CA, PR-28, approx 260p.

US Army Corps of Engineers, May 2000. Source Water Assessment, Fort Wainwright, Alaska. (Draft)

US EPA Office of Ground Water Protection, 1987. Guidelines for Delineation of Wellhead Protection Areas, Washington, DC. EPA 440/6-87-010.

US EPA Source Water Assessment website, 2003 (http://www.epa.gov/safewater/protect/assessment.html)

US Geological Survey, 2004. Calendar Year Streamflow Statistics for the Nation, online database: http://nwis.waterdata.usgs.gov/usa/nwis/annual/calendar_year.

US Geological Survey Short-Course: Modeling Gournd-Water Flow Using MODFLOW-2000 (GW2096), USGS National Center, Reston, VA, March 2003, class notes.

Viereck, L. A., K. Van Cleve, and C.T. Dyrness. 1986. Forest ecosystem distribution in the taiga environment *in* K. Van Cleve, F. S. Chapin III, P. W. Flanagan, L. A. Viereck and C. T. Dyrness, eds, Forest ecosystems in the Alaskan taiga: a synthesis of structure and function. Springer-Verlag, New York, pp. 22-43.

Wegner, M.A. 1997. Transient Groundwater and Surface-Water Interactions at Fort Wainwright, Alaska. M.S. Thesis, University of Alaska. 75 pp.

Yoshikawa, K. Personal communication, September 2004.

Youcha, E.K. 2003. *A Geohydrologic Analysis Of An Upland-Bedrock Aquifer System: Applications To Interior Alaska.* M.S. Thesis. University of Alaska Fairbanks. 140 pp.

APPENDIX A: FORT WAINWRIGHT PUMPING WELL INFORMATION

Table 18. Fort Wainwright pumping well information.

WELL ID	BUILDING LOCATION[b]	EASTING	NORTHING	DEPTH (fbgs)	SCREEN[f] (fbgs)	SLOT (inches)	DIAMETER[f] (inches)	OPERATION PERIOD	AVERAGE Q[b,f] (gpm)	CAPACITY (gpm)	PURPOSE	STATUS
3559 B	3559	3960211	241953.6	100	60-80	0.11	20	1998-present	1100	2200	drinking	active
3559 A	3559	3960229	241951.1	100	60-80	0.11	20	1998-present	1100	2200	drinking	active
5110	Range Shop	--	--	--	--	--	--	--	9	--	--	--
5108	Range Control	--	--	--	--	--	--	--	55	--	--	--
2095	2095 (golf course)	--	--	--	--	--	--	--	25	--	golf course maintenance	intermittent
128	3565	3959835	242176	202	180-200	0.1	16	1969-1988	1000	1000	drinking	back-up
127	5008 (DRMO)	3954866	255026.1	--	--	--	6	--	75	50-76	--	--
119	3564	3960105	242202.9	--	44-50	--	6	--	700	--	--	standby
110	1172 (ski lodge)	3971508	248400.4	260	94-100	--	6	--	136	--	--	standby
109	2092 (golf course)	3961180	254744.7	--	45-50	--	5	--	9	75	--	standby
106	5001	3954515	255257.1	--	--	--	6	--	--	13	--	standby
105	1173	3971846	241126.9	68	--	--	5	--	--	9	--	standby
104	1168	3966605	241871.3	45	--	--	8	--	--	--	--	standby
101	3563	3960386	242170.2	118	96-109	0.125	12	1952-1985	(1200-1400)/750[c]	1000	drinking	back-up
100	3405	3958218	245935.2	118	108-118	--	12	--	1000	1000	emergency	standby
98	4023	3961625	237570.9	--	40-50	--	12	--	500	750	emergency	standby
95	1011	3967009	251774.8	60	50-60	--	8	--	750	750	emergency	standby
86	1032	3967284	251571.9	58	48-58	--	12	--	1500	750	emergency	standby
71	3003	3961201	245852.5	160	150-160	--	8	--	600	600	emergency	standby
5	3598	--	--	--	--	--	--	--	--	--	industrial[d]	intermittent
4	3594 (power plant)	3959954	242617.2	--	--	--	12	--	--	--	industrial[e]	inactive

Sources: 1 ASCI/NANA, 2001, p.6
2 CH2MHILL, 1996b, p.5
3 US Army, 2000, p.6
4 ADEC, 2004 (all Fort Wainwright SWA Reports)
5 Miscellaneous spreadsheets given to USGS by Water Treatment Facility Operator Tony Miller

Notes: '--' = data unavailable
[a] Building location is used as the well identifier in some reports
[b] Q = volumetric discharge rate
[c] Pumped 1200-1400gpm unitl 1969; 750gpm 1969-1985 (CH2MHill, 1996b)
[d] Supplements cooling pond when water temperature reaches a certain threshold in summer (Malen, 2005)
[e] Installed for power plant supply, but mechanical difficulties prevented independent supply (ASCI/NANA, 2001)
[f] Reports contain conflicting values of diameter, screened interval, and pumping rates for many wells

APPENDIX B: FORT WAINWRIGHT SOIL MOISTURE DATA

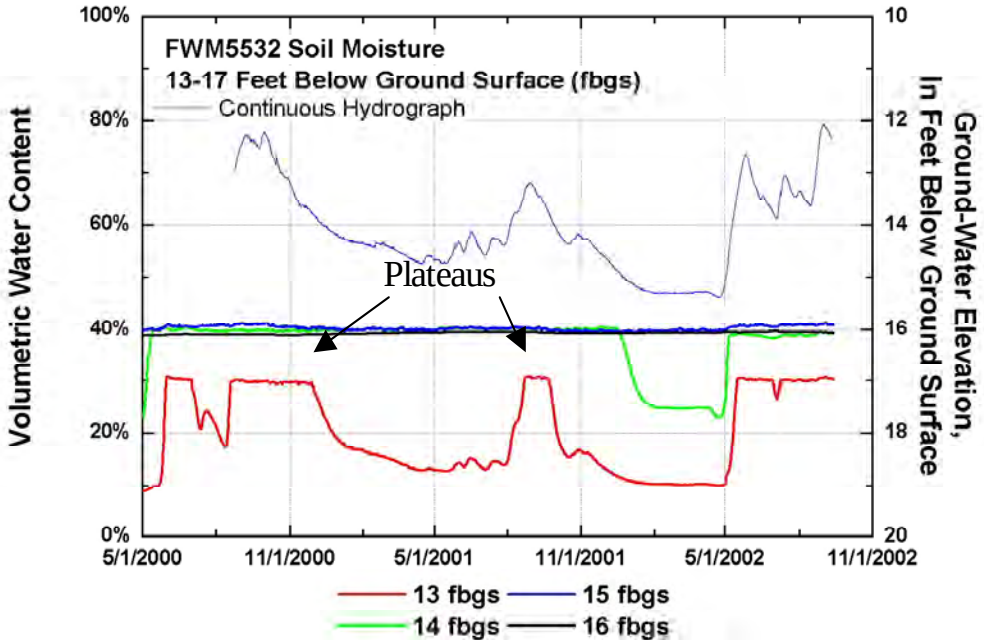

Figure 73. Volumetric water content of probes 13-16 fbgs at FWM 5532. Note plateaus of individual probe plots.

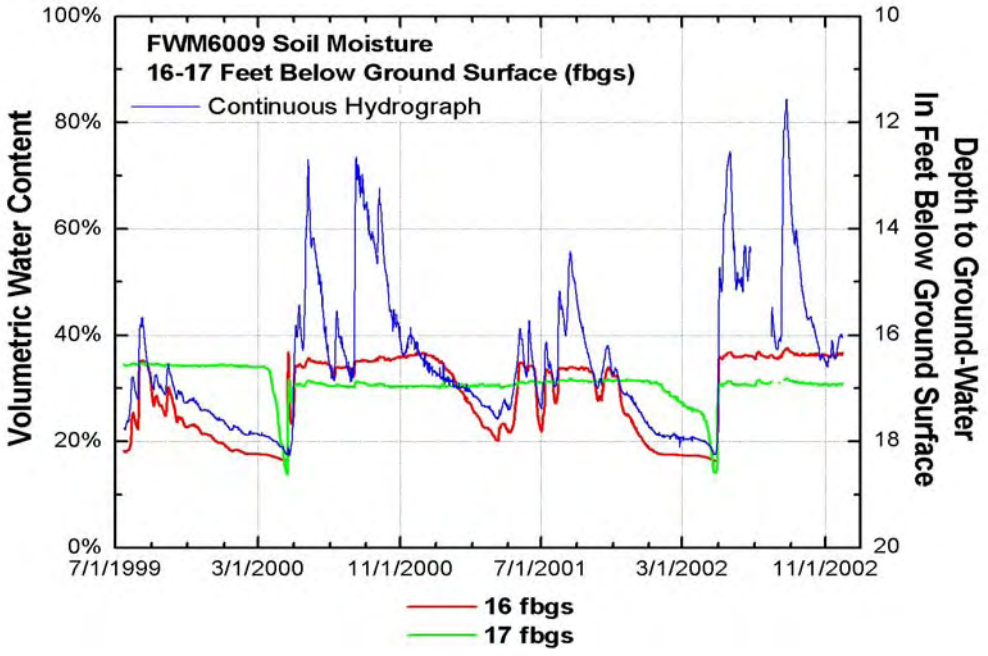

Figure 74. Volumetric water content of probes 16-17 fbgs at FWM 6009.

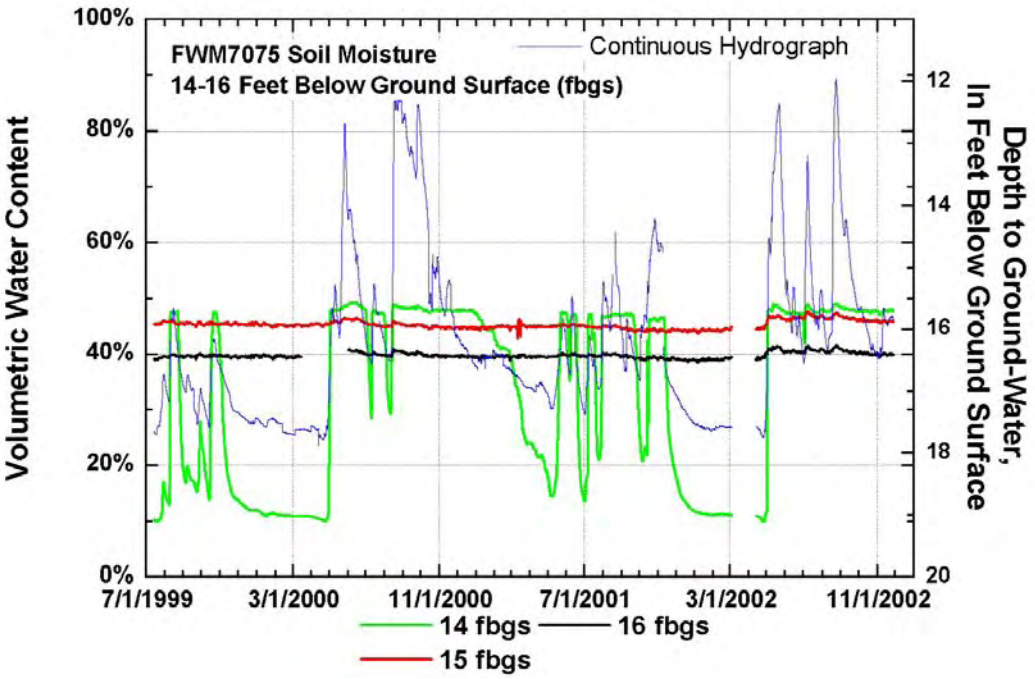

Figure 75. Volumetric water content of probes 14-16 fbgs at FWM 7075.

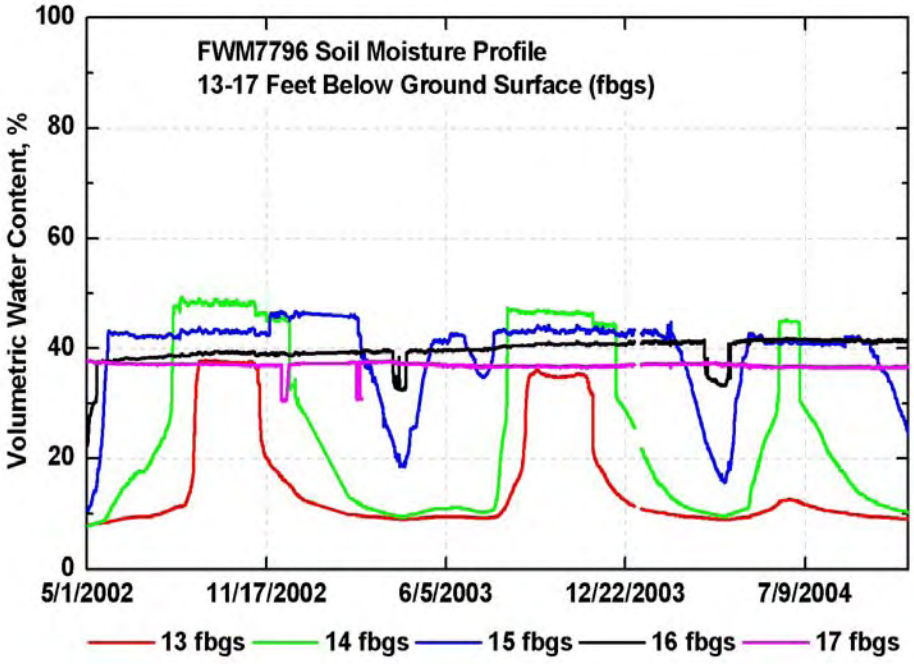

Figure 76. Volumetric water content of probes 13-17 fbgs at FWM 7796.

Figure 77. Aerial photo of Fort Wainwright showing soil moisture sites. Plotted sites are circled in red.

Table 19. Statistical analysis of saturated soil-moisture probes on Fort Wainwright

FWM ID	probe depth (fbgs)	always under water table?	number of plateaus	VOLUMETRIC WATER CONTENT (%) OF SOIL					
				max	min	average	median	variance	st dev
5532	13	NO	4	30.8	29.3	30.0	30.0	0.12	0.34
5532	14	NO	2	40.5	38.2	39.8	39.9	0.23	0.48
5532	15	YES	1	41.4	39	40.2	40.2	0.22	0.47
5532	16	YES	1	39.7	38.6	39.2	39.2	0.04	0.20
7796	13	NO	2	37.9	34	36.3	35.9	1.58	1.26
7796	14	NO	2	47.5	34.4	45.8	46.4	1.45	1.2
7796	15	NO	3	44.1	39.5	42.2	42.4	1.03	1.03
7796	16	NO	1	41.9	37.4	40.2	40.5	1.3	1.14
7796	17	YES	1	37.8	30.6	37.0	36.9	0.07	0.26
6009	16	NO	3	37.5	32.1	35.4	35.8	1.17	1.08
6009	17	NO	1	33.5	30	30.9	30.8	0.17	0.41
7075	14	NO	3	49.3	45.9	47.8	47.8	0.4	0.63
7075	15	NO	1	47.6	42.9	45.3	45.2	0.53	0.73
7075	16	NO	1	41.5	38.5	39.7	39.6	0.26	0.51
					Overall Average:	**39.3**			

Source: Fort Wainwright Geohydrologic Monitoring Project's data archive (http://www.uaf.edu/water/projects/ftww/ftww.html)

Notes: 1 4 of 11 Fort Wainwright soil moisture sites have probes clearly in fully-saturated soil

2 Of the 4 sites, there are a total of 14 probes in saturated soil

3 'Plateau' refers to shape of plot; a plateau indicates that probes is in fully-saturated soil if it is below the water table

4 FWM = Fort Wainwright Monitoring well

5 'st dev' = standard deviation

Table 20. Duration of soil moisture probe plateaus.

Individual probe plateaus				
FWM ID	**probe depth (fbgs)**	**start date**	**end date**	**period of record[g] (months)**
5532	13	5/31/2000	7/2/2000	1
5532	13	8/20/2000	11/28/2000	3
5532	13	8/23/2001	9/21/2001	1
5532	13	5/19/2002	9/11/2002	4
5532	14	5/15/2000	12/14/2001	23
5532	14	5/7/2002	9/12/2002	4
7796	13	9/3/2002	11/1/2002	2
7796	13	9/4/2003	11/8/2003	2
7796	14	8/12/2003	12/11/2003	4
7796	14	6/9/2004	7/3/2004	1
7796	15	5/24/2002	11/19/2002	6
7796	15	5/19/2003	6/28/2003	1
7796	15	7/28/2003	2/3/2004	6
7796	15	5/5/2004	9/21/2004	4
7796	16	5/20/2002	10/21/2004	27.5
7796	17	5/23/2002	10/21/2004	29
6009	16	5/4/2000	1/8/2001	8
6009	16	7/31/2001	9/26/2001	2
6009	16	5/4/2002	11/30/2002	6
6009	17	5/4/2000	11/30/2002	27
7075	14	5/1/2000	12/31/2000	7
7075	14	5/23/2001	11/12/2001	4.5
7075	14	5/16/2002	11/28/2002	6
7075	15	7/19/1999	11/28/2002	40
7075	16	7/19/1999	11/28/2002	40

[g]Period of record = 'end date' - 'start date' - any data gaps in record

APPENDIX C: SUB-REGIONAL MODEL DATA

Table 21. Input files required to run our MODFLOW simulation in MFI, and selected output files. All files are included in enclosed CD.

MODFLOW Package	Filename	Input Data files	Input File Contents
Name	thesis_final.nam		
Discretization	thesis_final.dis	top_elv.dat	top elevation of model
		m2l1elv.dat	layer 1 bottom elevations
		m2l2elv.dat	layer 2 bottom elevations
		m2l3elv.dat	layer 3 bottom elevations
		m2l4elv.dat	layer 4 bottom elevations
Basic	thesis_final.ba6	m2l1ib.dat	layer 1 IBOUND values
		m2l2ib.dat	layer 2 IBOUND values
		m2l3ib.dat	layer 3 IBOUND values
		m2l4ib.dat	layer 4 IBOUND values
		m2l1sh.dat	layer 1 starting heads
		m2l2sh.dat	layer 2 starting heads
		m2l3sh.dat	layer 3 starting heads
		m2l4sh.dat	layer 4 starting heads
Block-Centered Flow	thesis_final.bc6	m2l1conB.dat	layer 2 K values
		m2l2conB.dat	layer 1 K values
		m2l3trC.dat	layer 3 transmissivities
		m2l4tr.dat	layer 4 transmissivities
		m2l1vc8.dat	layer 1 VCONT values
		m2l2vc8.dat	layer 2 VCONT values
		m2l3vc8.dat	layer 3 VCONT values
Pre-Conjugate Solver	thesis_final.pcg		
Output Control	thesis_final.oc		
Recharge	thesis_final.rch	m2rch.dat	layer 1 recharge values
Well	thesis_final.wel		
River	thesis_final.riv		
Observation Process	thesis_final.obs		
	thesis_final.hob		
MODPATH	thesis_final.mpn		
	thesis_final.mp		

MODFLOW Output	Filename	Output File Contents
List	thesis_final.lst	model input and output data; simulation steps
Head	thesis_final.hed	head output of MODFLOW simulation
Budget	thesis_final.bud	cell-by-cell flow terms
Observed vs. Simulated	thesis_final._os	observed and simulated heads
Observation Residuals	thesis_final._w	observed heads - simulated heads

Table 22. Fort Wainwright monitoring well data used to calculate average March water levels.

				SUB-REGIONAL CELL ID			MARCH WATER-LEVEL AVERAGES (ft asl)								
FWM ID	NORTHING	EASTING	DEPTH (fbgs)	LAYER	ROW	COLUMN	1995	1996	1998	1999	2000	2001	2002	2003	OVERALL
5532	3961548	248752	23	1	67	125	432.7[i]	432.8[i]	--	431.77	431.92	432.99	432.2	433.04	432.38
4919	3956234	247630	24	1	78	122	--	--	--	435.23	435.28	436.38	435.65	--	435.64
5527	3965846	244240	24	1	59	115	--	--	426.63[i]	426.62	426.94	427.61	426.84	--	427.00
5534	3959426	248110	--	--	72	123	433.8[i]	--	--	433.03	--	--	--	--	433.03
5789	3966716	241515	59	1	57	110	--	--	--	425.96	426.1	426.74	426.05	--	426.21
5956	3961830	252187	--	--	67	131	434[i]	434.1[i]	--	433.18[i]	433.34[i]	434.4[i]	433.63[i]	--	433.78
6009	3966229	245174	29	1	58	117	--	--	--	427.02	427.28	427.97	427.25	427.99	427.50
6012	3965133	245876	28	1	60	118	--	--	--	427.71	427.83	428.83	428.12	--	428.12
6013	3965318	245040	27	3	60	117	--	--	--	428.23	425.60	431.79	--	--	428.54
6014	3965325	245057	18	2	60	117	--	--	--	427.47	427.87	--	429.96	--	427.67
6015	3965307	245059	29	1	60	117	--	--	--	427.26	427.46	428.41	427.38	--	427.71
6521	--	--	198.5	3	70	111	--	--	--	428.91	428.95	429.78[i]	429.10	--	428.99
6522	--	--	28	1	70	111	--	--	--	428.77	428.71	429.84[i]	429.06	--	428.85
6670	3963417	241096	29	1	64	109	427.2[i]	427.2[i]	--	426.36	426.71	427.25	426.71	--	426.76
6671	3963417	241096	76	2	64	109	427.2[i]	427.2[i]	--	426.41	426.64	427.23	426.61	--	426.72
6713	3966177	247539	103	2	58	122	430.01[i]	430.26[i]	--	427.86	428.12	428.99	428.19	--	428.29
7075	3966434	249456	75	2	58	125	--	--	--	427.17	427.26	428.07	427.32	428.17	427.59
7092	3965659	247559	66	1	59	122	428.76[i]	428.92[i]	--	--	--	429.14	428.31	--	428.72
7093	3965342	247538	62	1	60	122	--	429.1[i]	--	--	--	429.26	428.48	429.75	429.16
7162	--	--	29	1	58	113	--	--	--	426.41	426.67	427.15	426.40	--	426.66
7280	--	--	21	1	58	112	--	--	--	426.34	426.51	427.20	426.50	--	426.64
7350	3965769	248451	20	1	59	123	--	--	428.45	428.52	--	--	428.93	--	428.63
7546	--	--	19	1	60	125	--	--	--	429.51	429.84	430.63	429.90	--	429.97
50006	3960944	239350	113	2	69	105	--	--	--	427.20	427.42	428.08	427.30	--	427.50

Sources: 1 network-status02a.xls (hard copy), Table A, 1/21/2002
2 Fort Wainwright Geohydrologic Monitoring Project's data archive (http://www.uaf.edu/water/projects/ftww/ftww.html)

Notes: 1 Average March water levels were calculated from continuous (hourly) records of each well unless otherwise noted
2 [i] individual measurement rather than average of continuous data
3 FWM = Fort Wainwright Monitoring well
4 No data available for selected wells in 1997